https://ntrs.nasa.gov/search.jsp?R=19710005156 2020-03-12T00:01:06+00:00Z

MR-7009
Project 6910

A Study of High Frequency Nonlinear Combustion Instability in Baffled Annular Liquid Propellant Rocket Motors

Volume I

by

Samuel Z. Burstein

and

Harold S. Schechter

Final Report

to

National Aeronautics and Space Administration

Contract NAS7-752

August 31, 1970

TABLE OF CONTENTS

FOREWORD

This is the final report on Contract NAS7-752 for the National Aeronautics and Space Administration. The work was performed in the period from August 25, 1969 to September 25, 1970. The NASA program manager was Dr. Robert Levine, of the Office of Advanced Research and Technology, and the technical manager was Dr. Raymond Kushida, of the Jet Propulsion Laboratory.

NOTICE

This report was prepared as an account of Government-sponsored work. Neither the United States, nor the National Aeronautics and Space Administration (NASA), nor any person acting on behalf of NASA:

a) Makes any warranty or representation, expressed or implied, with respect to the accuracy, completeness, or usefulness of the information contained in this report, or that the use of any information, apparatus, method, or process disclosed in this report may not infringe privately-owned rights; or

b) Assumes any liabilities with respect to the use of, or for damages resulting from the use of, any information, apparatus, method, or process disclosed in this report.

As used above, "person acting on behalf of NASA" includes any employee or contractor of NASA, or employee of such contractor, to the extent that such employee or contractor of NASA or employee of such contractor prepares, disseminates, or provides access to any information pursuant to his employment or contract with NASA, or his employment with such contractor.

ABSTRACT

Computer experiments on the effect of baffles on the damping of bomb-like disturbances in simulated liquid rocket engines are reported herein. The method used is the direct numerical solution of the complete nonlinear gas dynamic equation with mass and energy sources in a cylindrical annular combustion chamber. The combustion model chosen for study is that of the Godsave's model of droplet vaporization augmented by an arbitrary pressure sensitive term of the form p-to-the λ power, when λ is a constant.

The original Godsave vaporization model has an effective λ of 0.0108, which did not yield steady oscillation, whereas $\lambda = 0.9$ did yield sustained periodic oscillation in an unbaffled chamber. Baffles damped this oscillation. Damping rates generally, although not always, increased with increase in baffle length. Drop size increase decreased oscillation amplitudes. Increasing the throat area, At/Ac, from .5025 to .6250 significantly increased damping rates. The results of systematic variation of the mass flux, the throat area, λ, and baffle length on the pressure history in the chamber are reported.

I. INTRODUCTION

This report describes the results of computer experiments that have been carried out using a numerical model of several of the processes occurring in the combustion chamber of an annular rocket motor. The companion report, which is the User's Guide[11], describes the details of the computer program, the difference method used, a sample case and program utilization. The fundamental assumption of the combustion process is that is is controlled by an evaporation mechanism. However, the model can be modified so as to include chemical kinetic energy release models. The model leads to a numerical simulation of the complete nonlinear gas dynamic flow field in an annular motor. The model considers three regimes of gas dynamic flow: the subsonic combustion zone adjacent to the injector face, the transonic region in the converging-diverging nozzle and the supersonic outflow region in the diverging section of the nozzle.

Interacting with the gas dynamic flow is a droplet field which has aerodynamic forces applied to it through a difference in velocities between the gas and droplet. The force field, resulting from the velocity field, is, of course, time-dependent and hence, motion of the droplet field is also time-dependent. The reinforcement of an initial pressure disturbance, present in the combustor, is then possible; dependence on the phase of the wave with respect to the time-dependent combustion field partially determines success or failure of the amplification process. The energy supplied to the wave versus energy outflow is another important criterion.

The coordinates are z, the axial length, θ, the angular coordinate, and time, t. This is the first model, to our knowledge, which is two-dimensional and time-dependent which includes the interaction of the combustion process with the nonlinear gas dynamic flow field. There have been[1,2] several analyses of a nonlinear form which come closest to modeling a physical combustion chamber[3] in which nonlinear effects are important. One could go to the literature[4,5] and obtain a rather complete introduction to linear theories of combustion instability. It has become apparent through the years that, although some qualitative aspects of the nonsteady combustion process can be described by a linear analysis, the degree of success that analysis will lend to design criterion in rocket engine technology clearly rests with nonlinear theory. Recent efforts[6] in this direction are appearing in the literature.

The model has the ability to describe baffles (up to six) placed at arbitrary angular positions and of arbitrary length. In addition to several calculations in which the drop parameters were allowed to vary, we include several calculations in this report in which the baffle length is allowed to vary. It is important to emphasize that these parameters are under the control of the rocket designer.

It is hoped that this report, which describes the continuation of an investigation in nonlinear rocket modeling, in two space dimensions, that was initiated with the Jet Propulsion Laboratories[7,8,9], will prove to be useful for analysis of stability limits in rocket motors yet to be designed and built.

II. MODEL CONSIDERATIONS

The computer program TRDL represents a numerical model of an annular combustion chamber with coordinates of axial length z and angle θ. The combustor is assumed to be of negligible radial thickness $\Delta r << R$, R being the annular chamber's mean radius. Then the equations of motion are

$$\begin{aligned}
&\rho_t + (\rho u)_z + \frac{1}{R}(\rho v)_\theta + \rho u \frac{\partial \mathrm{Ln}A}{\partial z} = \dot{m} \\
&(\rho u)_t + (\rho u^2 + p)_z + \frac{1}{R}(\rho uv)_\theta + \rho u^2 \frac{\partial \mathrm{Ln}A}{\partial z} = 0 \\
&(\rho v)_t + (\rho uv)_z + \frac{1}{R}(\rho v^2 + p)_\theta + \rho uv \frac{\partial \mathrm{Ln}A}{\partial z} = 0 \\
&E_t + \left[(p+E)u\right]_z + \frac{1}{R}\left[(p+E)v\right]_\theta + Eu \frac{\partial \mathrm{Ln}A}{\partial z} = \dot{E}
\end{aligned} \tag{1}$$

where

$\rho = \rho(z,\theta,t)$ = mass/unit volume of combustion gas

$u = u(z,\theta,t)$ = velocity of combustion gas in axial direction

$v = v(z,\theta,t)$ = velocity of combustion gas in tangential direction

$E = E(z,\theta,t)$ = total energy/unit volume of combustion gas

To be more specific, the total energy is related to the internal energy/unit mass, e, and kinetic energy by

$$E \equiv \rho\left(e + \tfrac{1}{2}(u^2+v^2)\right) \tag{2}$$

The pressure may be eliminated as a variable through the equation of state

$$r_\ell < .1 r_\ell^o$$

since the mass associated with the drop would be less than one-thousandth the original injected value.

The combustion model we have used is based on a modified Godsave model. The basic equations to obtain $\dot{m}$ and $\dot{E}$ required in equations (1) are:

$$a_{p_o} = 3.73 \times 10^{-5} T + 1.855$$
$$a_p = a_{p_o} (p/p_o)^{\lambda} \qquad (9)$$

where p is the local pressure in psia, p_o is the steady state pressure and T is the gas temperature in degrees Rankine. The parameter a_{p_o} was determined previously for the hydrogen/N_2O_4 propellant mixture[8]. The fuel droplet burning rate is then given by:

$$\dot{m}_F = \frac{2\pi k}{c_p} d_\ell a_p (1 + 0.276 (Re)^{\frac{1}{2}} (Pr)^{1/3}) \qquad (10)$$

where k is the thermal conductivity of the fuel vapor, c_p is the specific heat capacity of the fuel vapor, d_ℓ is the drop diameter, Re is the droplet Reynolds number and Pr is the Prandtl number of the surrounding gas. Finally, $\dot{m}$ and $\dot{E}$ are obtained by the relations:

$$\dot{m} = \dot{m}_F \left(1 + \frac{1}{\phi f_s}\right) N$$
$$\dot{E} = \dot{m}_F \left(Q - L_F - \frac{L_o}{\phi f_s}\right) N \qquad (11)$$

where N is the number density of the drop spray (see Appendix), ϕf_s is the local fuel/oxidant mass ratio, ϕ is the heat of reaction per unit mass of fuel, L_f is the latent heat of vaporization of the fuel and L_o is the latent heat of vaporization of the oxidizer.

In the original analysis given in reference 8, λ for the Godsave vaporization model was found to be 0.0108. However, as will be described later in this report, this model did not lead to sustained oscillation in the combustor. Therefore, the value of λ was not fixed but imputted as an arbitrary parameter.

The terms in equations (1) involving $\frac{\partial LnA}{\partial z}$ are added to simulate a convergent-divergent nozzle in the annular chamber[8]. The cross-sectional area is approximated by a quadratic function

$$A/A_c = 1-\alpha(z-L_c)+\beta(z-L_c)^2 \qquad L_c \leq z \leq L;\ A/A_c=1\ z \leq L_c$$

where A_c is the area of the chamber and L_c and L are the length of the chamber and motor respectively.

The need of introducing a nozzle into the calculation is related to one's inability to describe the correct nonlinear time-dependent downstream boundary condition. The nozzle is a valve that controls the pressure level in the combustor and hence the dependence of the outflow of combustion products from the combustor. One does not have to prescribe arbitrary conditions at the exit plane of the combustor. Rather, the flow is allowed to accelerate to a supersonic state within the nozzle and then the downstream boundary condition reduces to an extrapolation of flow conditions in the neighborhood of the supersonic boundary. The

error introduced by this procedure, even though it can be made small, cannot propagate upstream into the chamber because the particle speed exceeds the signal speed, i.e., signals are swept out of the domain of integration.

It is felt that the methods used in determining the outflow conditions in the one-dimensional "annular" motors[2,6] be reexamined more critically. This is needed since the computation of the gradients of gas velocity, density and temperature in the z-direction in the plane z=constant require an assumption that introduces an integral condition over the entire domain of interest. This means that, if attention is directed to any arbitrary mesh point θ_i at time t, the dependence of the solution at θ_i at time $t+\Delta t$ depends not only on data at time t at mesh points θ_{i-1}, θ_i, θ_{i+1} (introduced from the difference quotients in the difference equation) but on all mesh values θ_k, k=1,2,...,J. This is seen from the integration formulas used. Hence, at any time $t+\Delta t$ at point θ_i the solution depends on all other θ_k, k=1,2,...,J, since the weights in the integration procedure (Simpson's Rule) are uniform over $0 \leq \theta \leq 2\pi$. This means that information at a point θ_p, which is, say, $R(\theta_i-\theta_p)$ units to the left of θ_i can reach θ_i in the time

$$\Delta t = \frac{R(\theta_i-\theta_p)}{u+a}$$

From fluid dynamic considerations this implies a violation of the rule of forbidden signals. The Courant-Friedrichs-Lewy Condition, which can be written as

$$\Delta t \leq \frac{R(\theta_i - \theta_{i-1})}{u+a}, \quad (\theta_i - \theta_{i-1}) < (\theta_i - \theta_p)$$

is a necessary condition for stability for explicit difference schemes; here u and a are the particle velocity and sound speed respectively. For implicit methods this restriction may be relaxed; indeed, the method may be unconditionally stable. However, for this class of difference methods, the dependence of the solution at a mesh point on neighboring mesh points will decrease with increasing mesh distance. This characteristic of difference methods is needed to model the behavior of the original differential equation.

So far we have described a nonlinear model of fluid motion of a cylindrical column of gas coupled to an energy source which is distributed in space and time. It has long been known (from the work of Lord Rayleigh) that it is possible to stimulate motion of large amplitude waves in geometries such as those defining the domain of gas flow in rocket motors. If the phase relationship between the wave position and the energy release position, as well as energy source strength, is correct, reinforcement of wave motion will occur. It will be shown, further on in this report, that the above assumed model can simulate the reinforcement process.

The question which is raised at this point is: if a sustained oscillation of the gas dynamic field is achieved with a particular set of parameters input to the combustion model, how can the reinforcement process be attenuated by introducing changes in the

geometry of the domain of the gas flow. The purpose of this report is to describe the behavior of the model when changes are introduced in the geometry of the combustion zone. We consider the geometry to be changed through the insertion of baffles into the chamber and seek the effect that these baffles have on the stability of the combustion process. The baffles are assumed to start at the injector face and to extend an arbitrary length, up to, but never exceeding, the combustion chamber length. These baffles also can be arbitrarily spaced in the theta direction.

As a result of the baffles being in the chamber, one can see that the periodicity of the flow field in the theta direction will be destroyed. Hence the pattern of wave motion in the chamber will be substantially changed. One would suspect, that as a result of the influence of the baffles on the characteristics of the two-dimensional chamber flow, the relationship between the energy source strength and phase and the wave pattern will change. The pattern of change that will occur in a rocket combustion chamber with the introduction of baffles is one of the main concerns of the rocket motor designer. It is also the subject of this report.

III. PRELIMINARY NONSTEADY CALCULATIONS

The two sets of calculations presented in this section were carried out during the testing and debugging phase of the development of program TRDL. They are of interest because the range and value of parameters chosen differ from those presented in Section IV, where the program was used to analyze a physical annular motor operated by Richard M. Clayton at the Jet Propulsion Laboratories[12]. In addition, the general discussion of program TRDL, contained in this section, is meant to be complementary to the discussion in Section II.

We have carried out a series of computations involving a 'pop' type of disturbance superimposed on the self-consistent steady state. By a self-consistent steady state we mean a numerical solution to the complete set of gas dynamic equations and droplet equations solved simultaneously and whose solution is characterized by the vanishing of time derivatives. In the annular model we prescribe the dependence of the burning rate on the pressure by first carrying out a series of calculations using a variation of the Godsave model[10] in a parametric calculation. The dependence of the burning rate a_p in equation (9) on pressure in thus determined.

The calculations presented in this section are with two drop sizes $r_\ell^\circ=50\mu$ and $r_\ell^\circ=100\mu$ and with combustion sensitivity $\lambda=0.0108$ and $\lambda=0.90$. Most of the calculations were performed with a two baffle configuration in the motor. The baffles were placed at

θ_1=171 degrees and θ_2=351 degrees. (See Figure 1.) The baffle lengths, ℓ, in inches are prescribed as input data to the computer code. The location and the strength of the pulse, E_{bomb}/E_c, (or pop) are input parameters.

In all calculations presented in this section, the disturbance center is located at $\theta_{bomb}=270^\circ$ close to the injector face. The combustion chamber L_c is equal to 2.1 times the chamber radius, R, while the nozzle length L_N is equal to 0.9 times the chamber radius.

The calculation starts by computing the steady state flow field, and then superimposing the disturbance field of the bomb in terms of a distribution of pressure and density centered about $\theta=270^\circ$ and z=1.5 in. If present, the baffle geometry is prescribed as is the shutter which focuses the initial disturbance field. The time duration over which the shutter is present in the combustor is another parameter. When baffles are present, the shutter is absent. The shutter is merely a single baffle placed near the initial disturbance and removed after a specified time.

The time evolution of the chamber pressure, density, velocity and combustion field $\dot{m}(\theta,z,t)$ and $\dot{E}(\theta,z,t)$ is determined from the solution of the explicit finite difference equations[11]. Plotting routines are used to graph the pressure field and velocity field at prescribed values of time. The energy source $\dot{E}$, as a function of z, is plotted at equal intervals of θ at the same values of time. The primary indicator of the disturbance level in the combustor is given by the pressure history in the combustor which,

in turn, is plotted at several discrete points in the chamber. The envelope of maximum and minimum chamber pressure is also shown on the same plot. It is clear that by observing the level of the pressure disturbances generated from a particular run one is given an indication of how to rate the overall sensitivity of the combustion zone-pressure wave interaction process on combustor stability.

Periodic Oscillation

Figures 2 through 5 show the result of a calculation with a shutter in a combustor with no baffles present. Here $\lambda=0.9$, the flow rate is 2.2 lbm/sec-in^2 with a steady injector end pressure level of 300 psia. The initial drop radius is 50 microns. The maximum pulse pressure is almost 6000 psia; its exact value and the distribution of the pressure pulse is shown in Figure 2. Figure 3 shows the distribution $\dot{E}(z)$ for four values of θ at a value of time close to the end of the run. The nonuniform energy release is apparent; the largest rate exists in the region around $\theta=90^{\circ}$ and, as one sees from Figure 4, this coincides with the peak of a pressure wave which is spinning in the chamber. To see this, one observes from Figure 5 the periodic behavior of the pressure oscillations at the three pressure tap positions. The oscillation is strongest near the injector (p_1,p_2). Here, the peak to trough level of the oscillations are of the order of 400 psia on top of a base pressure of 300 psia. Downstream (p_3) the pressure oscillation has a peak level of approximately 400 psia with a trough level of about 300 psia.

Figure 6 shows the behavior of the solution if there is no shutter in the combustion chamber. The oscillation is not as strong as in the previous calculation even though the combustion parameters are exactly the same as in the previous case. It is clear that the shutter, which is set equal to the chamber length and is located at approximately 320°, reinforces the original disturbance by reflecting some of the wave energy forward towards the front of the pulse. The user of the program can then examine the pressure history curves and obtains an estimate of the relative combustor stability by comparing one run, with a given set of parameters, against another. The dynamic behavior of the wave as measured by the rate of change of the pressure at a particular location, $\dot{p}$, indicates if the disturbance is a continuous compression wave or a shock. The wave amplitude as well as the envelope of the wave train are useful measures of stability. The behavior of the maximum pressure envelope also gives an indication of the smoothness of the particular 'engine firing'.

Effect of Baffle Length

Figures 7, 8 and 9 show the pressure history obtained for this combustor when two baffles are inserted. The results shown in the three figures correspond to combustors with baffle lengths 3, 6 and 11.55 inches respectively. In comparing the calculation shown in Figures 6, with no baffle, and 7, with 3 inch baffles, we see (+) the fairly prominent periodic pressure wave detected at pressure tap p_2. The qualitative difference is clear: with the

baffle, the pressure wave has a longer rise time. This implies that the waves in the chamber without baffles may be shocklike, while with the baffles present, there is an insufficient tangential distance for the wave to propagate and 'shock up' since it collides with the baffles. Figures 8, with 6 inch baffles, and 9, with 11.55 inch baffles, show this general trend. Indeed, when the baffle length is 11.55 inches, equal to the chamber length, one sees a trend towards steady state for t*3 milliseconds. Figures 10 and 11 show the energy release rate, $\dot{E}$, for the completely unbaffled and baffled engine. The rates are essentially the same.

Effect of λ

If we decrease the pressure sensitivity of the combustion process, by letting λ=0.0108, we see by comparing Figures 9 and 12 that the motor stabilizes more quickly, i.e., at t≈1 millisecond the oscillation decays and the flow becomes essentially one-dimensional and time independent. In Figure 12, the lines of constant pressure (isobars) are vertical indicating that the pressure has no (or only a slight) θ-dependence. Figure 14 shows the lower energy release rate as a function of pressure obtained with this value of λ. The energy release extends over much of the combustor which can also be seen from Figure 13. This figure shows the rather gradual pressure gradient associated with the extended combustion length. In contrast, the pressure gradient in the nozzle is quite steep.

Effect of Drop Size

In Figures 15 (λ=0.9) and 16 (λ=0.0108) we indicate the pressure history for the combustor when the drop radius is 100 microns whereas the previous calculations were for 50 microns. The value of pressure at the injector in Figure 15 at 3 milliseconds is about 150 psia while the value for Figure 16 is 265 psia. The case where λ=0.9 is more oscillatory but at a lower pressure level. This is due to the form of the pressure sentitivity law: $a(p) \sim (p(t)/300)^{\lambda}$. If $p(t)<300$ then the function $a(p)$ is smaller than when $p(t)>300$ for a given λ.

The reason the pressure level falls below 300 psia can be seen from the energy release rates given in Figures 17 and 18. Here the evaporation of the 100μ drop is not complete by the end of the combustor. The energy release rate for λ=0.0108 is seen to be greater than for λ=0.9 at these pressure levels. For this case then, one can conclude that the value of N chosen should be increased somewhat to take into account the incomplete evaporation. Indeed, $N=5\times10^{7}$ was our first choice based on consideration of the droplet radius assuming complete evaporation.

Effect of the Number of Baffles

After completion of the two baffle calculation, the code TRDL was tested on a four baffle motor which was similar to but not geometrically the same as Clayton's (Reference 12) annular motor. For this calculation, the baffles were placed at positions $\theta=45^{\circ}$, 135°, 207° and 333°. They were each 6 inches long in a chamber which is 11.55 inches long. The value of the pressure index,

λ=0.9 was used in the droplet model which was given an initial drop radius of 50 microns. The steady state was pulsed, at t=0, with a bomb whose center resides on the line $\theta=270^{\circ}$.

The pressure history at discrete points in the combustor is given in Figure 19. This calculation may be compared directly to Figure 8 where there are two baffles and with Figure 6 with no baffles. We see from Figure 19 that there is almost no oscillatory pressure history at pressure tap 1 located approximately at the center of the bomb. The strongest oscillation occurs in the baffle diametrically opposite to the bomb location. There are no pressure taps available for evaluation in the baffled cavities defined for values of θ satisfying $333^{\circ}\leq\theta\leq45^{\circ}$ and $135^{\circ}\leq\theta\leq207^{\circ}$ since the maximum number of pressure taps available in TRDL, when this run was made, was four. The most interesting fact observed when comparison is made to the two baffle motor configuration is that the pressure trace at p_2 is much smoother for the four baffle motor than that shown for the two baffle motor. The rise time of the pressure oscillation decreases with the number of baffles in the chamber. This would imply that the baffles are reducing the distance required for wave coalescence in the tangential direction. The induced velocity field of the gas behind the wave would then be decreased reducing the level of droplet evaporation rates. Comparison can be made with Figure 6 which shows the pressure history in the unshuttered unbaffled engine. The maximum chamber pressure in the unbaffled engine is 550 psia at 3.008 milliseconds while it is 526

psia at 3.030 milliseconds in the four baffle engine (approximately the same in the two baffle engine). For this calculation the ratio of the throat area to chamber area is 0.7 with $N=4.0\times10^8$ drops/ft^3, $r_\ell^o=50$ microns and injection velocity of the drop $u_\ell^o=120$ ft/sec.

Four Baffle Engine

For the last set of calculations presented in this section, the drop density $N=7.25\times10^8$ drops/ft^3, $r_\ell^o=50$ microns, the droplet injection velocity $u^o=100$ ft/sec and the ratio of the throat area to chamber area is 0.5025. The chamber pressure is $p_o=100$ psia with a pressure index $\lambda=1.1$ and with a flow rate per unit area of 0.37 lbm/sec-in^2. We have found that for the given injection parameters, the steady state that one obtains depends quite strongly on the individual values of the initial droplet radius, r_ℓ^o and the droplet number density, N. The axial injection velocity u_ℓ^o has not been varied over a large enough range to see its effect on the steady state solution while the tangential injection velocity v_ℓ^o is always set to zero. The results which we present here, in Figures 20 through 31, are based on the above parameters.

The Figures 20 through 31 are identified by the computer run at the top of each figure. There are two sets of pressure plots per run. The plots are presented in order of decreasing stability as measured by the oscillatory pressure level of the tangential

wave in the neighborhood of the injector face (as measured by P(4)). In the table below we identify each of the runs as to the single element of variation from one run to another - the baffle geometry.

Figures	Baffle Configuration
20-21	no baffle
22-23	a single removable baffle - a shutter
24-25	$\theta_1=81^\circ, \theta_2=153^\circ, \theta_3=243^\circ, \theta_4=315^\circ, \ell=1.375$ inches
26-27	$\theta_1=81^\circ, \theta_2=153^\circ, \theta_3=243^\circ, \theta_4=315^\circ, \ell=2.875$ inches
28-29	$\theta_1=81^\circ, \theta_2=153^\circ, \theta_3=243^\circ, \theta_4=315^\circ, \ell=4.375$ inches
30-31	$\theta_1=81^\circ, \theta_2=153^\circ, \theta_3=243^\circ, \theta_4=315^\circ, \ell=5.375$ inches

The last four runs are carried out with four baffles at the indicated θ positions with length ℓ in a chamber of length equal to 15.8 inches. The baffle positions in Clayton's experimental engine are reported at θ values of 80°, 155°, 245° and 320°.

It is clear that with the introduction of baffles the engine experiences stronger oscillations than without baffles. The wave slope, however, is not as large as observed in the nonbaffled run 3 or shuttered run 4. One possible reason for this behavior is that, for this computation only, burning was excluded in the neighborhood of the baffle face so that gradients of pressure are generated by the nonuniform burning field.

The period of the wave is seen to increase with baffle length from a value of approximately 1 millisecond for the unbaffled and 1.375 inch baffled engines to about 1.5 milliseconds for the last

three baffled runs. There is apparently a sharp increase in the wave period between a baffle length of 1.375 inches and 2.875 inches remaining approximately constant up to the baffle length of 5.375 inches.

The decay rate of the oscillation is more pronounced for the nonbaffled runs than for the last four baffled runs. Even more pronounced is the large amount of energy contained over a period in a wave for the baffled engines as against the unbaffled engine.

IV. NUMERICAL EXPERIMENTS - J.P.L. ANNULAR MOTOR

A. Description of the Experiments

We have completed a limited series of computer runs with program TRDL with input data describing the geometry of Richard Clayton's experimental rocket motor[12]. Various parameters, input to the program, were systematically changed to observe their effect on the stability of the numerical motor. The result of these experiments will be described in this section and tentative conclusions, to be drawn from these runs performed using the model, will be elaborated upon.

TABLE I

Input and Computed Data For a Steady State (Clayton Motor)

$\gamma = 1.2$	$E_{bomb}/E_c = 0.1$	$p_o = 100.0$ psia
$M = 23.0 \frac{lbm}{mole}$	$N = 7.0 \times 10^7$ drops/ft^3	$T_o = 4000.0\ ^oR$
$R = 0.60917$ ft.	$d_\ell = 100.0$ microns	$a_o = 3220.7$ ft/sec
$L_c = 1.32167$ ft	$u_\ell = 100.0$ ft/sec	$\rho_o = 0.0536$ lbm/ft^3
$L_t = 1.85167$ ft.	$\lambda = 0.5$	$t_o = 0.1891$ millisec
$A_t/A_c = 0.5025$	$K = 1.0$	$\dot{m} = 0.35$ lbm/sec-in^2
$\ell = 0.$ ft.	fudg = 0.85	$p_c = 95.6$ psia
$\Delta z = 0.18080$ ft.		
$\Delta\theta = 0.31416$		

In the above table the first two columns contain input data or data computed from principle input data. The variables with a subscript zero, in the third column, are reference variables used to nondimensionalize the difference equations. The flow rate and pressure, shown in this column, are printed in the output of the program when steady state is reached. The pressure is measured at the injector face while the gas flow rate is determined at the exit of the combustion chamber (which is the entrance to the nozzle). Since the flow at steady state is one-dimensional, there is just one value of pressure at the injector face and one value of flow rate at the entrance to the nozzle.

The data given in Table I yields a self-consistent (fluid dynamic and droplet evaporation) steady state which closely approximates the experimental runs of Reference 12. Here the experimentally measured flow rate is 0.31 lbm/sec-in^2 while the measured chamber pressure is 100 psia. The data given in Table I form the data base from which variations to the basic motor were generated (runs 2 through 8). This data base, or set of initial and boundary conditions, was generated by the one-dimensional option contained in TRDL with E_{bomb}/E_c set equal to zero. The run labeled Clayton Motor 1 corresponds to this perturbed steady state with $E_{bomb}/E_c = 0.1$, i.e., with a bomb energy corresponding to 10% of the steady state chamber energy.

Table II indicates the variable that was changed from the value given in Table I. There are a total of twenty-four runs which are headed Clayton Motor 1 through 24 and Table II gives the value of the parameter that was changed for runs 2 through 24. Each of the runs were pulsed with the same bomb energy (E_{bomb}/E_c = 0.1).

Run number 9 corresponds to a pulsed Clayton Motor, but with a lowered steady state flow rate per unit area of 0.28 lbm/sec-in^2. The one-dimensional option in TRDL was used to generate the steady state. Runs 10 through 16 are stability runs based on this steady state, the values of all other variables, in this series, being given in Table I and the value of the perturbed variable being given in Table II.

Run 17 corresponds to a pulsed Clayton Motor, but with an increased flow rate per unit area of 0.42 lbm/sec-in^2. Again the one-dimensional option in TRDL was used to generate the steady state with this flow rate. Runs 18 through 24 are stability runs based on this steady state, the values of all other variables, in this series, being given in Table I with the value of the perturbed variable being given in Table II.

TABLE II

Value of Perturbed Variables in Stability

Runs 2 through 24

Run Number	Data: Table I except	Run Number	Data: Table I except
1		9	$N=5.8 \times 10^7$ drops/Ft^3 and
2	$A_t/A_c=0.3750$	10	$A_t/A_c=0.3750$
3	$A_t/A_c=0.6250$	11	$A_t/A_c=0.6250$
4	$\lambda=1.2$	12	$\lambda=1.2$
5	$\ell=5.375$ in.	13	$\lambda=0.1$
6	$\ell=4.375$ in.	14	$\ell=5.375$ in.
7	$\ell=2.875$ in.	15	$\ell=4.375$ in.
8	$\lambda=0.1$	16	$\ell=2.875$ in.

Run Number	Data: Table I except
17	$N=8.0 \times 10^7$ drops/Ft^3 and
18	$A_t/A_c=0.3750$
19	$A_t/A_c=0.6250$
20	$\lambda=1.2$
21	$\lambda=0.1$
22	$\ell=5.375$ in.
23	$\ell=4.375$ in.
24	$\ell=2.875$ in.

The perturbed flow rate data, given in columns two and three correspond to a steady state injector head pressure level of 76.5 psia ($\dot{m}$ = 0.28 lbm/sec-in^2) and 112.1 psia ($\dot{m}$ = 42 lbm/sec-in^2) respectively.

With the set of runs presented, one can then

a) describe the sensitivity of the stability of the motor as a function of flow rate, $\dot{m}$;

b) as a function of the pressure sensitive index, λ;

c) as a function of the reciprocal contraction ration, A_t/A_c;

d) as a function of the baffle length, ℓ.

The number of baffles is limited to four for this series of runs, the location of each, in the chamber, is specified by the length, ℓ, and the angular orientation, θ_i i = 1,2,3,4, i.e., $\theta_1 = 81^\circ$, $\theta_2 = 153^\circ$, $\theta_3 = 243^\circ$, and $\theta_4 = 315^\circ$. The position of each of the pressure taps (there are a total of 6 for each run) are indicated, on the pressure plots, by their distance from the injector face and their angular orientation.

B. Presentation of Results

For each of the twenty-four runs presented in this section, there are two figures for each run. The first of each contains the maximum and minimum pressure history envelope for the combustion chamber as well as two pressure histories at the indicated

tap position. The second graph shows the four pressure histories obtained from the remaining four pressure taps.

Figures 32 and 33 show the stability behavior of the model approximation to Clayton's motor with no baffles or shutter present. We did not use the shutter option for this entire series of computer experiments.

The tangential wave moving past the pressure taps located along $\theta = 0$ are seen to be almost in phase along the length of the combustor. Upon close inspection, one observes that there is a small shift in arrival time; the wave front is leading near the injector and trailing near the nozzle entrance. Maximum pressure levels exist at the injector end and decrease towards the nozzle end of the combustor.

Figures 34 and 35 corresponds to the previous motor calculation but with a larger nozzle contraction ratio, 0.3750^{-1}. This motor is clearly more unstable than the previous motor since it exhibits a higher amplitude wave whose decay rate is lower than that observed in Run 1. It should be observed that the period of rotation for this motor is fairly constant at 1 millisecond for all runs presented in this section. Figures 36 and 37 show the pressure history for the same motor configuration but with a smaller contraction ratio of 0.6250^{-1}. Clearly, this motor is more stable than the previous two motors since the decay rate of the disturbance is greatest.

Figures 38 and 39 show the pressure history for a larger pressure sensitive index; here $\lambda = 1.2$. The oscillatory nature of the solution is much more severe than for $\lambda = 0.5$, as one would suspect. This solution should be compared to the solution for $\lambda = 0.1$ given in Figures 46 and 47. Here there is very little amplification of the spinning wave by the combustion process due to the relative insensitivity of the combustion process to pressure.

Figures 40 and 41, 42 and 43, and 44 and 45 show the effect of baffles on the fundamental solution, Figures 32 and 33. The baffle lengths $\ell = 5.375$ inches, 4.375 inches, 2.875 inches and 0.0 inches correspond respectively to the above figures. In this series of runs, one observes that the peak pressure levels decrease with increasing baffle length. In the transient phase of the bomb pulse the maximum pressure levels reached in each of the motors are 240 psia, 211 psia, 184 psia and 164 psia in order of increasing baffle length. There is a uniform decrease in the peak pressure levels observed for baffle lengths between 0.0 inches and 5.375 inches. With increasing baffle length attenuation of the amplitude of the pressure oscillations in the chamber increases along with an increase in the rise time of the wave as measured as it sweeps past a pressure tap position. This implies that the baffles tend to surpress the coalescence properties of the finite amplitude wave by internal reflections.

Figures 48 and 49 show a pulsed solution for the Clayton motor with a flow rate per unit area of 0.28 lbm/sec-in^2 which may be compared to the solution shown in Figures 32 and 33. The solutions are similar, the lower flow rate yielding correspondingly smaller amplitude oscillations.

Figures 50 and 51 and Figures 52 and 53 show the effect of changing the nozzle contraction ratio to a value which is larger and smaller respectively than the value used in Figures 48 and 49. The effect of changing the contraction ratio is quite similar to that already discussed above as observed by comparing the figures of Runs 2 and 3 with Runs 10 and 11.

In Figures 55 and 56, the value of the pressure index, λ, was increased from a value of 0.5 to 1.2. The pressure oscillations are much larger than that shown in Figures 48 and 49, where $\lambda = 0.5$, but they are also larger than that shown in Run 4, Figures 38 and 39, especially at the pressure taps located far downstream, i.e., there is, in Run 12, a more uniform amplitude tangential wave spinning with a smaller decay of amplitude with downstream position.

When $\lambda = 0.1$, in Figures 56 and 57, the pressure wave is again, as in Run 8 (Figures 46 and 47), only slightly amplified. For small λ, there does not appear to be much of an effect of flow rate on the amplitude of oscillatory waves in the nonsteady solution. Run 21, shown in Figures 72 and 73, with a flow rate per unit area of 0.42 lbm/sec-in^2, or 1.5 times that in Run 13, has oscillations that are still quite small.

Figures 58 and 59, 60 and 61 and 62 and 63 correspond to baffled runs (with a flow rate of 0.28 lbm/sec-in^2) with baffle lengths of ℓ = 5.375 inches, 4.375 inches and 2.875 inches respectively. And, again, the greater the baffle length, the greater the stability. There is a similar decrease in the maximum oscillatory pressure for baffled Runs 14, 15 and 16 similar to the previous series of calculations (where $\dot{m}$ = 0.35 lbm/sec-in^2). We note, again, a rather uniform decrease in the maximum observed pressure in the maximum pressure envelope from 232 psia for the zero baffle length case (Run 9) to 202 psia to 170 psia to 145 psia for the maximum baffle length of 5.375 inches.

Figures 65 and 66, Run 17, show the oscillatory solution for λ = 0.5 and $\dot{m}$ = 0.42 lbm/sec-in^2. Here, for this higher flow rate, we see that the tangential wave leads slightly at the injector end while being retarded at the nozzle end. This small effect is also present in Run 1 (Figures 32 and 33) and to a smaller extent Run 9 (Figures 48 and 49). However, it is clear that increasing the flow rate increases the phase angle between the head and tail of the spinning wave.

Figures 66 and 67 and 68 and 69 show the effect of varying the reciprocal contraction ratio for this higher flow rate. In the first two figures A_t/A_c = 0.3750 while A_t/A_c = 0.6250 for the last two figures. It is clear that smaller throat areas for a given chamber area allows for greater permanence of the spinning wave in the combustor. And, the way to amplifying this effect is to increase the flow rate over its design value.

The value of the pressure index was again varied from λ = 0.5 in Figures 63 and 64 to λ = 1.2 in Figures 70 and 71 and λ = 0.1 in Figures 72 and 73. It is clear, by comparing these three sets of figures, that, in addition to the greater amplification of the spinning wave with increasing λ, the wave front increases its lead, at the injector end of the combustion chamber, over the wave front at the nozzle end of the combustion chamber.

The last three runs, 22, 23 and 24, that correspond to Figures 74 and 75, 76 and 77 and 78 and 79, respectively, were nonsteady runs of the baffled combustion chamber with the flow rate of 0.42 lbm/sec-in^2. Peak maximum pressure amplitudes for the unbaffled motor and 2.875 inch, 4.375 inch and 5.375 inch baffled motors are 276 psia, 218 psia, 198 psia and 183 psia respectively. Again we see that the baffle reduces the wave amplitude. In this series of runs, the introduction of the 2.875 inch baffle causes a 60 psia change in peak pressure while approximately doubling the baffle length still further reduces the peak measured pressure by only 30 psia. Upon close examination (compare Run 17 with Run 22) we observe the wave front near the nozzle leading the front near the injector. This effect is not observed in the other two sets of experiments.

V. CONCLUSIONS

This report presents results obtained from the code TRDL, a program describing a computational algorithm of a two-dimensional time-dependent nonlinear formulation of an evaporation rate controlling combustion model in an annular rocket engine. We have presented results which describe the influence of drop diameter, mass flow rate per unit area, pressure sensitive burning index, contraction ratio and the number and length of baffles on the stability process. These are just a few of the input parameters available in the model which have been varied (over the limited range presented in this report).

The User Manual (Ref. 11) for the program TRDL can be referred to so that additional experimentation, by the interested reader, can be carried out. The combustion model itself, because it is contained in a single subroutine, can be substituted with other models more appropriate for different fuel oxidizer combinations so that comparisons can be made between models.

We have shown the model contains the following characteristics:

a) A bomb, pulsing an initially steady flow, leads to a solution containing a finite amplitude wave which spins in the chamber. By focusing the initial pulse using a shutter (a baffle which can be removed after a few tens of cycles of computation) the amplitude of the induced spinning wave can be increased significantly over a wave which has not been focused.

b) A large drop diameter introduces inertia into the evaporation process so that oscillations of the gas are lower for larger drops.

c) The greater the flow rate, the greater the energy available for wave amplification; hence a stronger tangential wave.

d) Values of the pressure sensitive index, of the order of unity, lead to oscillatory pressure levels which seem quite reasonable. The larger the index the more unstable the engine.

e) The nozzle to combustion chamber area ratio significantly effects the chamber stability. Smaller values of this parameter lead to more unstable motors.

f) The introduction of baffles into the combustion chamber reduces the amplitude of the wave while increasing the rise time of the wave - both effects stabilizing the motor.

g) We have also shown that for some values of several of the above variables the oscillatory solution yields a spinning wave in phase over the entire chamber length; for other values the injector end of the wave leads the nozzle end of the wave.

The exact quantitative measure of each of these effects would require more extensive testing of program TRDL than has been completed thus far. But, it is clear from the tests and runs completed that the program is quite flexible as it can compute the motion of extremely strong bomb transients successfully. We feel that we have produced a useful engineering tool (if the program is used it may prove useful) for the design of liquid propulsion rocket engines.

NOMENCLATURE

A_c	cross-sectional area of chamber
A_t	cross-sectional area of throat
a_p	dimensionless mass burning rate at pressure p
a_o	reference sound speed
C_D	drag coefficient
c_p	specific heat at constant pressure
d_ℓ	diameter of drop
Δt	time stepsize
$\Delta\theta$	tangential stepsize
Δz	axial stepsize
E	total energy per unit volume of gas
E_{bomb}/E_c	ratio of bomb energy to steady-state chamber energy
e	internal energy per unit mass
γ	specific heat ratio
ℓ	length of baffles
L_c	length of chamber
L_N	length of converging-diverging nozzle
L_t	length of motor to throat
λ	pressure index in burning rate law
M	molecular weight of gas
$\dot{m}_F$	mass burning rate
N	drop number density
p	pressure of gas
p_o	reference pressure

r, R	radius of chamber
r_ℓ	radius of drop
ρ	density of gas
ρ_o	reference density
T	temperature of gas
T_o	reference temperature
t	time
t_o	reference time
θ	tangential coordinate
u	axial velocity of gas
v	tangential velocity of gas
W	vector of fluid properties
z	axial coordinate

REFERENCES

1. Priem, R.J. and Heidmann, M.F., "Propellant Vaporization as a Design Criterion for Rocket-Engine Combustion Chambers", NASA TR R-67, 1960.

2. Priem, R.J. and Gruentert, D.C., "Combustion Instability Limits Determined by a Nonlinear Theory and a One-Dimensional Model", NASA TN D-1409, 1962.

3. Clayton, R.M. and Rogero, R.S., "Experimental Measurements on a Rotating Detonation-like Wave Observed During Liquid Rocket Resonant Combustion", J.P.L. TR No. 32-788, August 15, 1965.

4. Crocco, L. and Cheng, S.I., "Theory of Combustion Instability in Liquid Propellant Rocket Motors", AGARD Monograph No. 8, Butterworths Scientific Publications, Ltd., London, 1956.

5. Crocco, L., Greg, J. and Harrje, D.T., "Theory of Liquid Propellant Rocket Combustion Instability and its Experimental Verification", ARS Journal, Vol. 30, No. 2, Feb. 1960.

6. Campbell, D.T. and Chadwick, W.D., "Combustion Instability Analysis at High Chamber Pressure", Final Report, AFRPL-TR-68-179, Rocketdyne August, 1968.

7. Burstein, S.Z., "Nonlinear Combustion Instability in Liquid-Propellant Rocket Engines: The Transverse Mode 1. The Hydrodynamic Differential and Difference Equations and Computer Algorithm", NASA TR 32-1111, Sept. 15, 1967.

8. Burstein, S.Z., Chinitz, W., and Schechter, H.S., "Nonlinear Combustion Instability in Liquid-Propellant Rocket Motors", MAGI Final Report to J.P.L., Contract No. 951946, July, 1970.

9. Burstein, S.Z. and Schechter, H., "Nonlinear Combustion Instability: Computer Experiments Using Codes COMB and TRDL", MAGI Final Report of J.P.L., Contract No. 952505, July, 1969.

10. Peskin, R.L. and Wise, H., AIAA Journal, 4, p. 1646 (1966).

11. Schechter, H.S. and Burstein, S.Z., "A Study of High Frequency Nonlinear Combustion Instability in Baffled Annular Liquid Propellant Rocket Motors, Vol. II - A User Manual For Computer Programs TRDL and TRDPLT", MAGI Final Report to NASA, Contract No. NAS7-752, August 31, 1970.

12. Clayton, R.M., "Resonant Combustion", J.P.L. Space Programs Summary 37-55, Vol. 3, February 28, 1969.

LIST OF FIGURES

Figures:

Figures:	Parametric Experiments on Clayton Motor
32-33	Unbaffled, $\dot{m}$=0.35, A_t/A_c=0.5025, λ=0.5
34-35	Unbaffled, $\dot{m}$=0.35, A_t/A_c=0.3750, λ=0.5
36-37	Unbaffled, $\dot{m}$=0.35, A_t/A_c=0.6250, λ=0.5
38-39	Unbaffled, $\dot{m}$=0.35, A_t/A_c=0.5025, λ=1.2
40-41	Baffled, ℓ=5.375", $\dot{m}$=0.35, A_t/A_c=0.5025, λ=0.5
42-43	Baffled, ℓ=4.375", $\dot{m}$=0.35, A_t/A_c=0.5025, λ=0.5
44-45	Baffled, ℓ=2.875", $\dot{m}$=0.35, A_t/A_c=0.5025, λ=0.5
46-47	Unbaffled, $\dot{m}$=0.35, A_t/A_c=0.5025, λ=0.1
48-49	Unbaffled, $\dot{m}$=0.28, A_t/A_c=0.5025, λ=0.5
50-51	Unbaffled, $\dot{m}$=0.28, A_t/A_c=0.3750, λ=0.5
52-53	Unbaffled, $\dot{m}$=0.28, A_t/A_c=0.6250, λ=0.5
54-55	Unbaffled, $\dot{m}$=0.28, A_t/A_c=0.5025, λ=1.2
56-57	Unbaffled, $\dot{m}$=0.28, A_t/A_c=0.5025, λ=0.1
58-59	Baffled, ℓ=5.375", $\dot{m}$=0.28, A_t/A_c=0.5025, λ=0.5
60-61	Baffled, ℓ=4.375", $\dot{m}$=0.28, A_t/A_c=0.5025, λ=0.5
62-63	Baffled, ℓ=2.875", $\dot{m}$=0.28, A_t/A_c=0.5025, λ=0.5
64-65	Unbaffled, $\dot{m}$=0.42, A_t/A_c=0.5025, λ=0.5
66-67	Unbaffled, $\dot{m}$=0.42, A_t/A_c=0.3750, λ=0.5
68-69	Unbaffled, $\dot{m}$=0.42, A_t/A_c=0.6250, λ=0.5
70-71	Unbaffled, $\dot{m}$=0.42, A_t/A_c=0.5025, λ=1.2
72-73	Unbaffled, $\dot{m}$=0.42, A_t/A_c=0.5025, λ=0.1
74-75	Baffled, ℓ=5.375", $\dot{m}$=0.42, A_t/A_c=0.5025, λ=0.5
76-77	Baffled, ℓ=4.375", $\dot{m}$=0.42, A_t/A_c=0.5025, λ=0.5
78-79	Baffled, ℓ=2.875", $\dot{m}$=0.42, A_t/A_c=0.5025, λ=0.5

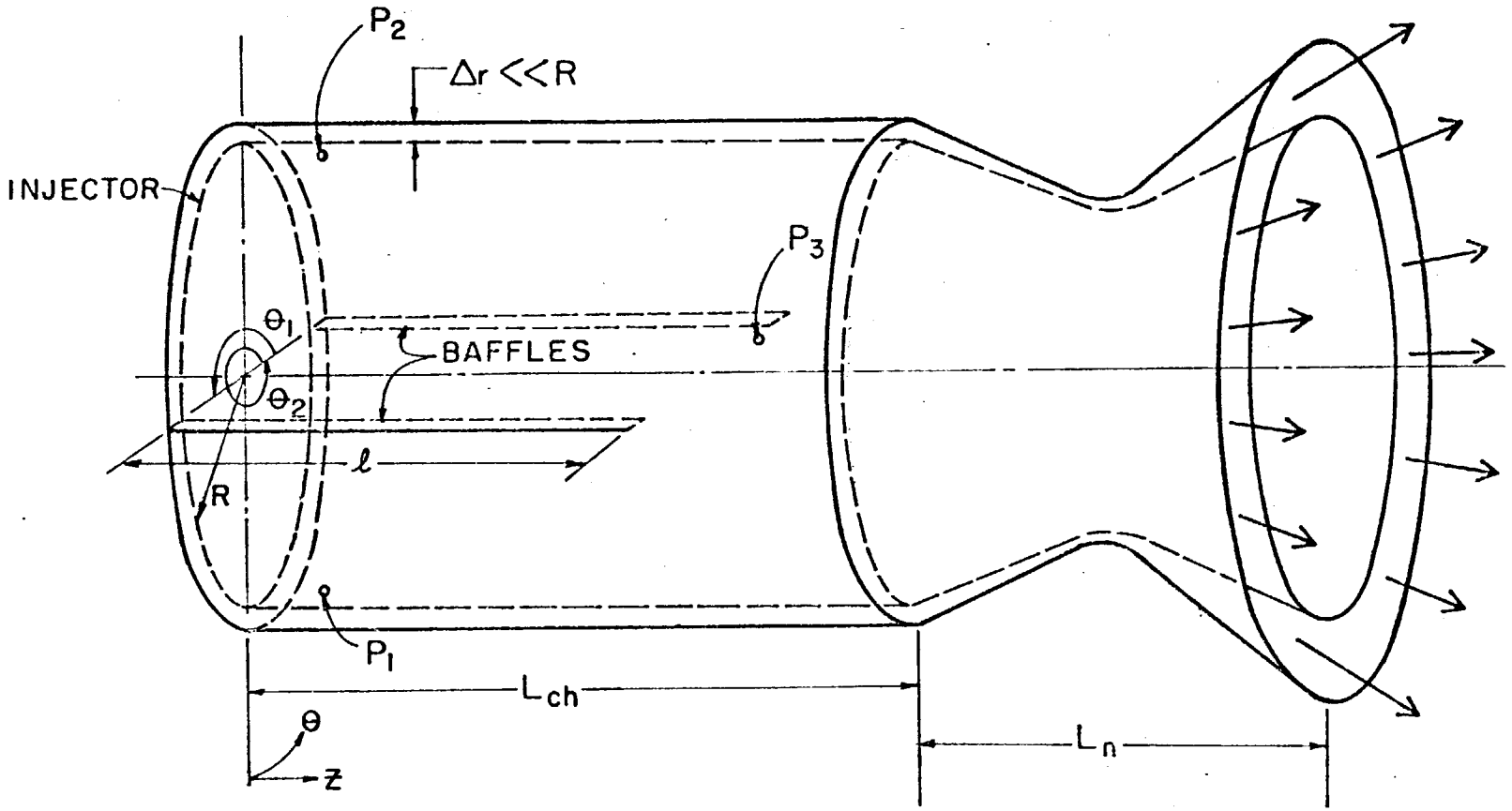

FIGURE 1 2 - BAFFLE ENGINE GEOMETRY

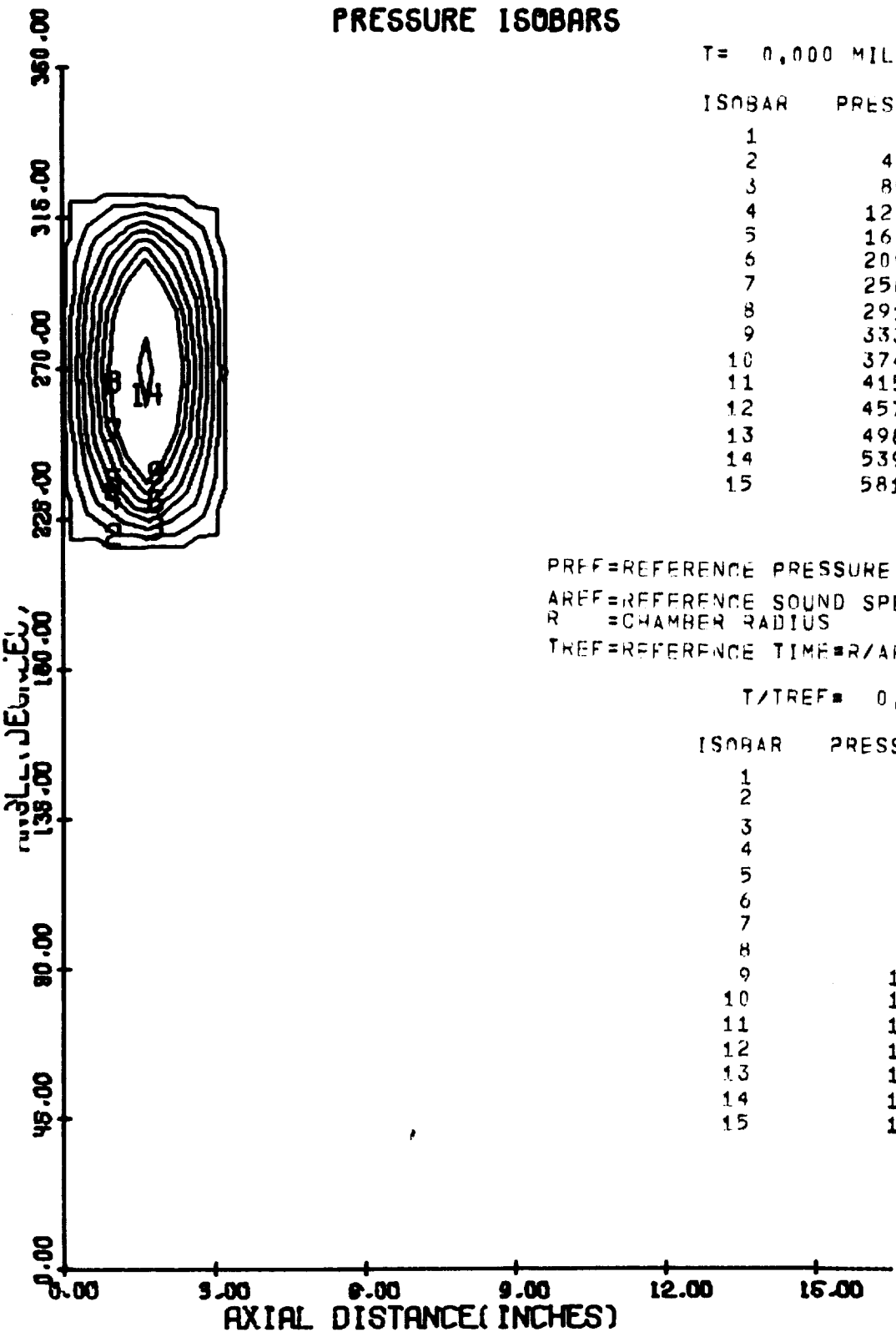
PRESSURE ISOBARS
T= 0.000 MILLISECONDS
ISOBAR PRESSURE(PSI)
1 25,154
2 438,404
3 851,654
4 1264,904
5 1678,154
6 2091,404
7 2504,654
8 2917,904
9 3331,154
10 3744,405
11 4157,655
12 4570,905
13 4984,155
14 5397,405
15 5810,655
PREF=REFERENCE PRESSURE = 300.00 PSI
AREF=REFERENCE SOUND SPEED= 3220.7 FT/SEC
R =CHAMBER RADIUS = .45830 FEET
TREF=REFERENCE TIME=R/AREF=.0001423 SEC
T/TREF= 0.00000
ISOBAR PRESSURE/PREF
1 .084
2 1.461
3 2.839
4 4.216
5 5.594
6 6.971
7 8.349
8 9.726
9 11.104
10 12.481
11 13.859
12 15.236
13 16.614
14 17.991
15 19.369
360.00
315.00
270.00
225.00
180.00
135.00
90.00
45.00
0.00
0.00
3.00
6.00
9.00
12.00
15.00
AXIAL DISTANCE(INCHES)
T= 0.000 MILLISECONDS

Figure 2

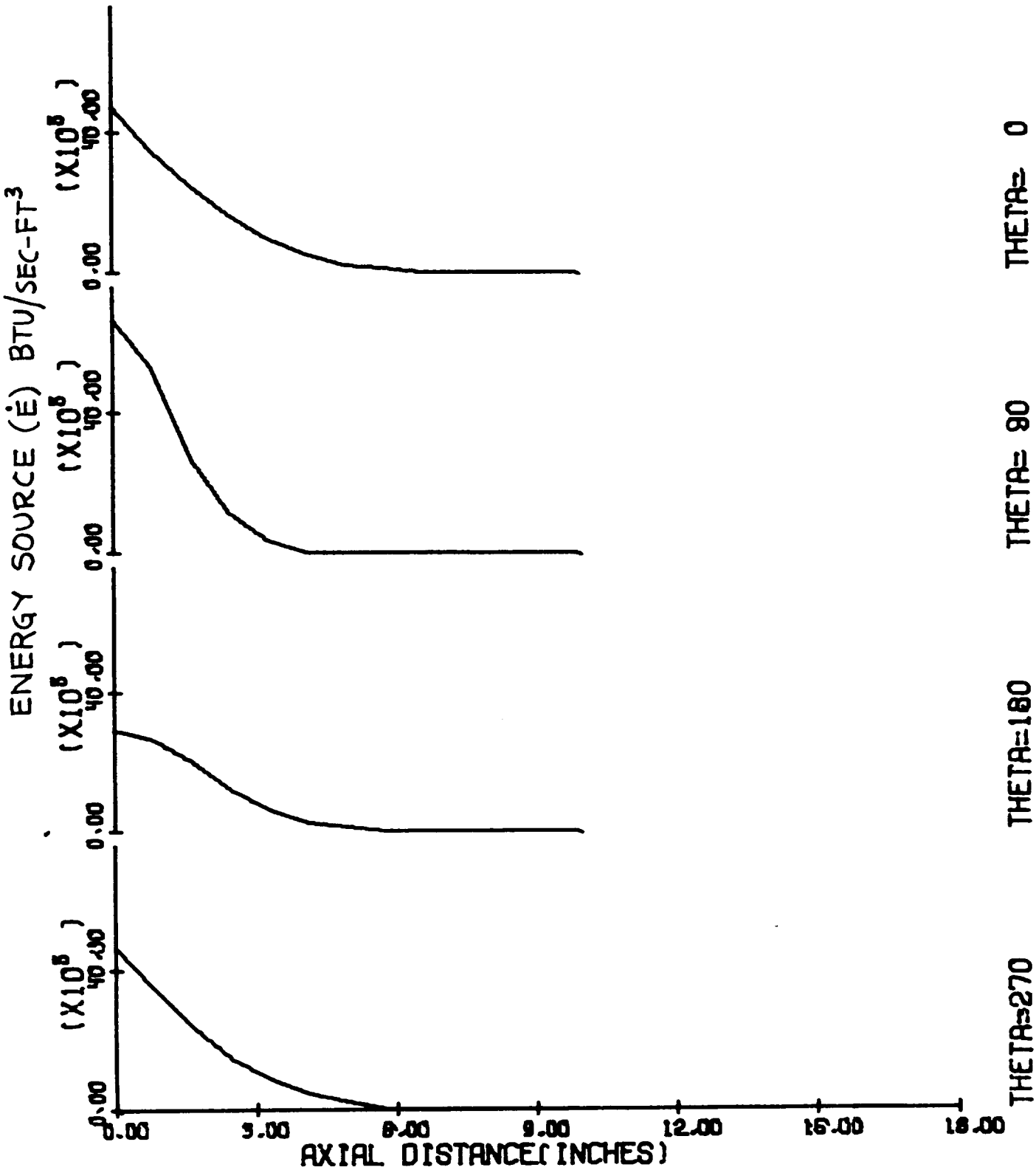

T= 3.008 MILLISECONDS

Figure 3

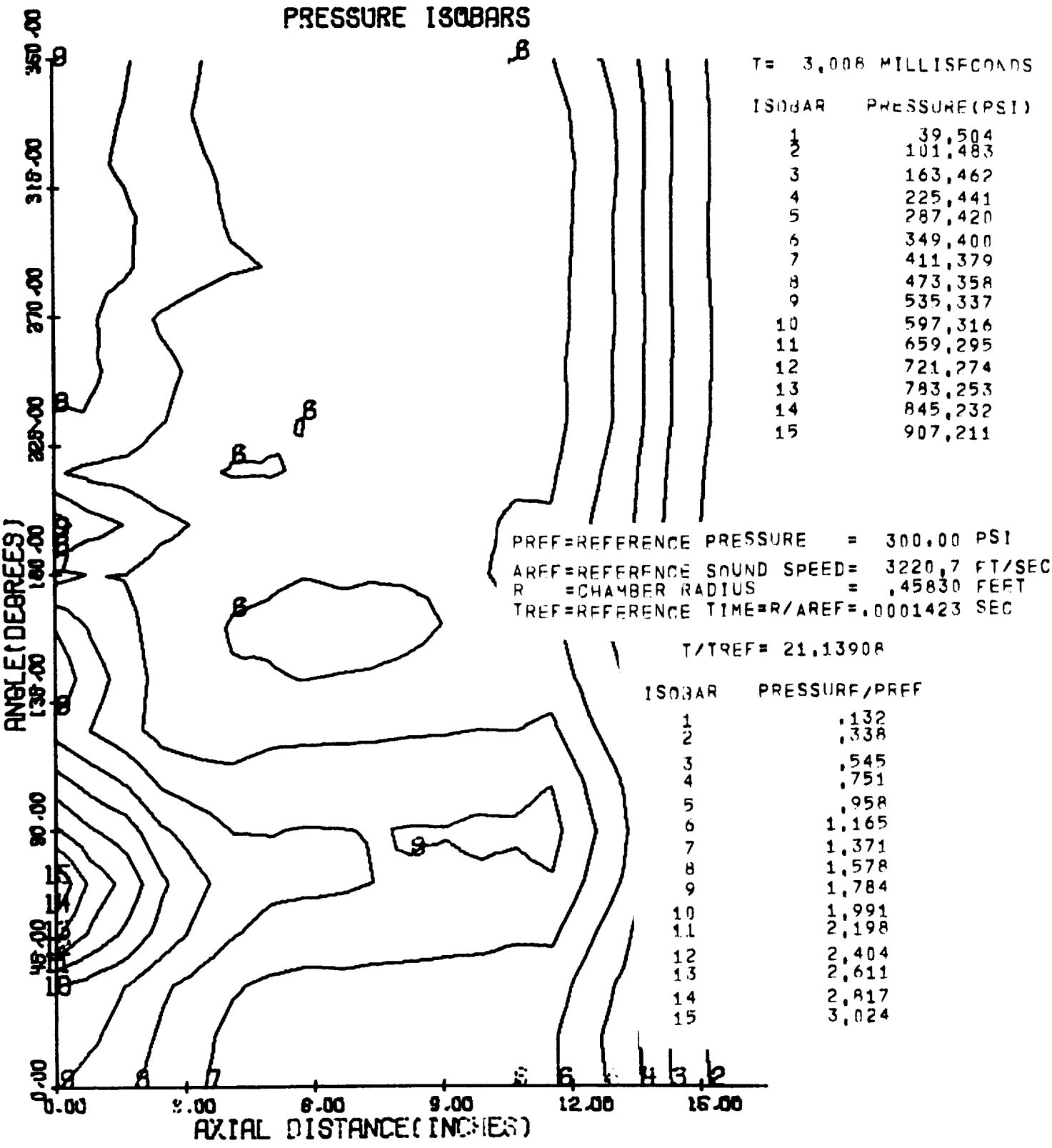
PRESSURE ISOBARS
T= 3.008 MILLISECONDS
ISOBAR PRESSURE(PSI)
1 39.504
2 101.483
3 163.462
4 225.441
5 287.420
6 349.400
7 411.379
8 473.358
9 535.337
10 597.316
11 659.295
12 721.274
13 783.253
14 845.232
15 907.211
PREF=REFERENCE PRESSURE = 300.00 PSI
AREF=REFERENCE SOUND SPEED= 3220.7 FT/SEC
R =CHAMBER RADIUS = .45830 FEET
TREF=REFERENCE TIME=R/AREF=.0001423 SEC
T/TREF= 21.13908
ISOBAR PRESSURE/PREF
1 .132
2 .338
3 .545
4 .751
5 .958
6 1.165
7 1.371
8 1.578
9 1.784
10 1.991
11 2.198
12 2.404
13 2.611
14 2.817
15 3.024
ANGLE(DEGREES)
AXIAL DISTANCE(INCHES)
0.00
3.00
6.00
9.00
12.00
15.00
T= 3.008 MILLISECONDS

Figure 4

SHUTTER ENGINE, UNBAFFLED λ=0.90

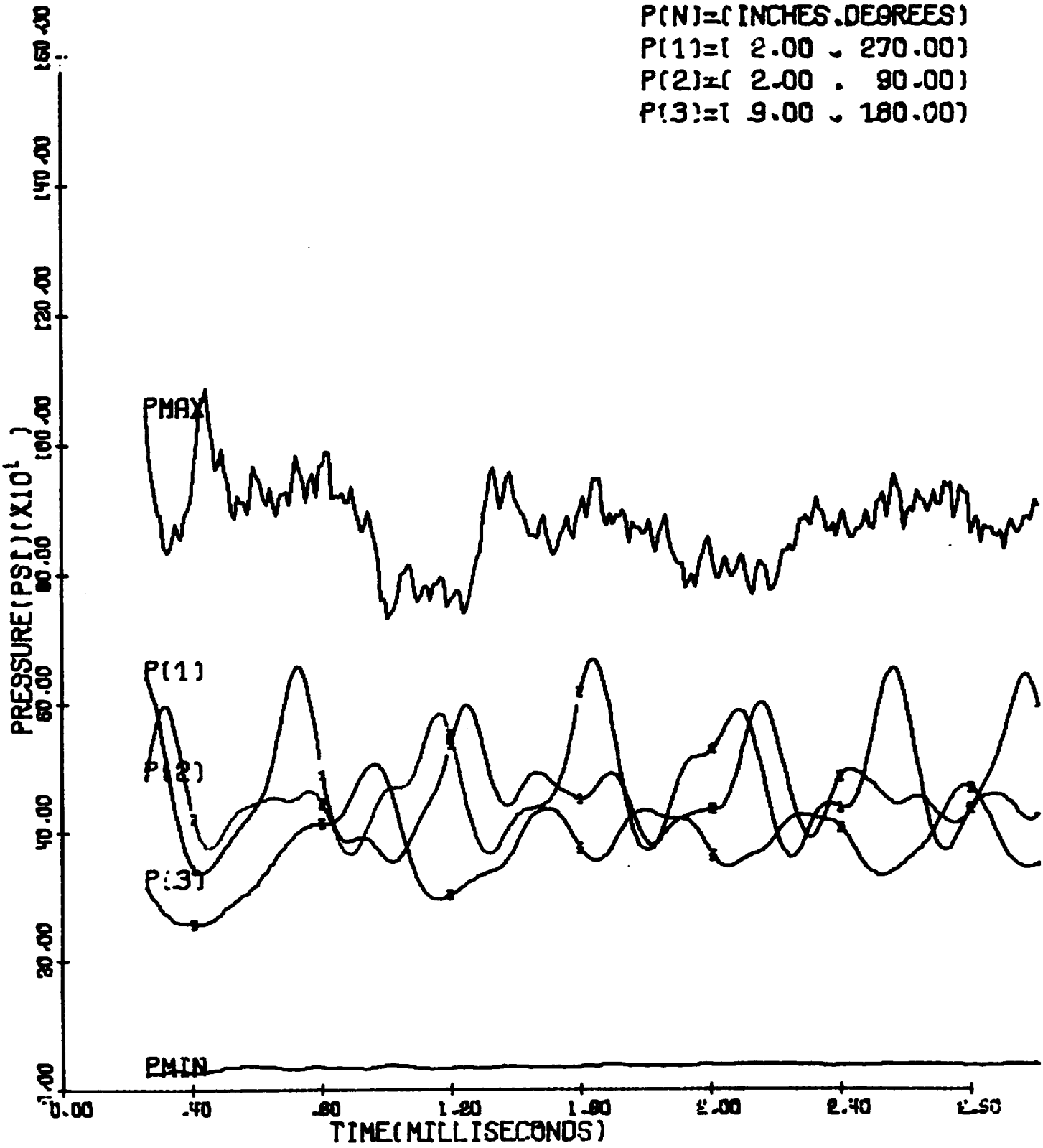

Figure 5

UNSHUTTED ENGINE, UNBAFFLED λ=0.90

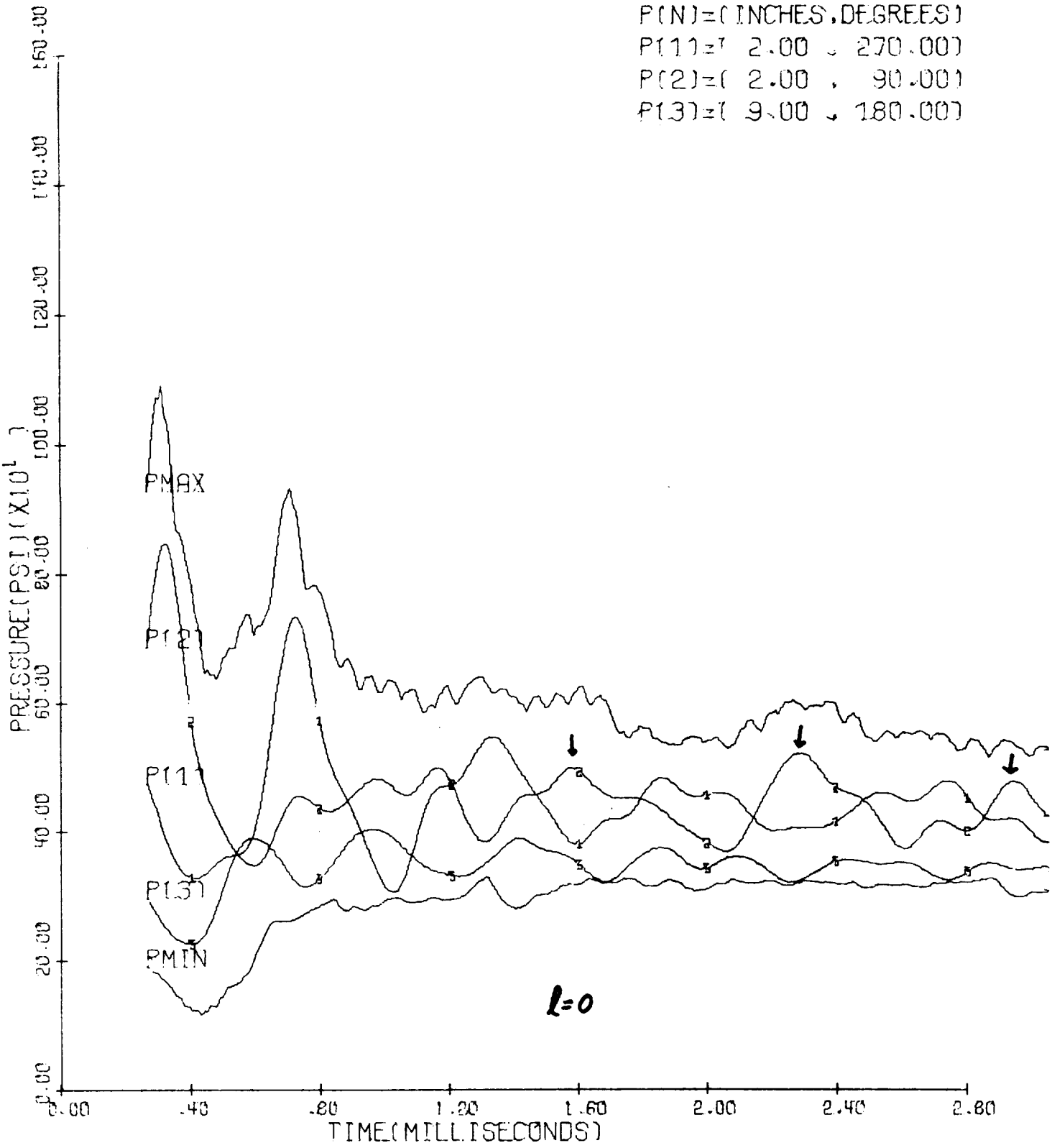

Figure 6

2-BAFFLE ENGINE, ℓ=3", λ=0.90

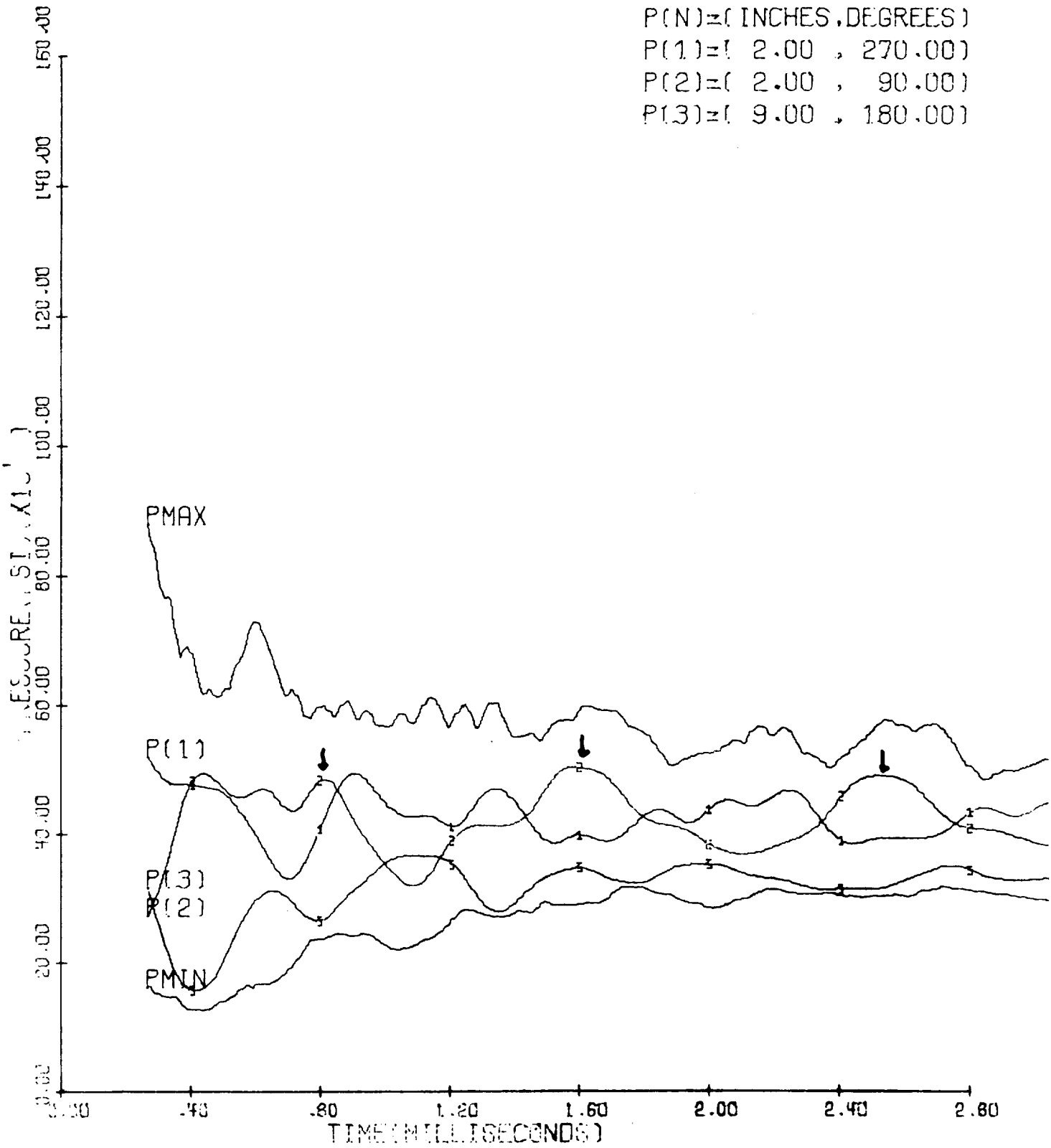

Figure 7

2-BAFFLE ENGINE, ℓ=6", λ=0.90

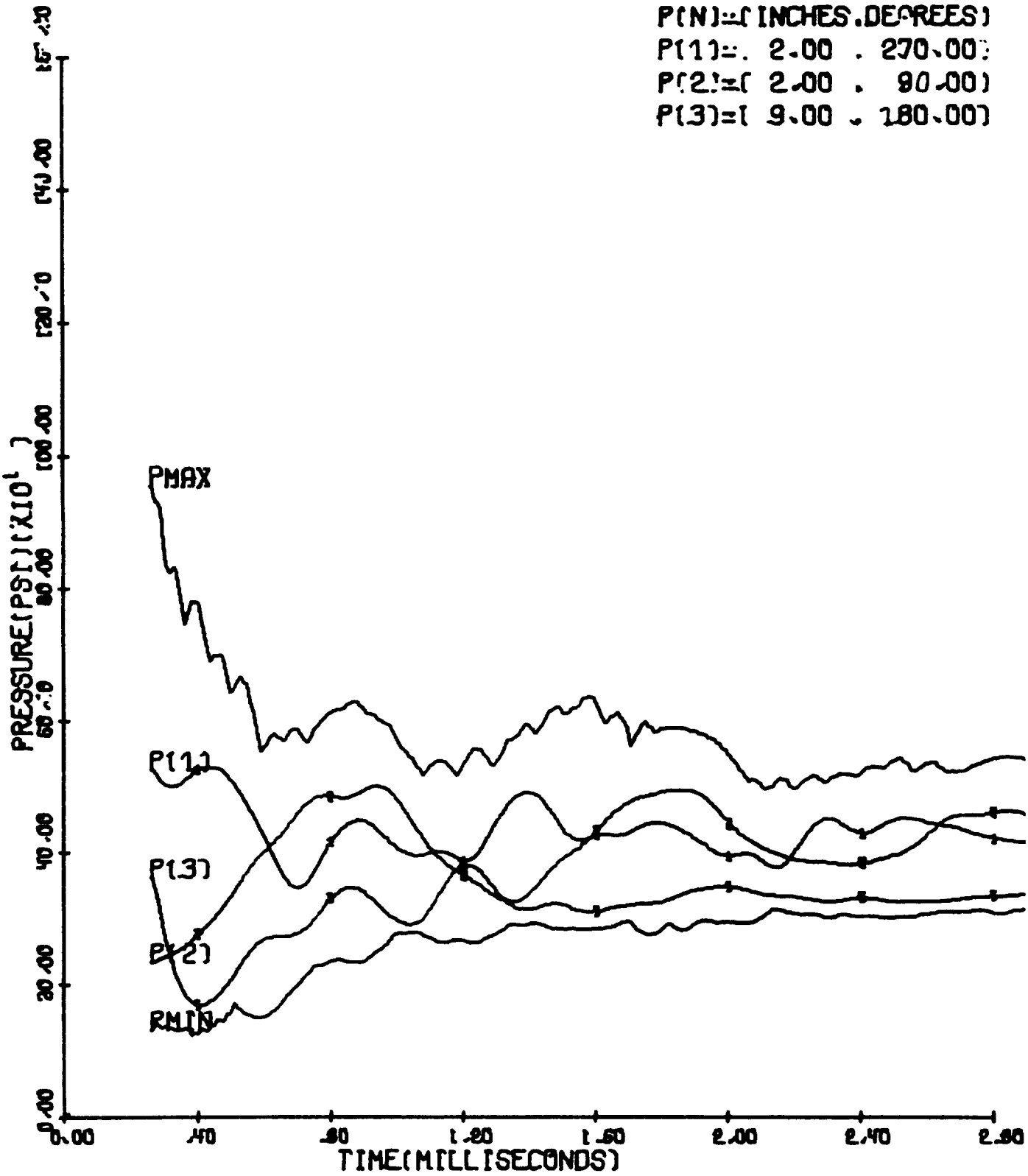

Figure 8

2-BAFFLE ENGINE, L=11.55", λ=0.90

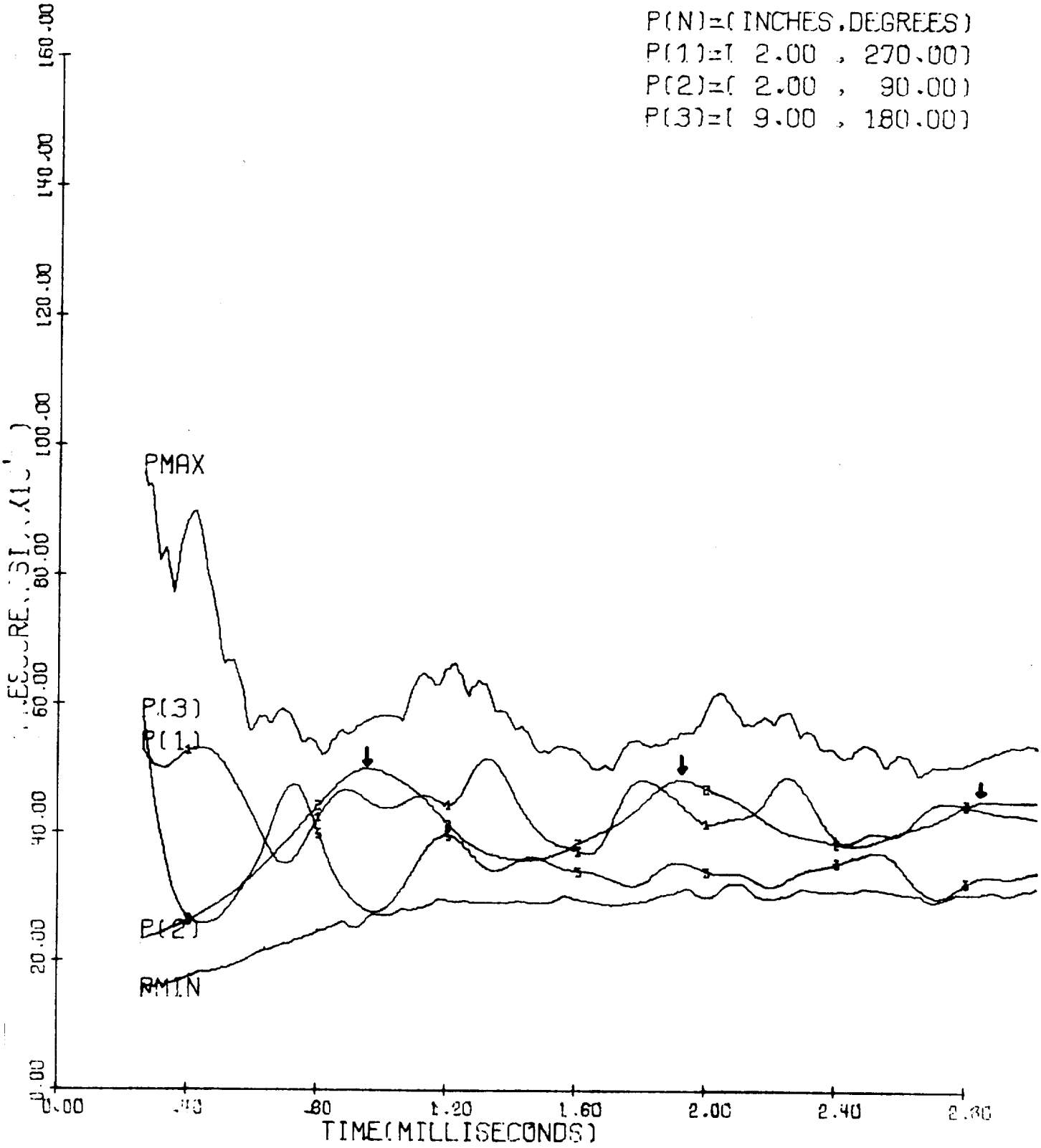

Figure

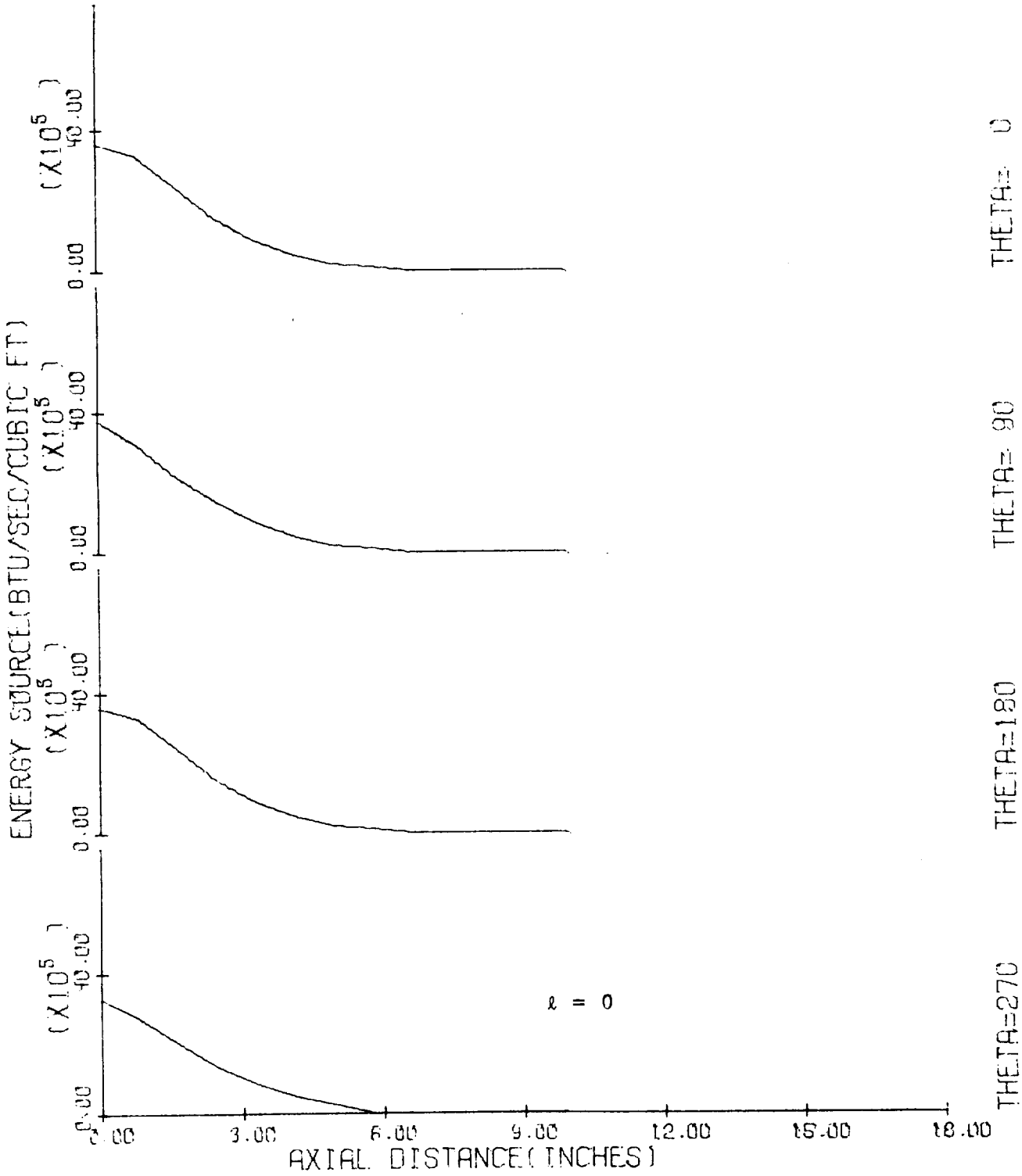

T= 3.057 MILLISECONDS

Figure 10 ---

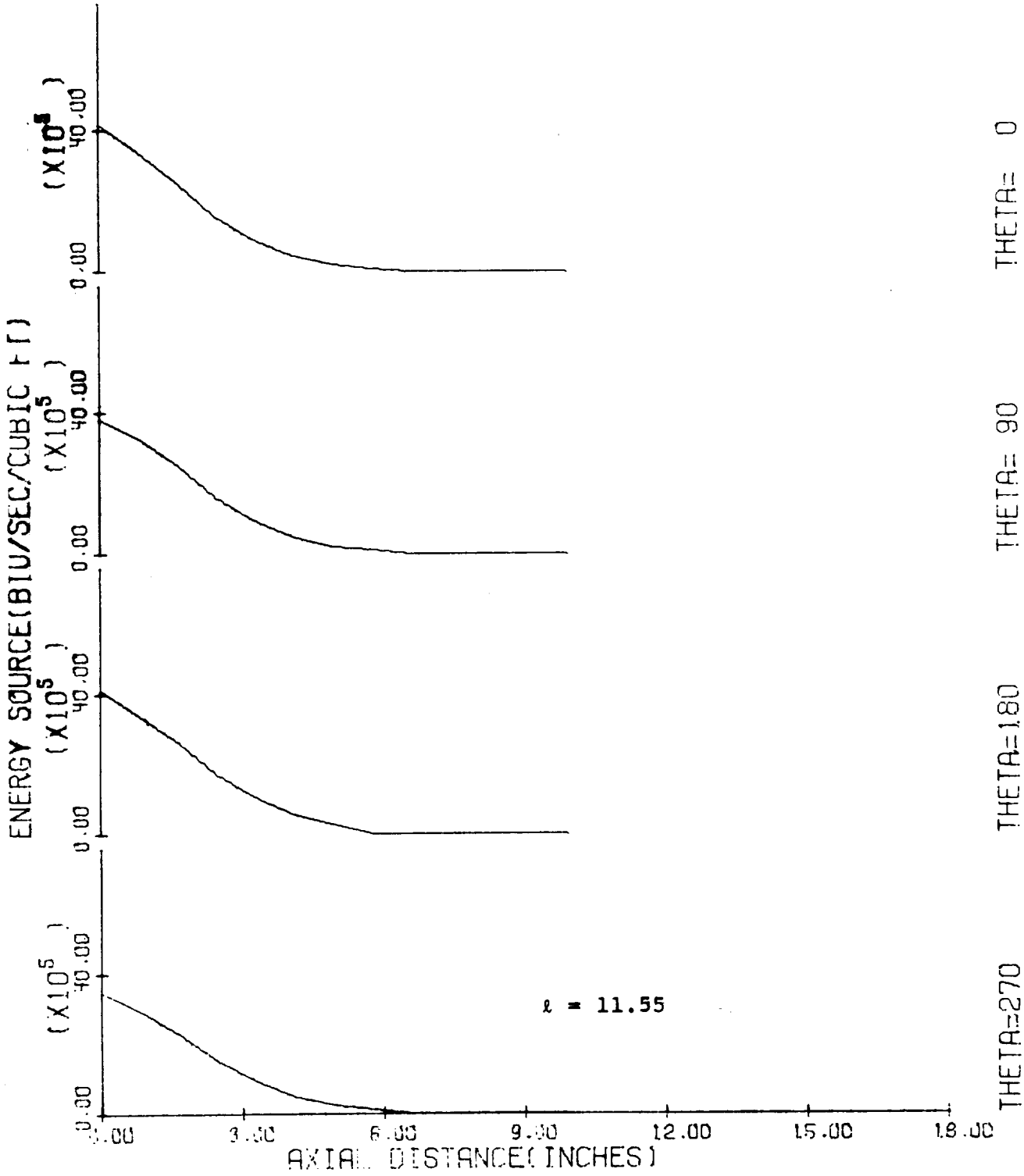

T= 3.024 MILLISECONDS

Figure 11

2-BAFFLE ENGINE, ℓ=11.55", λ=0.0108

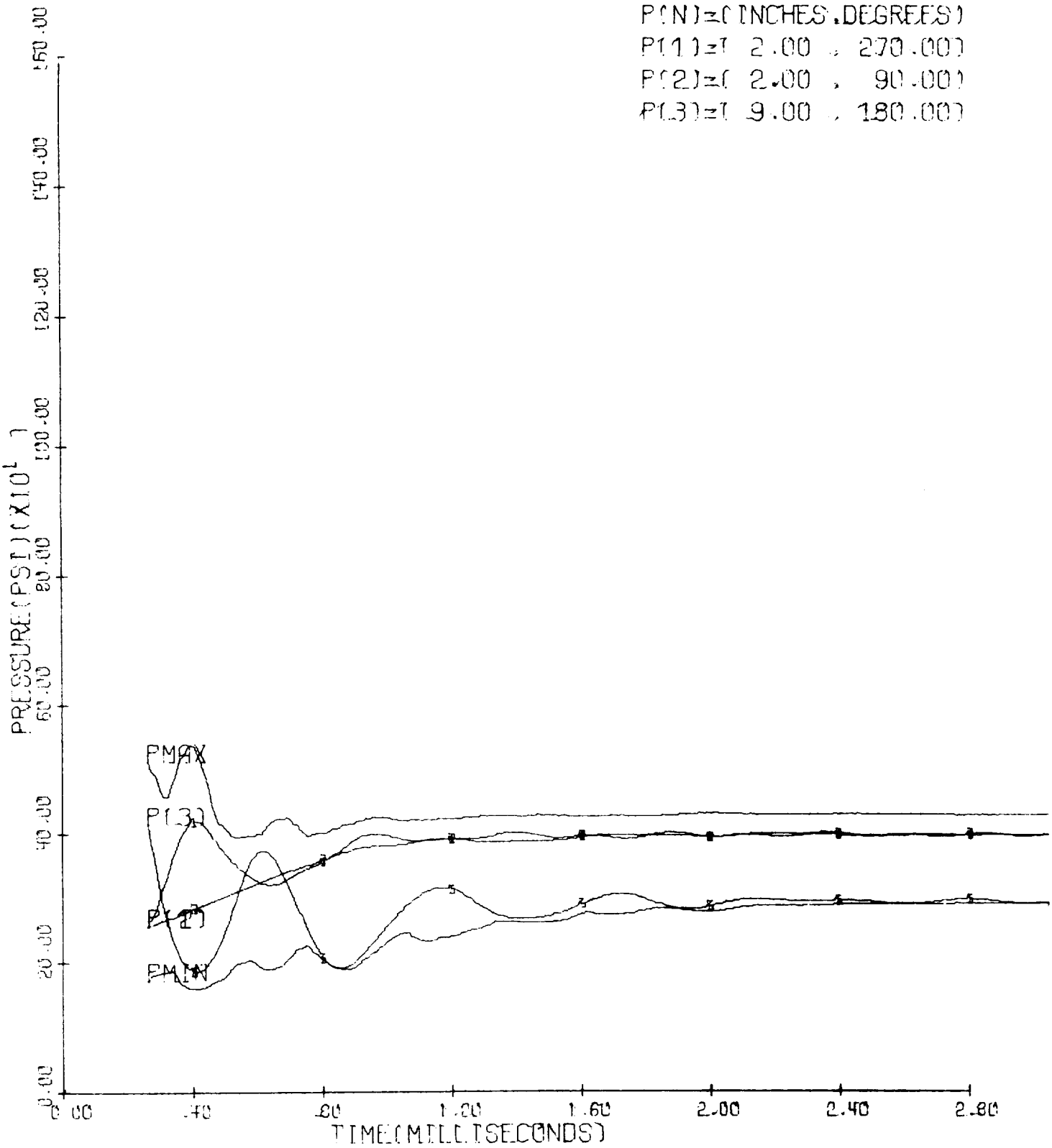

Figure-12

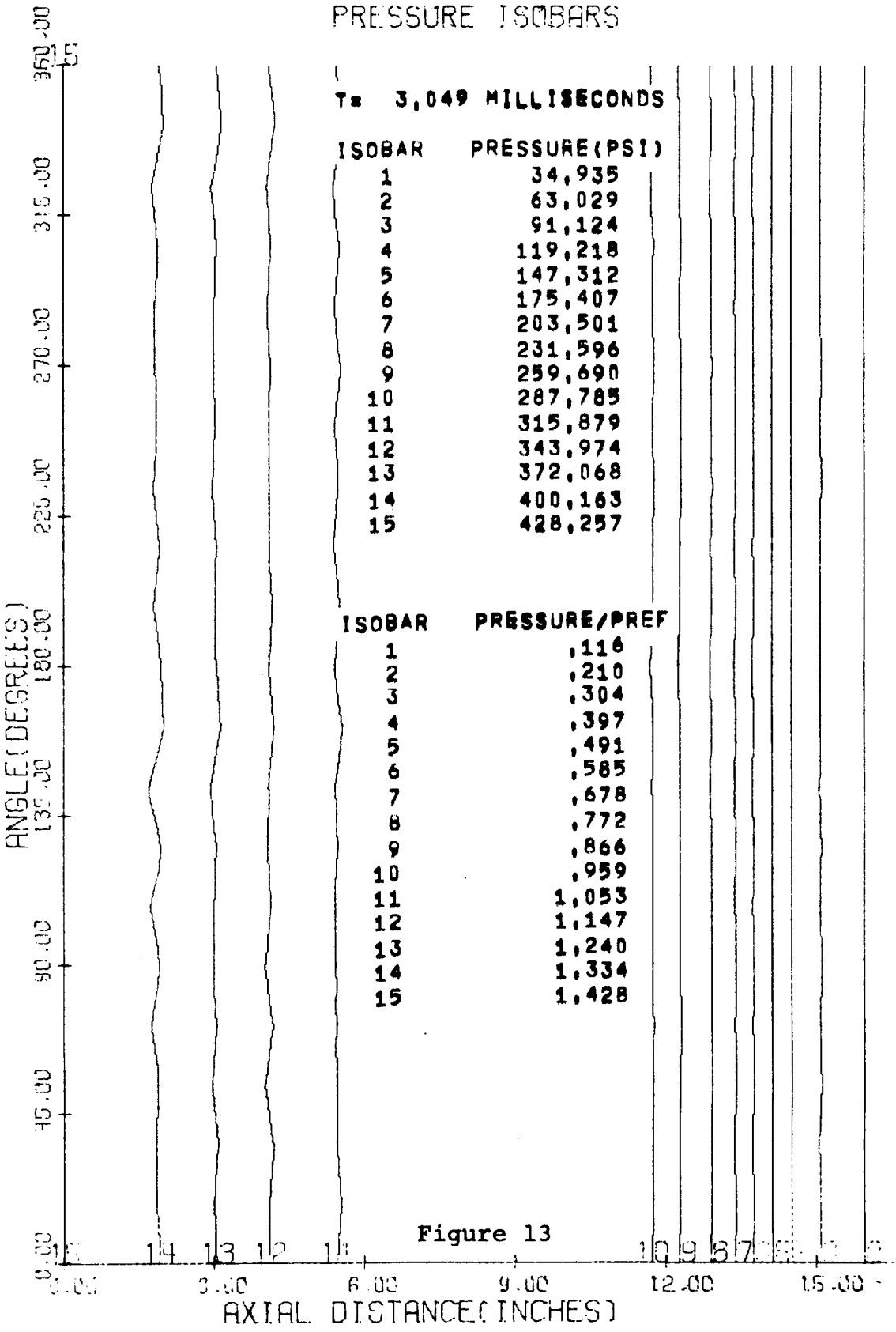

Figure 13

PREF=REFERENCE PRESSURE = 300,00 PSI
AREF=REFERENCE SOUND SPEED= 3220,7 FT/SEC
R =CHAMBER RADIUS = ,45830 FEET
TREF=REFERENCE TIME=R/AREF=,0001423 SEC

T/TREF= 21,42993

2-BAFFLE ENGINE, ℓ=11.55", λ=0.0108

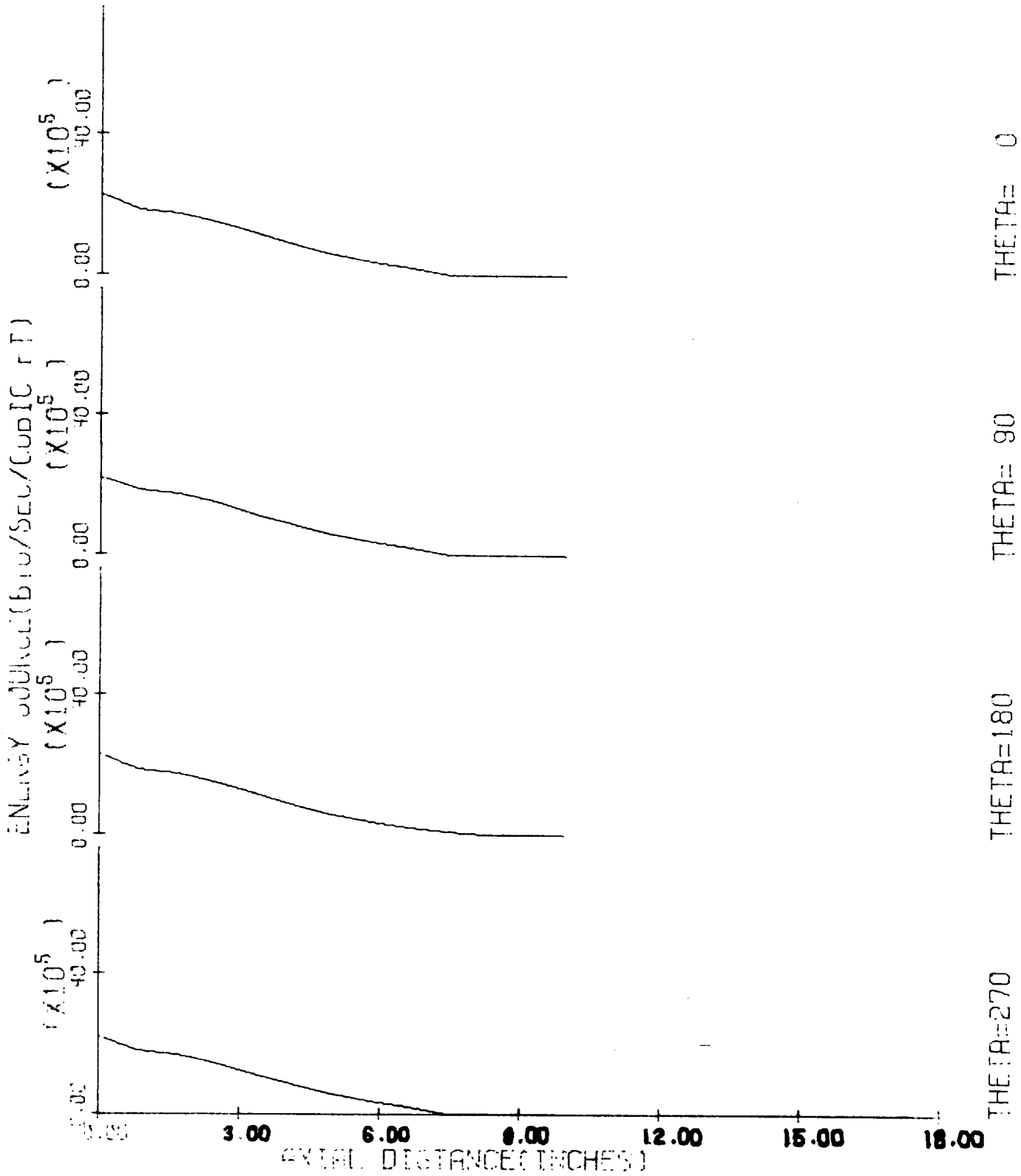

T= 3.049 MILLISECONDS

Figure 14

2-BAFFLE ENGINE, ℓ=6", λ=0.9, r_e=100

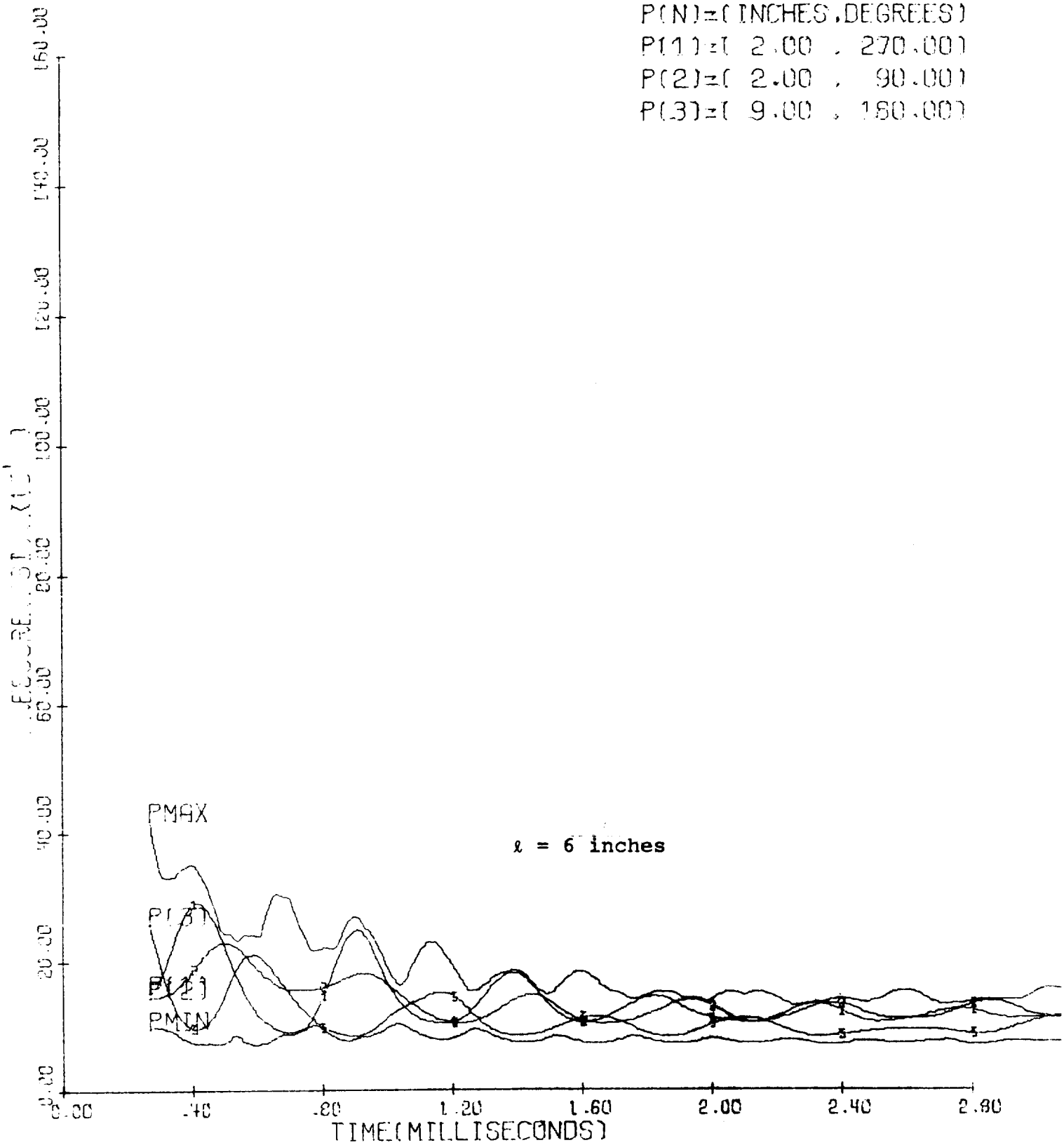

Figure 15

2-BAFFLE ENGINE, ℓ=6", λ=0.0108, r_e=100

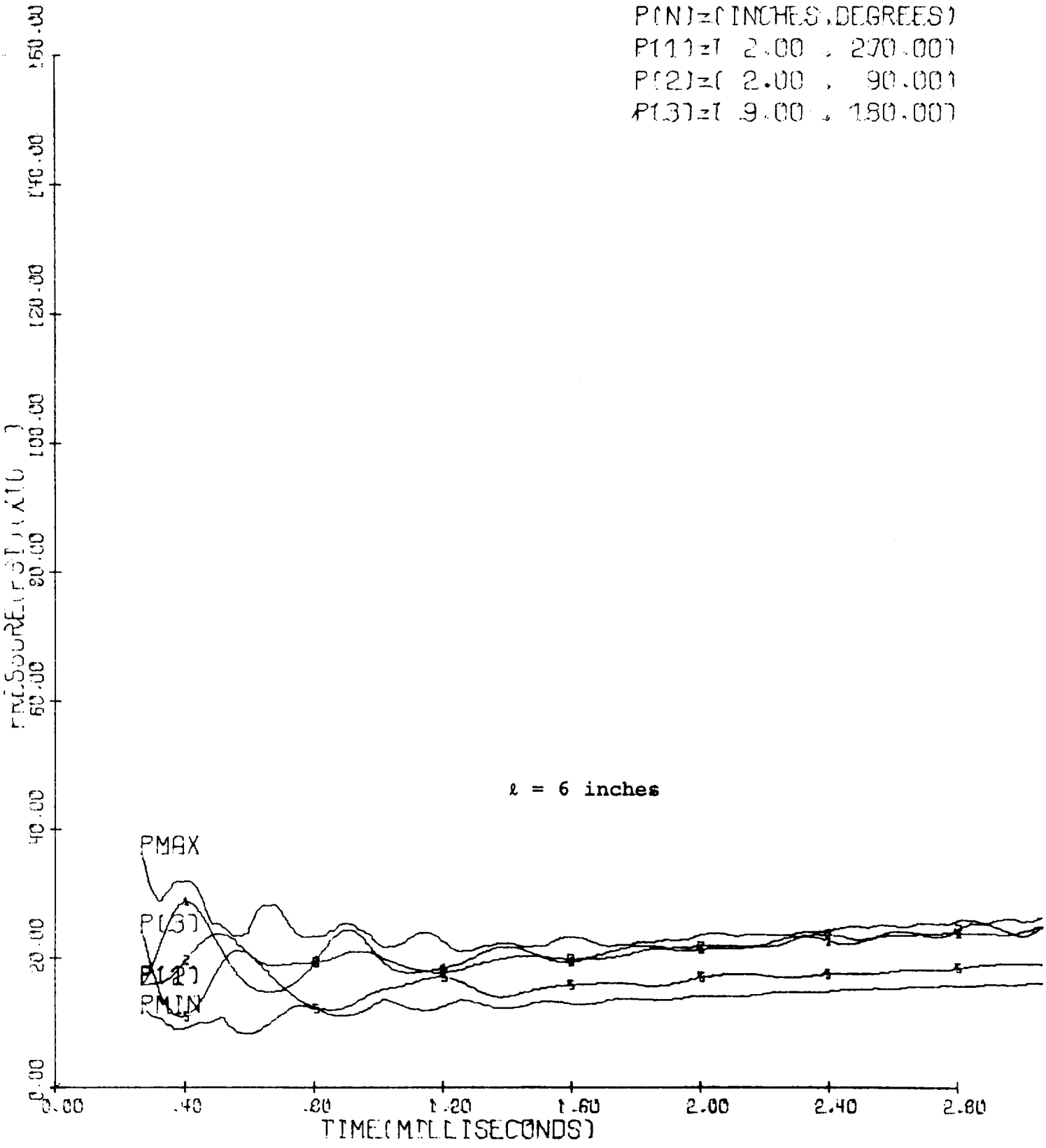

ℓ = 6 inches

Figure 16

ENERGY RELEASE RATE E, CORRESPONDING TO FIGURE 15

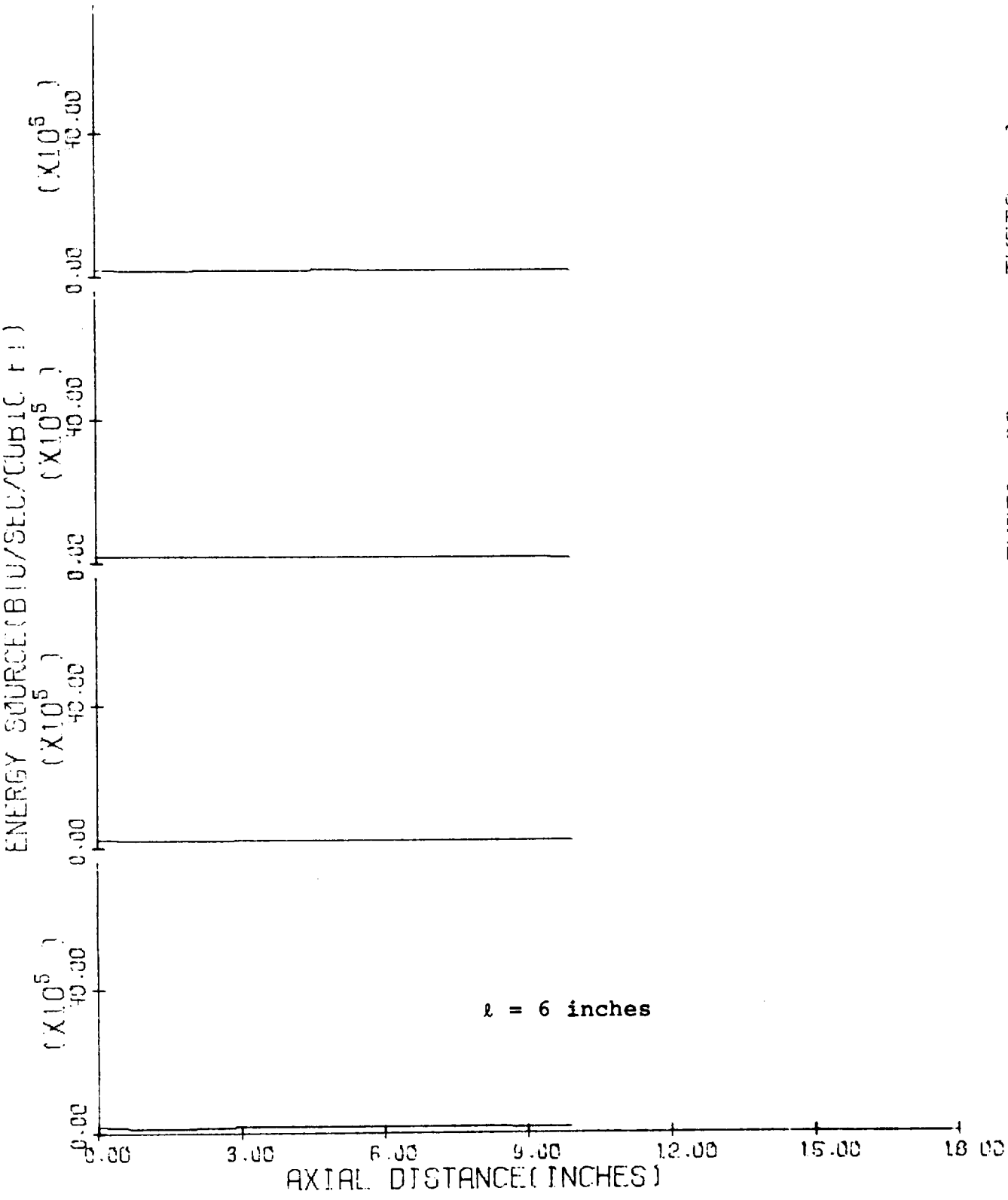

Figure 17

ENERGY RELEASE RATE Ė, CORRESPONDING TO FIGURE 16

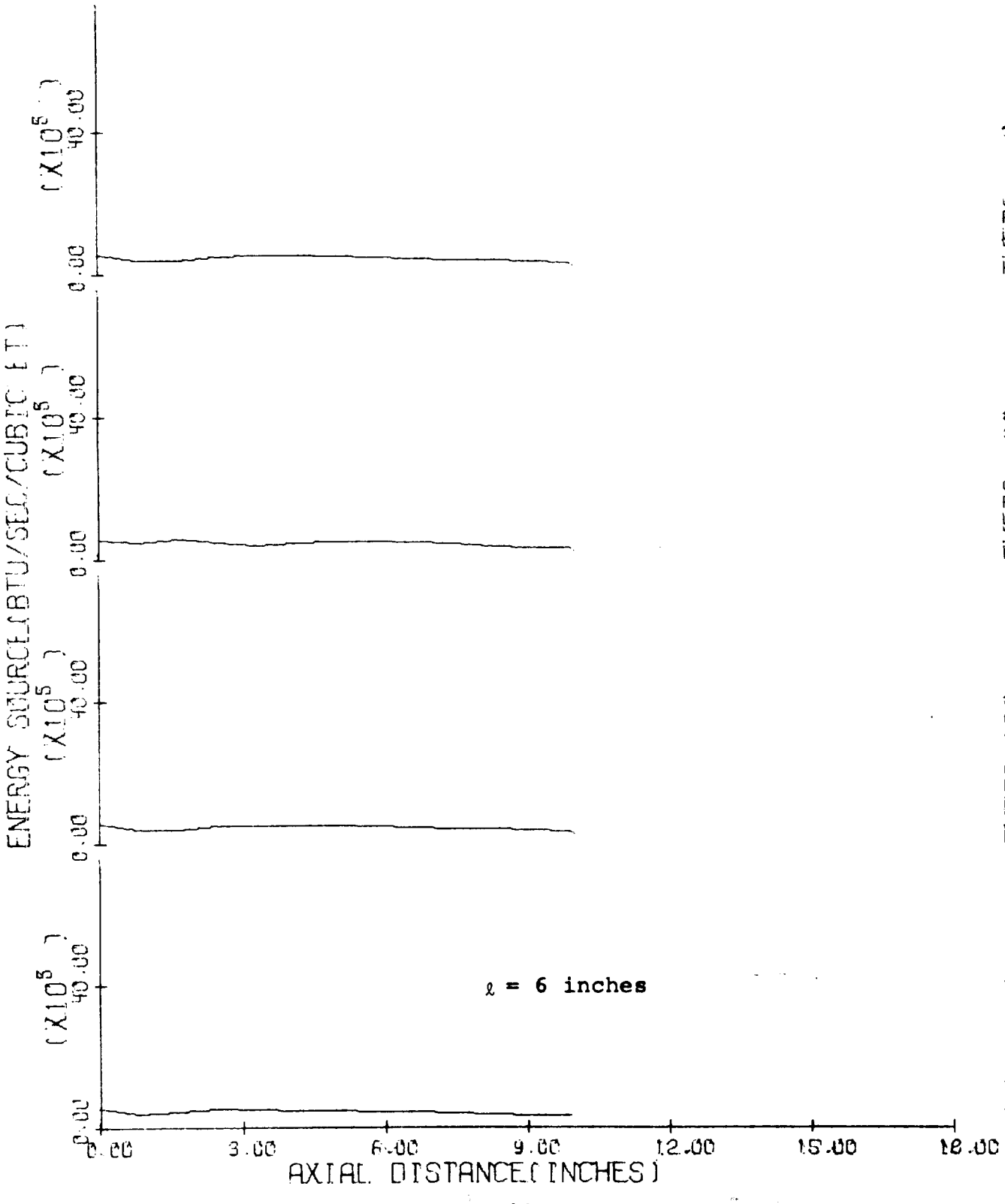

Figure 18

4-BAFFLE ENGINE, p_c=300 psia, λ=0.9 ℓ=6"

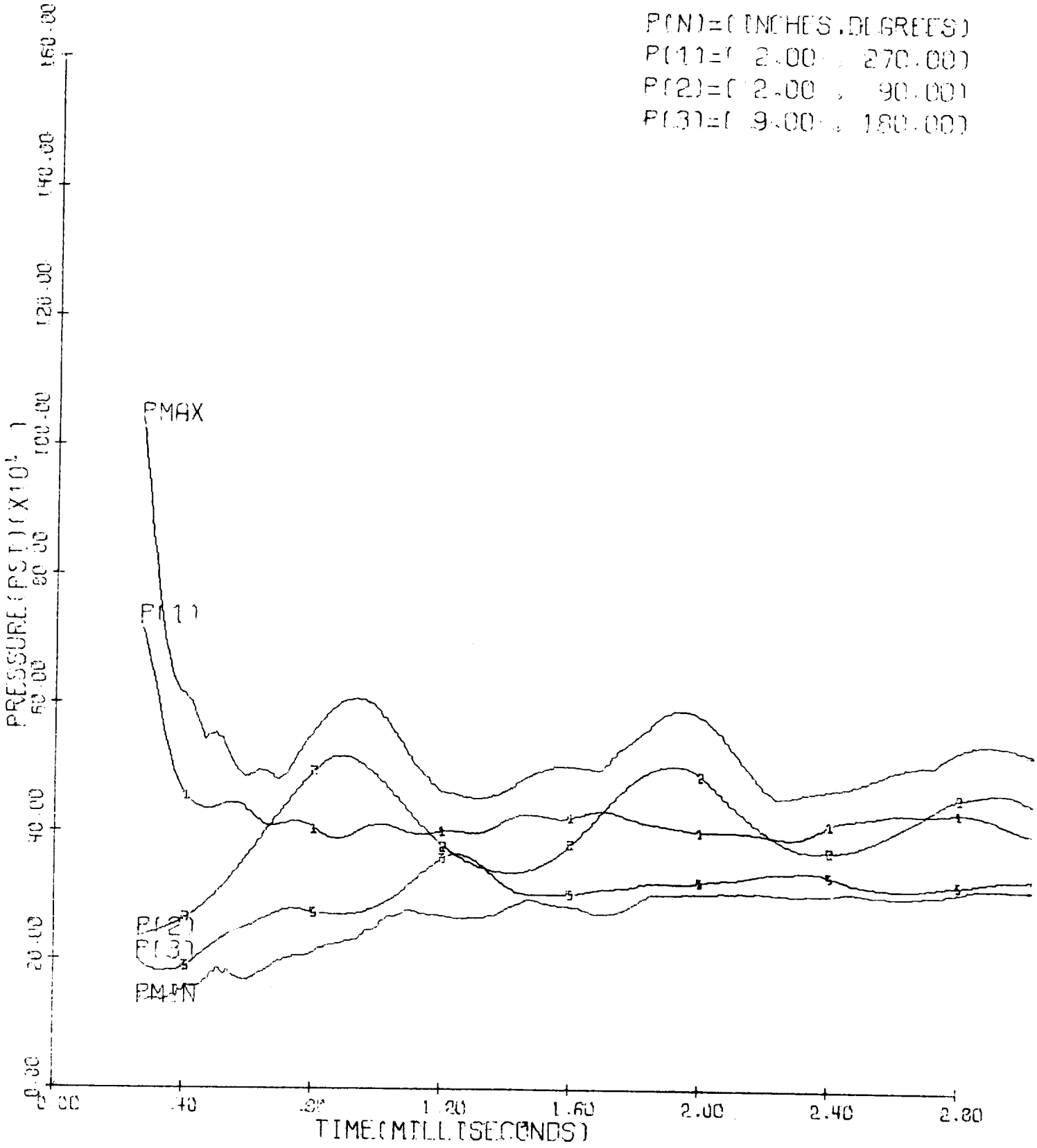

Figure 19

PRELIMINARY EXPERIMENT, CLAYTON MOTOR, NO SHUTTER OR BAFFLE

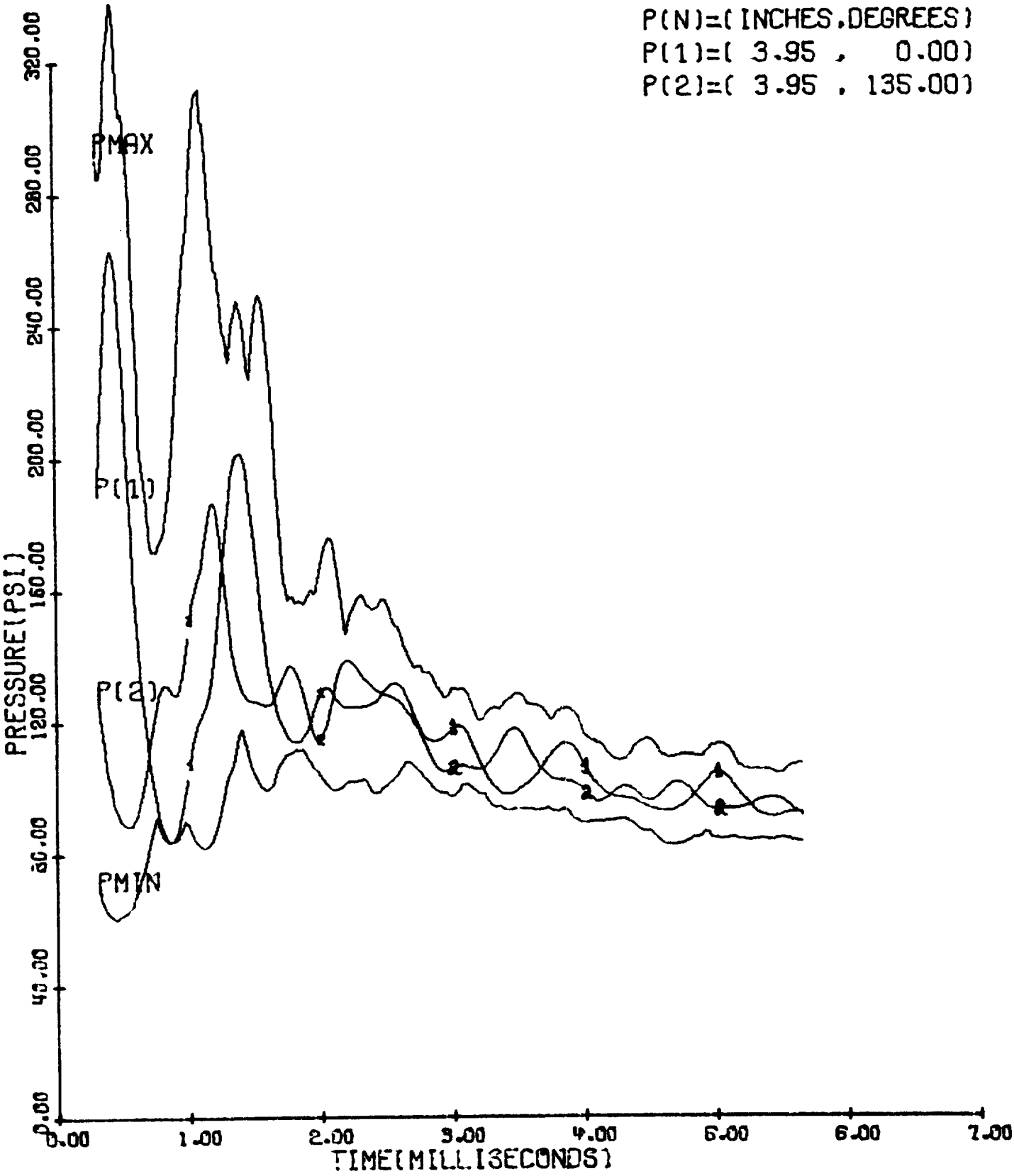

Figure 20

PRELIMINARY EXPERIMENT, CLAYTON MOTOR, NO SHUTTER OR BAFFLE

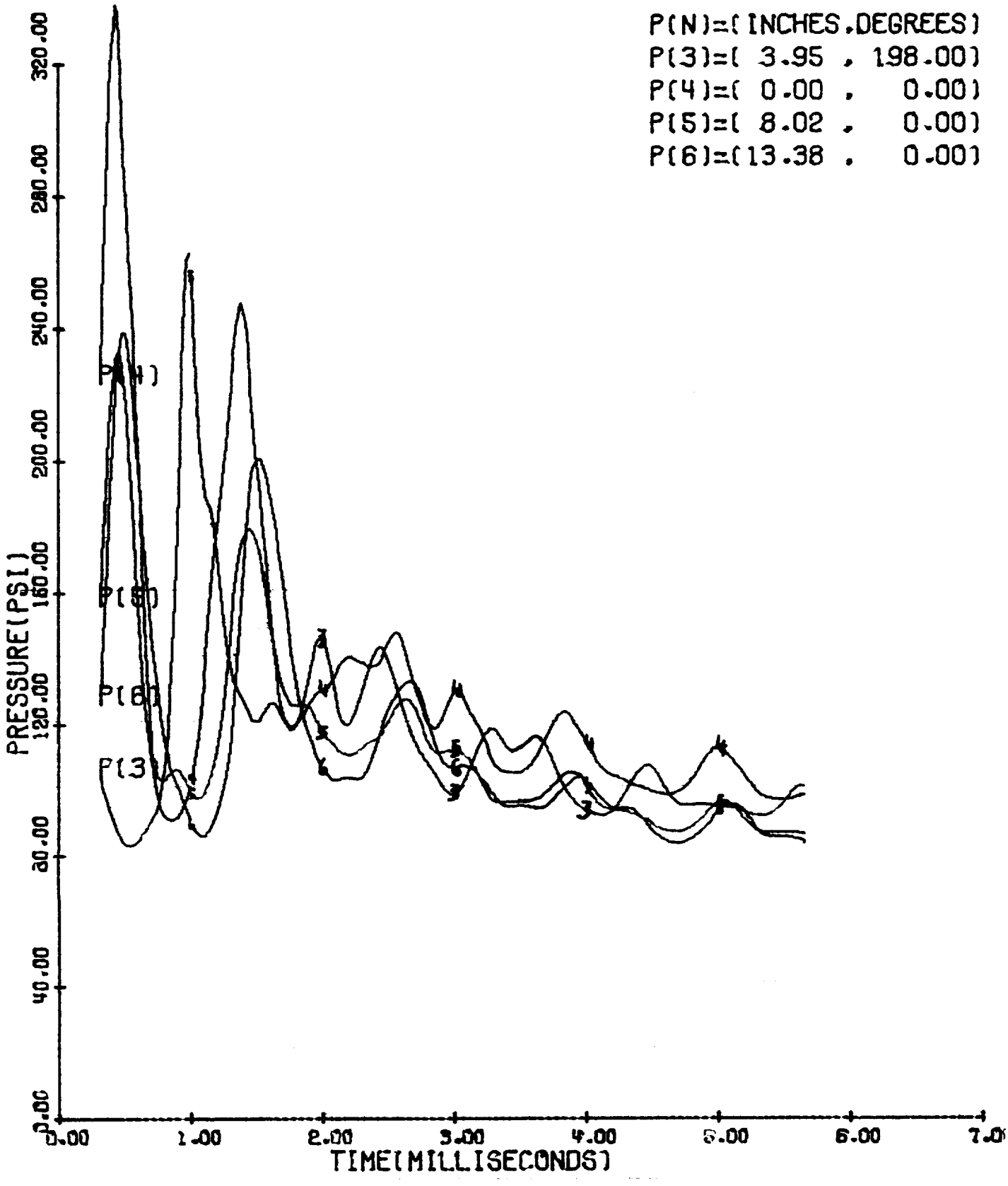

Figure 21

PRELIMINARY EXPERIMENT, CLAYTON MOTOR,
SHUTTERED BUT NOT BAFFLED

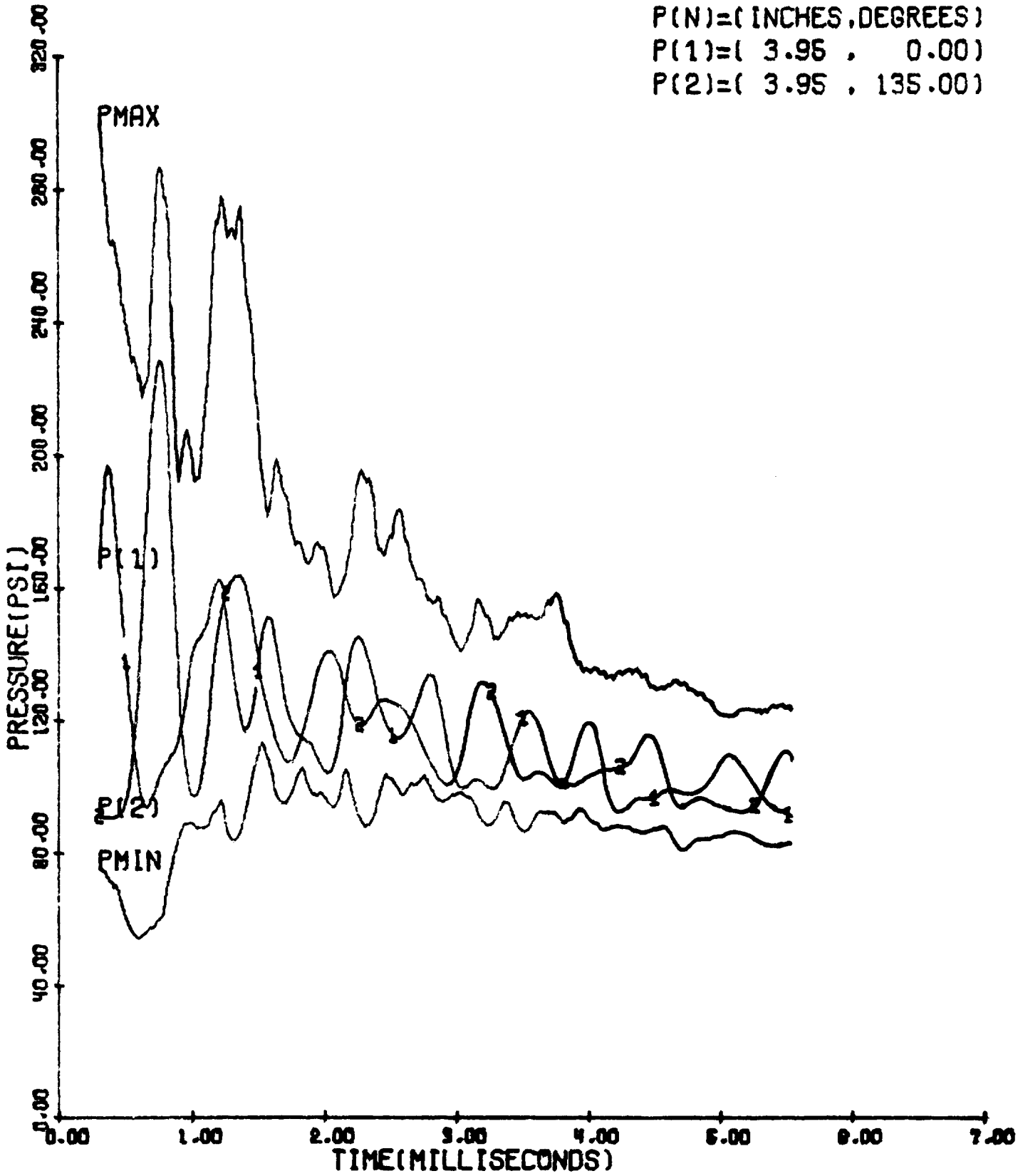

Figure 22

PRELIMINARY EXPERIMENT, CLAYTON MOTOR,
SHUTTERED BUT NOT BAFFLED.

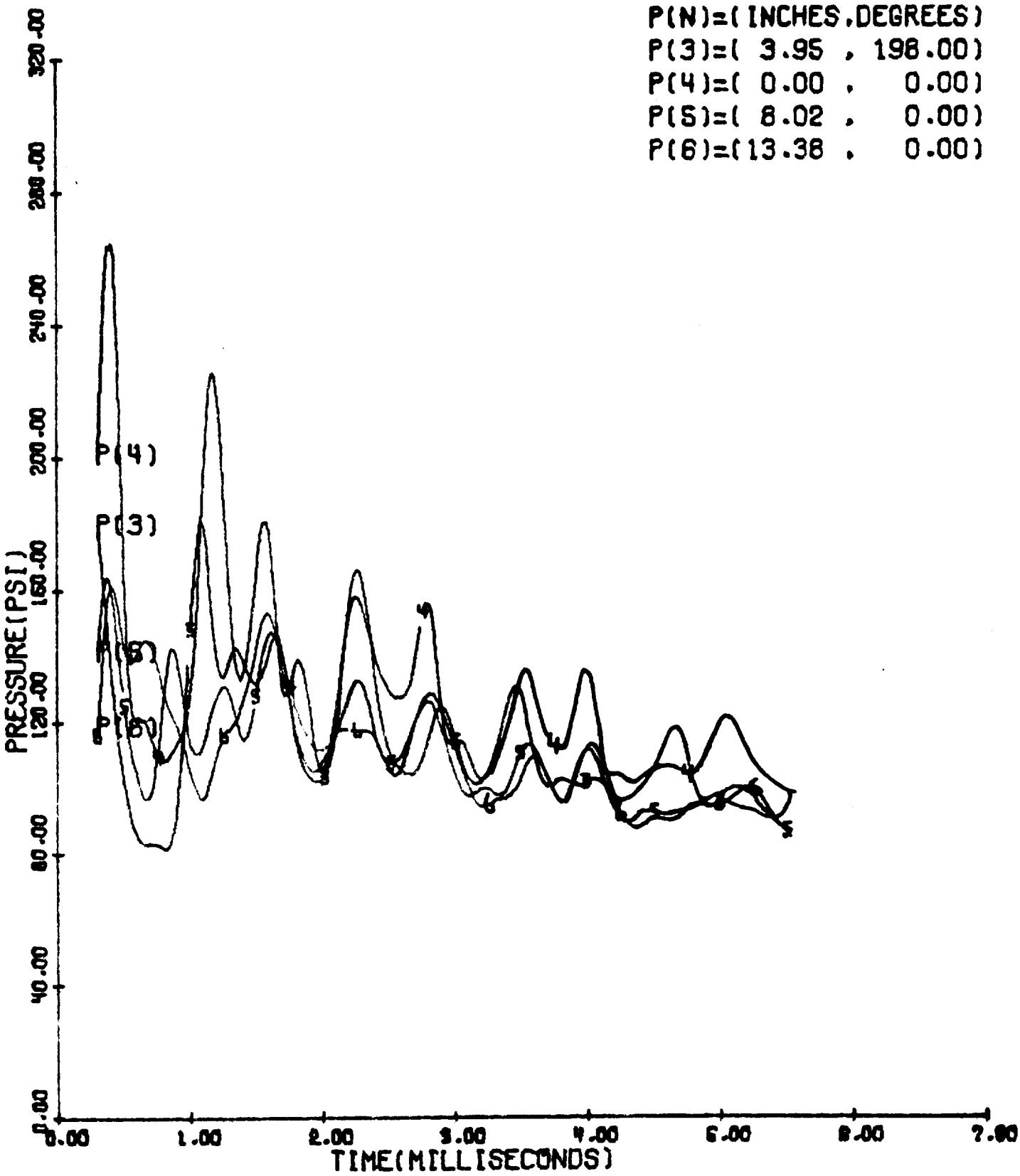

Figure 23

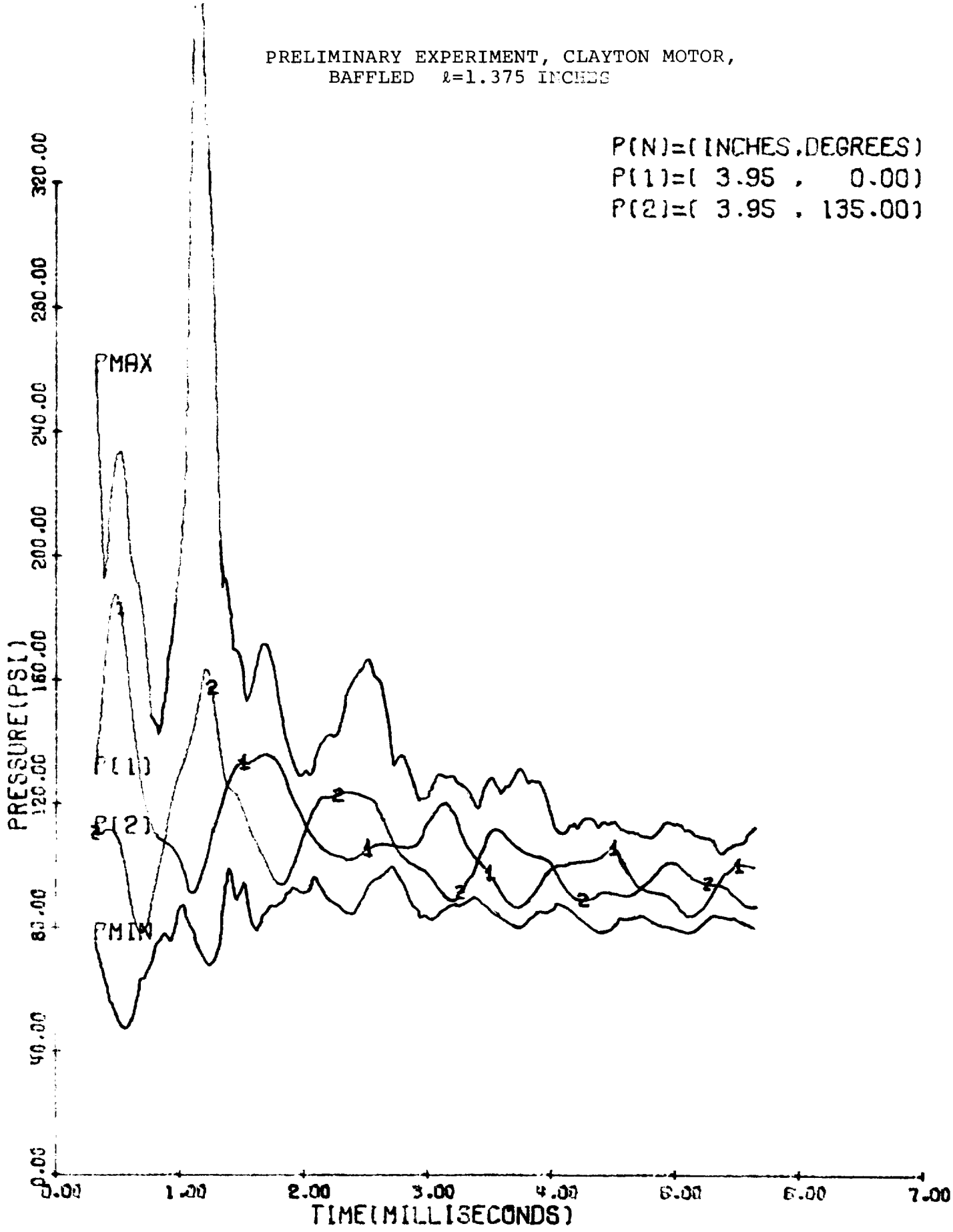
PRELIMINARY EXPERIMENT, CLAYTON MOTOR,
BAFFLED ℓ=1.375 INCHES
P(N)=(INCHES,DEGREES)
P(1)=(3.95 , 0.00)
P(2)=(3.95 , 135.00)
PMAX
P(1)
P(2)
PMIN
PRESSURE(PSI)
320.00
280.00
240.00
200.00
160.00
120.00
80.00
40.00
0.00
1.00
2.00
3.00
4.00
5.00
6.00
7.00
TIME(MILLISECONDS)

Figure 24

PRELIMINARY EXPERIMENT, CLAYTON MOTOR,
BAFFLED ℓ=1.375 INCHES

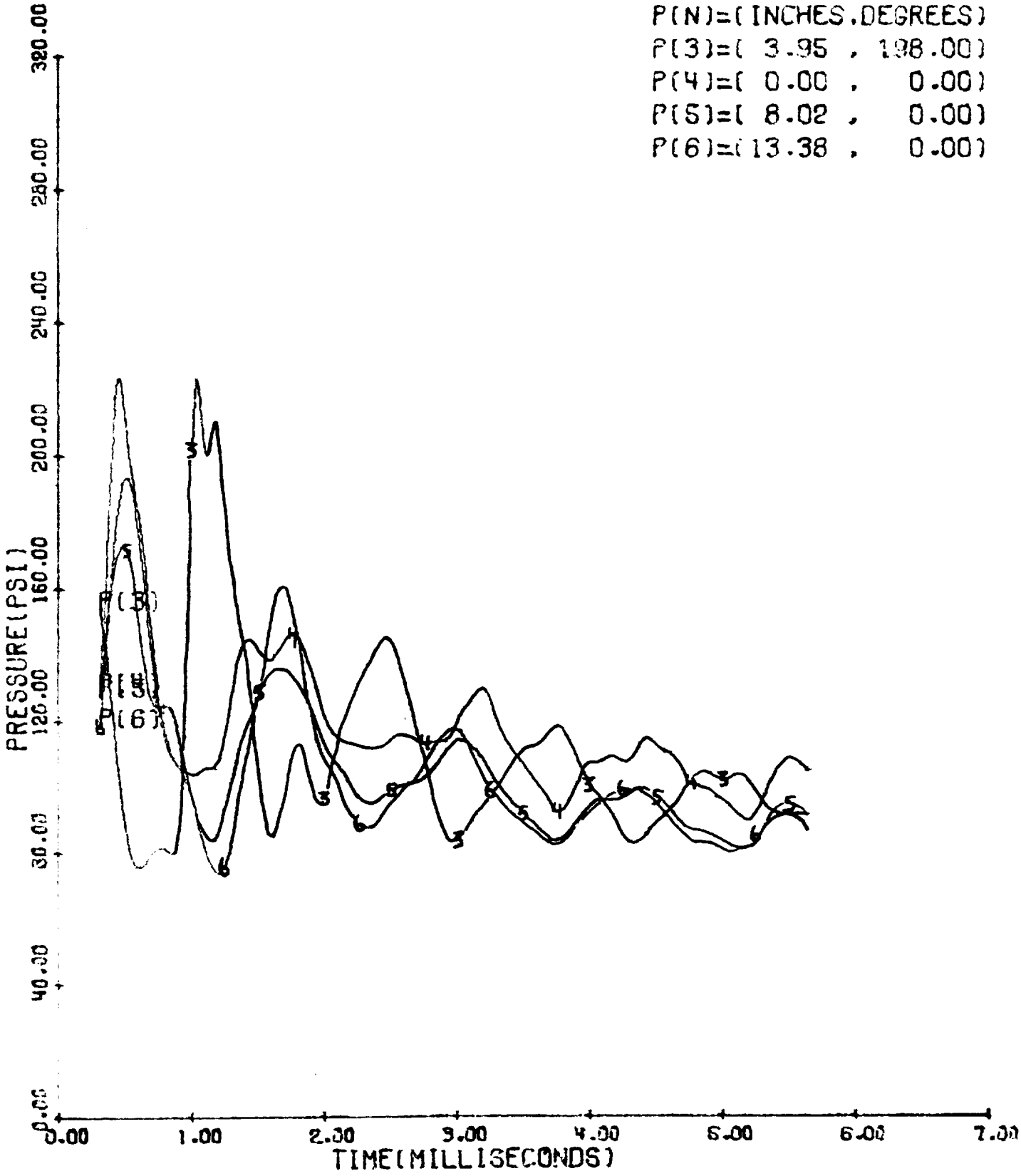

Figure 25

PRELIMINARY EXPERIMENT, CLAYTON MOTOR,
BAFFLED ℓ=2.875 INCHES

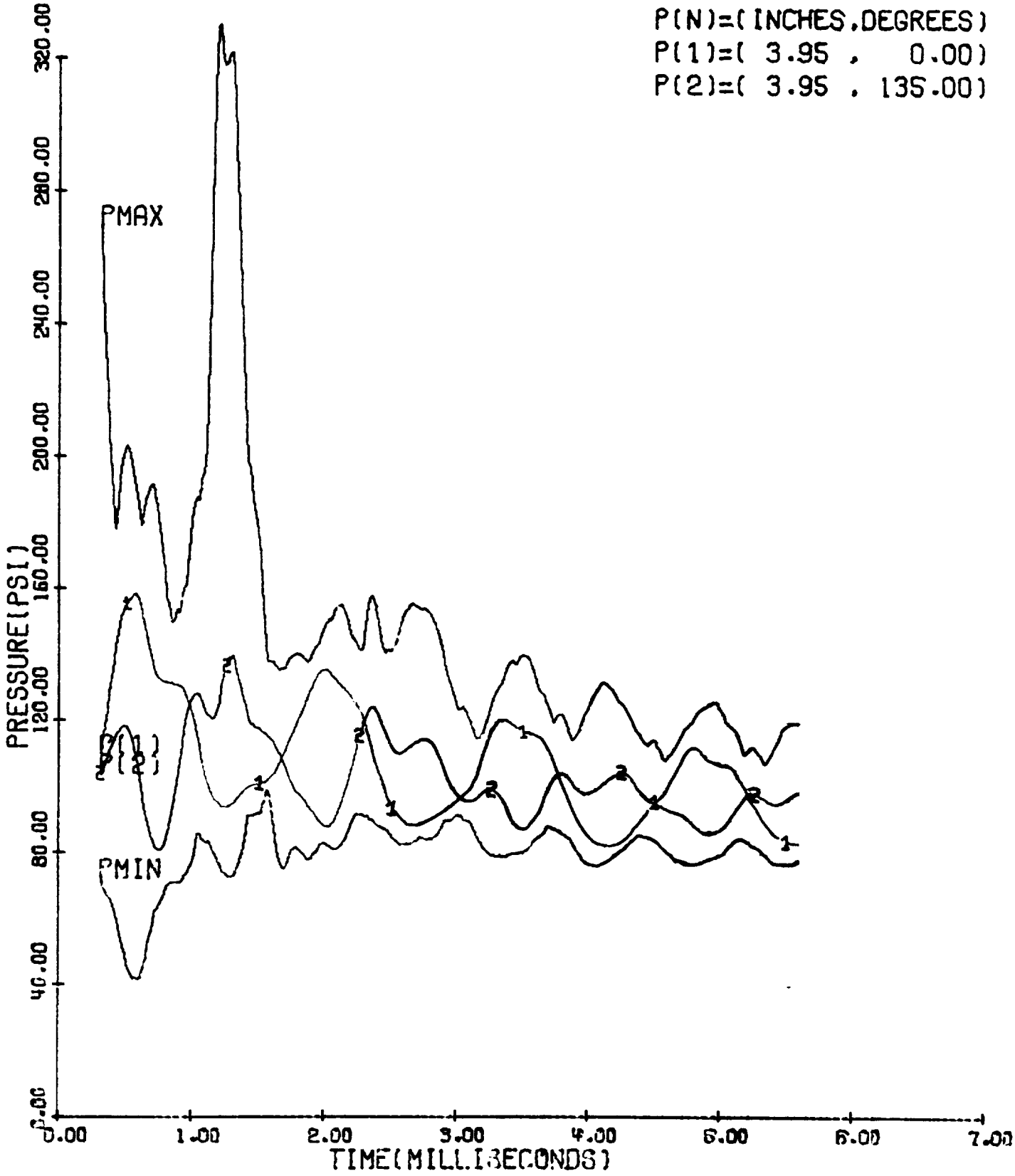

Figure 26

PRELIMINARY EXPERIMENT, CLAYTON MOTOR,
BAFFLED ℓ=2.875 INCHES

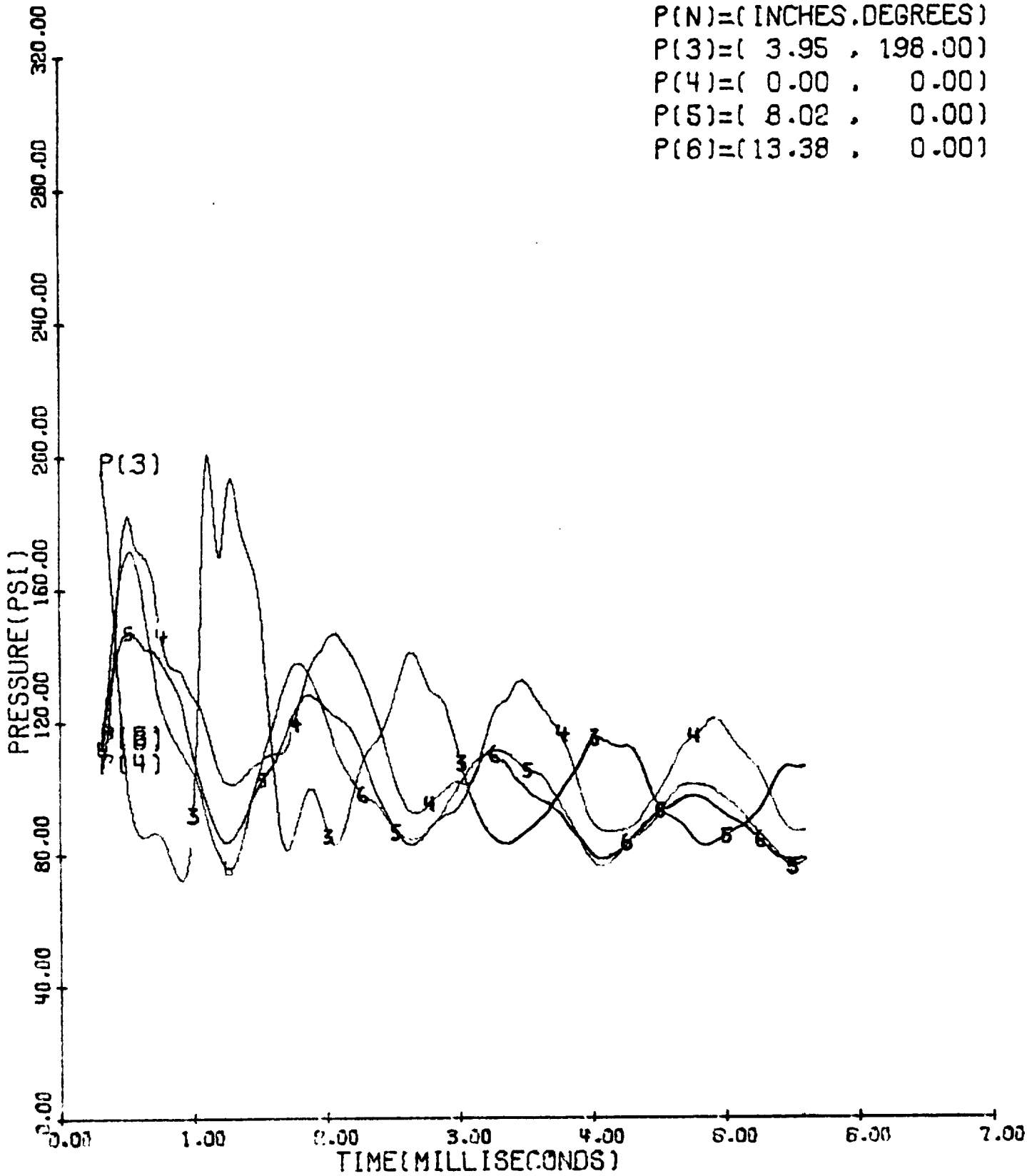

Figure 27

PRELIMINARY EXPERIMENT, CLAYTON MOTOR,

BAFFLED ℓ=5.375 INCHES

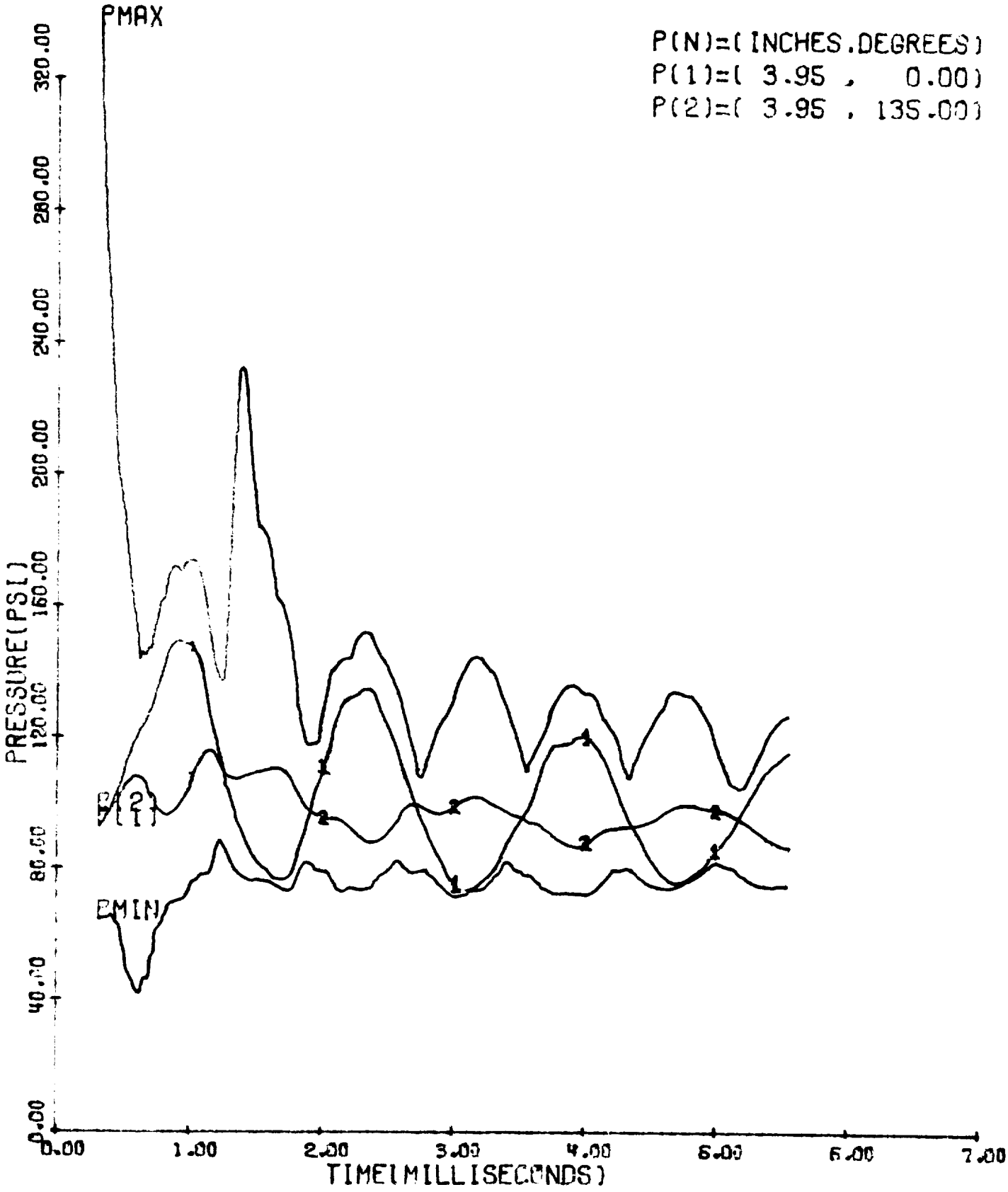

Figure 30

PRELIMINARY EXPERIMENT, CLAYTON MOTOR,

BAFFLED ℓ=5.375 inches

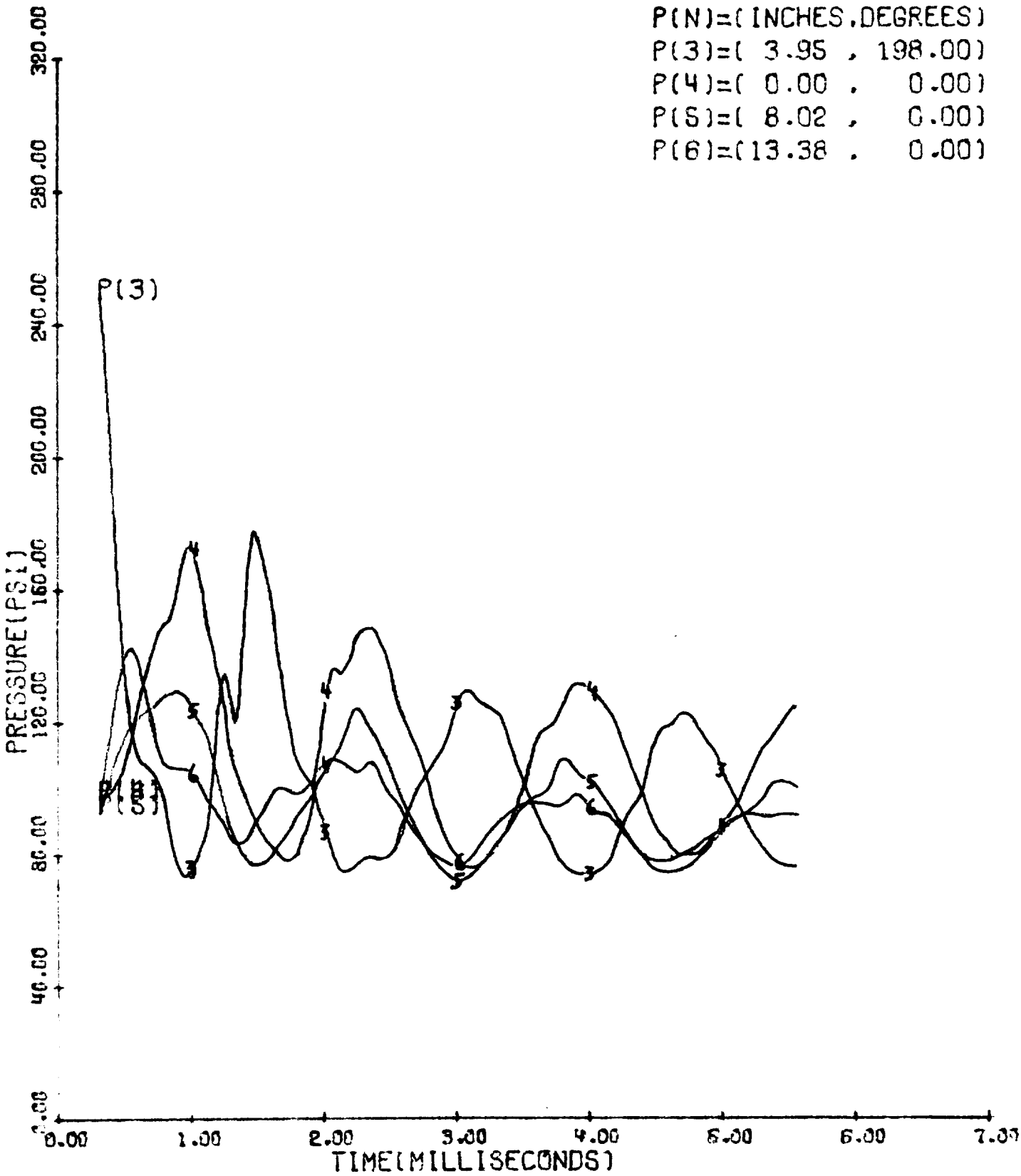

Figure 31

UNBAFFLED, $\dot{m}$=0.35, A_t/A_c=0.5025, λ=0.5

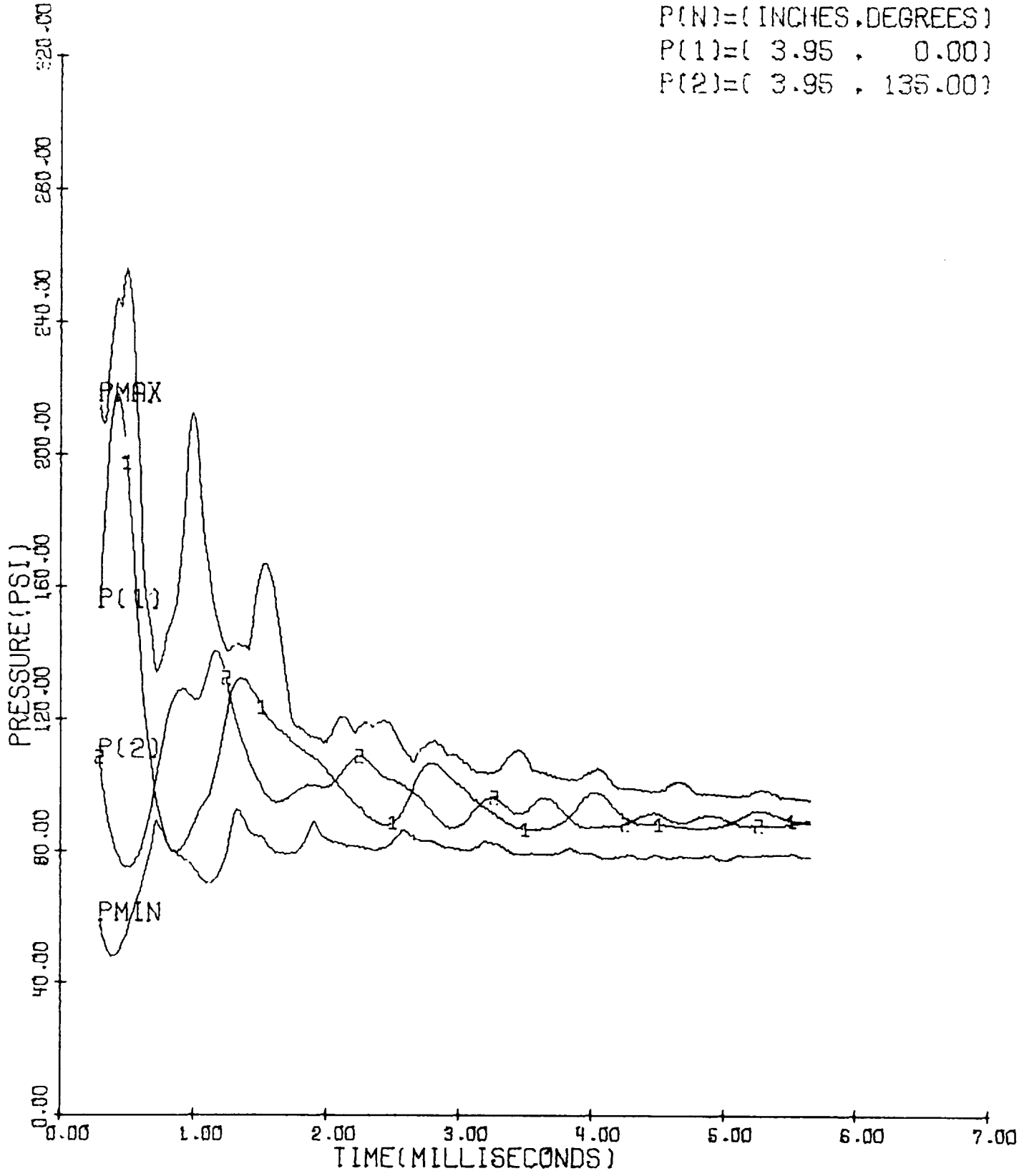

Figure 32

UNBAFFLED $\dot{m}=0.35$, $A_t/A_c=0.5025$, $\lambda=0.5$

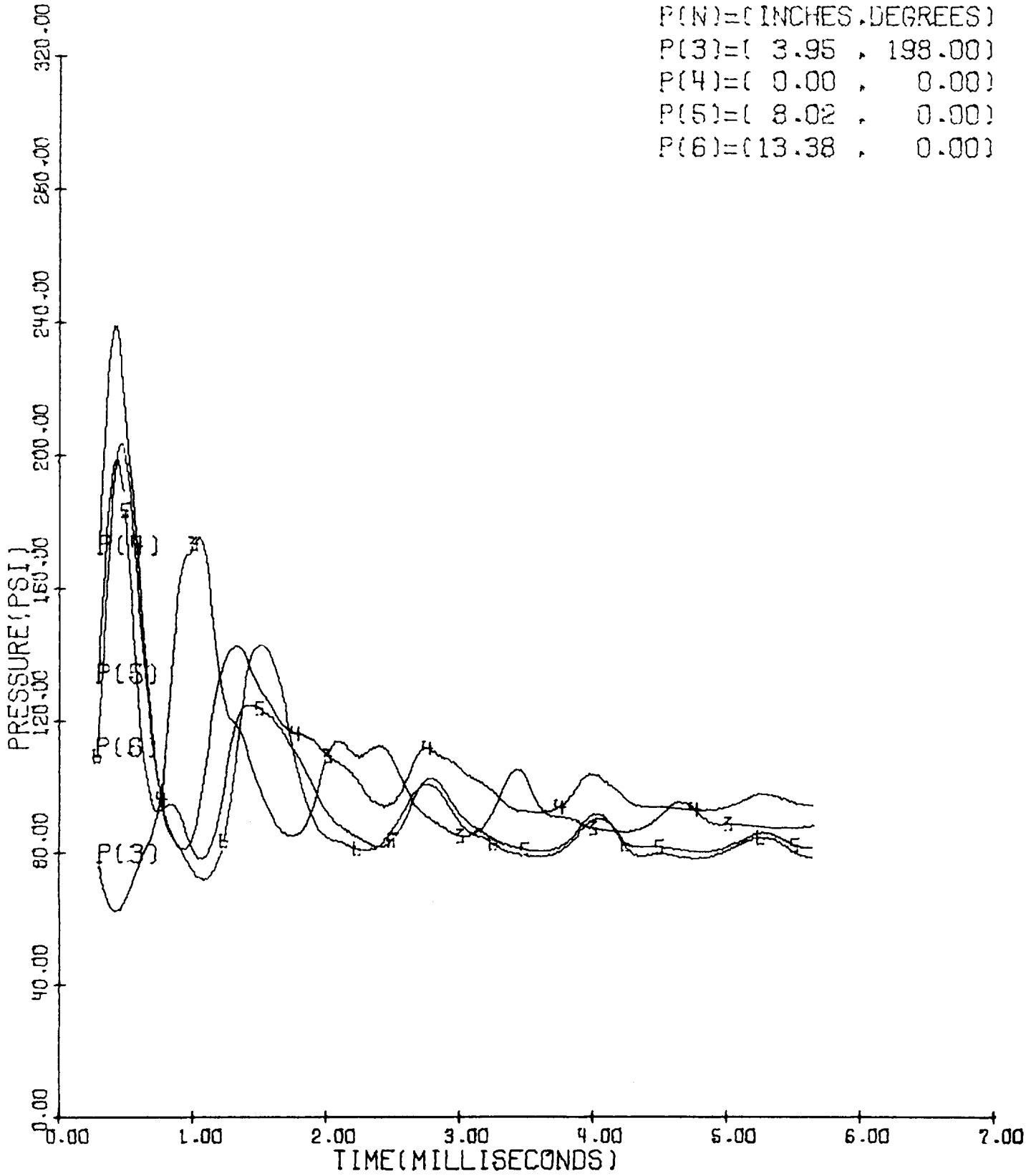

Figure 33

UNBAFFLED $\dot{m}=0.35$, $A_t/A_c=0.3750$, $\lambda=0.5$

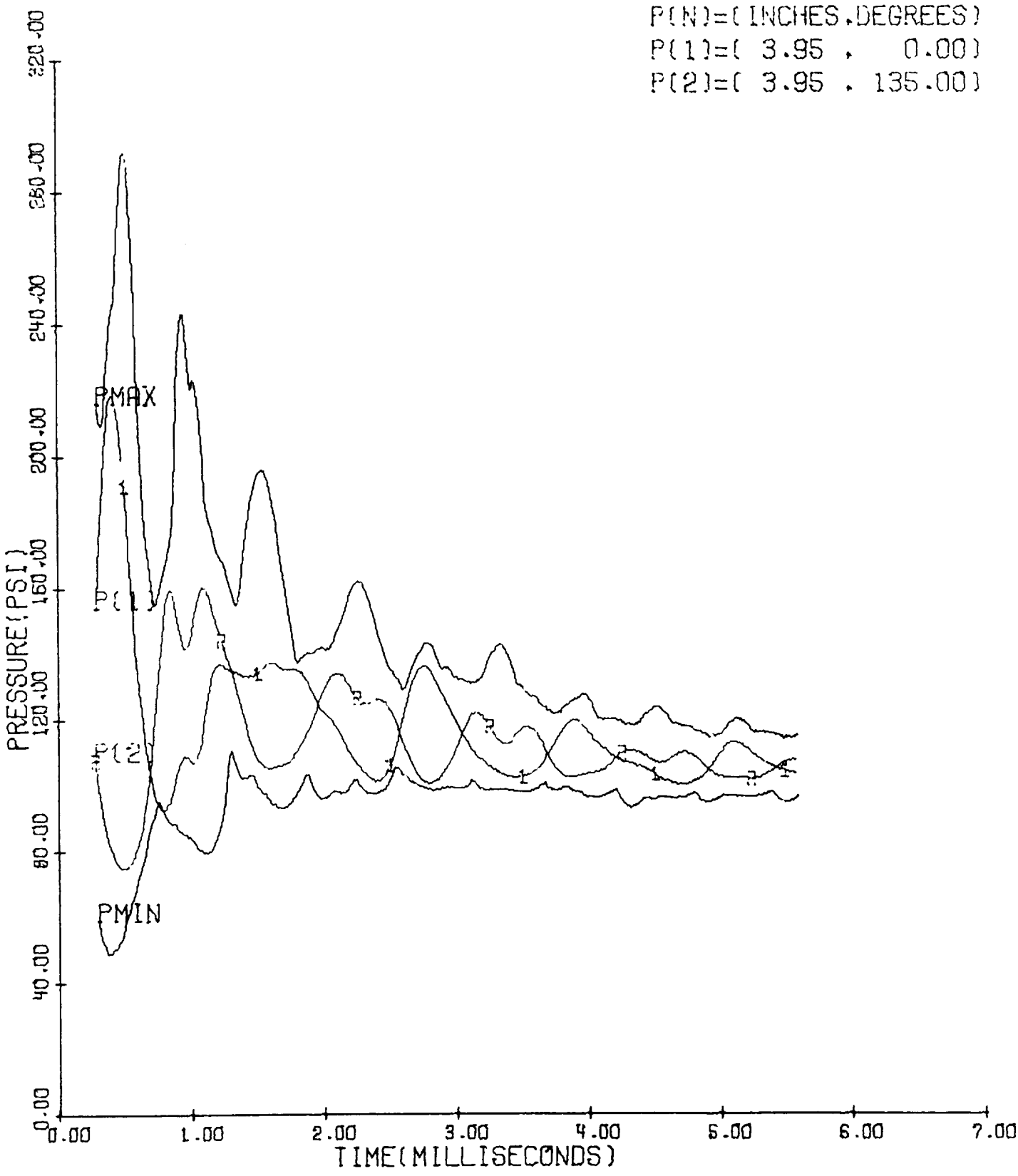

Figure 34

UNBAFFLED $\dot{m}=0.35$, $A_t/A_c=0.3750$, $\lambda=0.5$

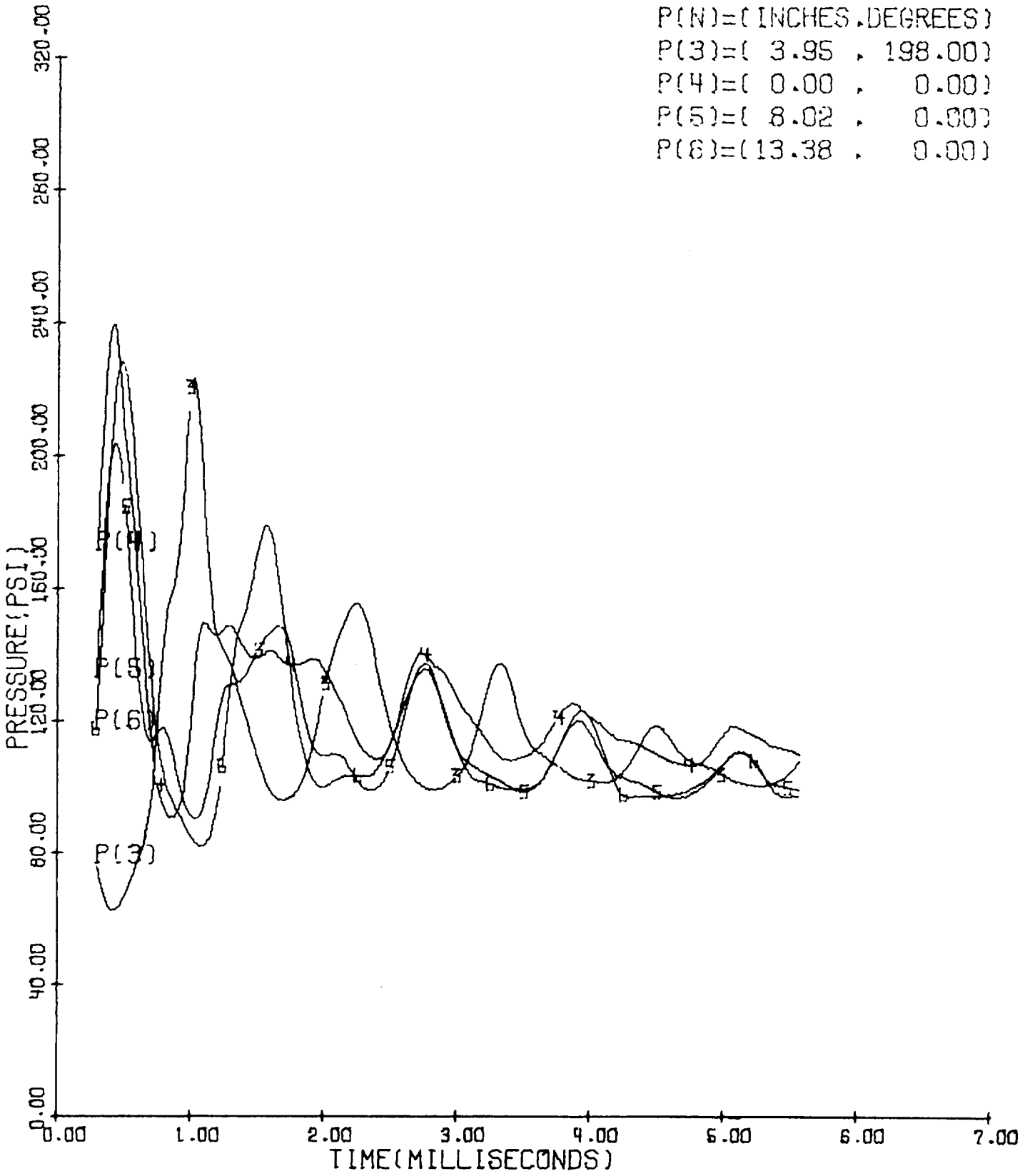

Figure 35

UNBAFFLED $\dot{m}=0.35$, $A_t/A_c=0.6250$, $\chi=0.5$

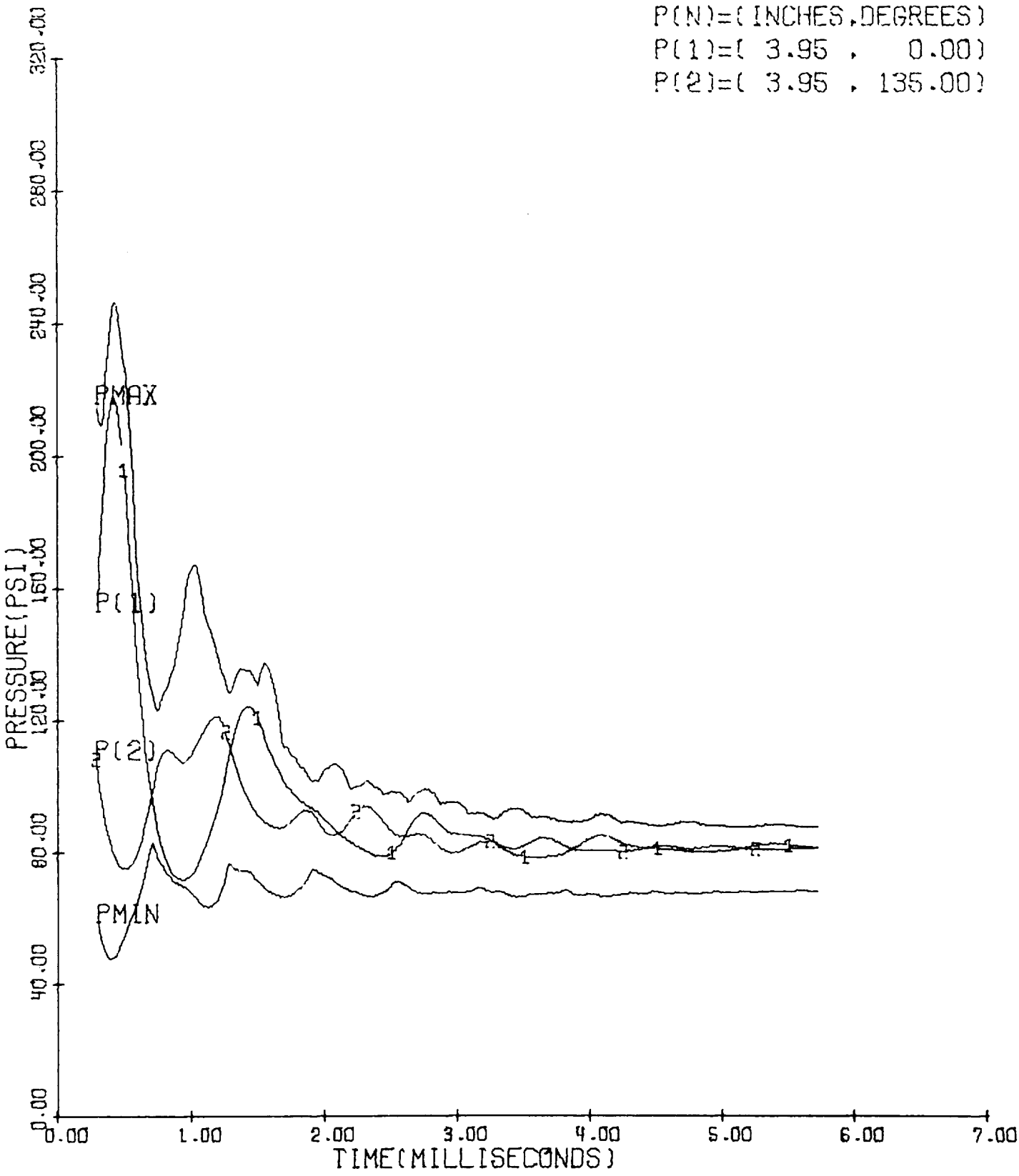

Figure 36

UNBAFFLED $\dot{m}=0.35, A_t/A_c=0.6250, \ell=0.5$

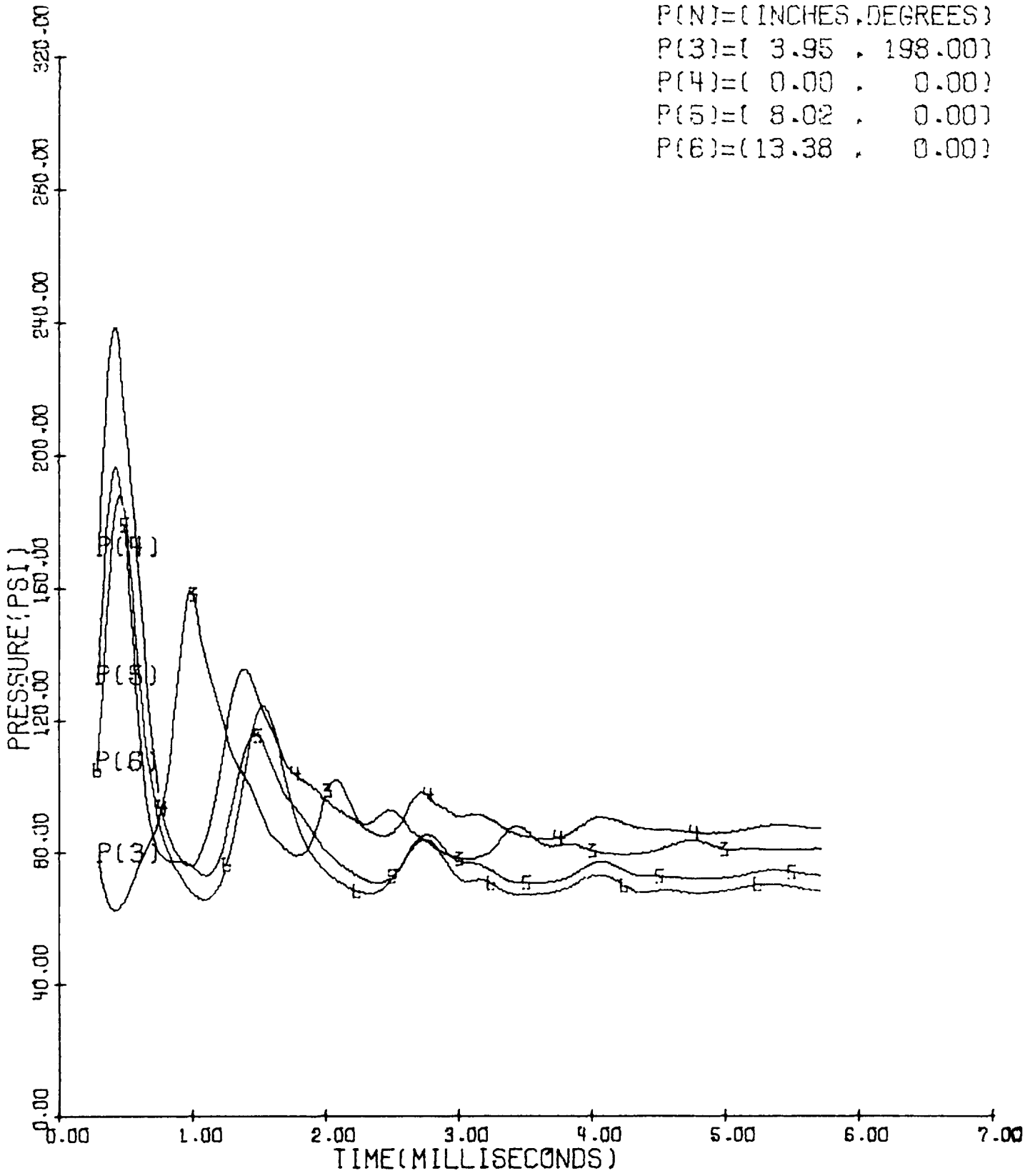

Figure 37

UNBAFFLED, $\dot{m}$=0.35, A_t/A_c=0.5025, λ=1.2

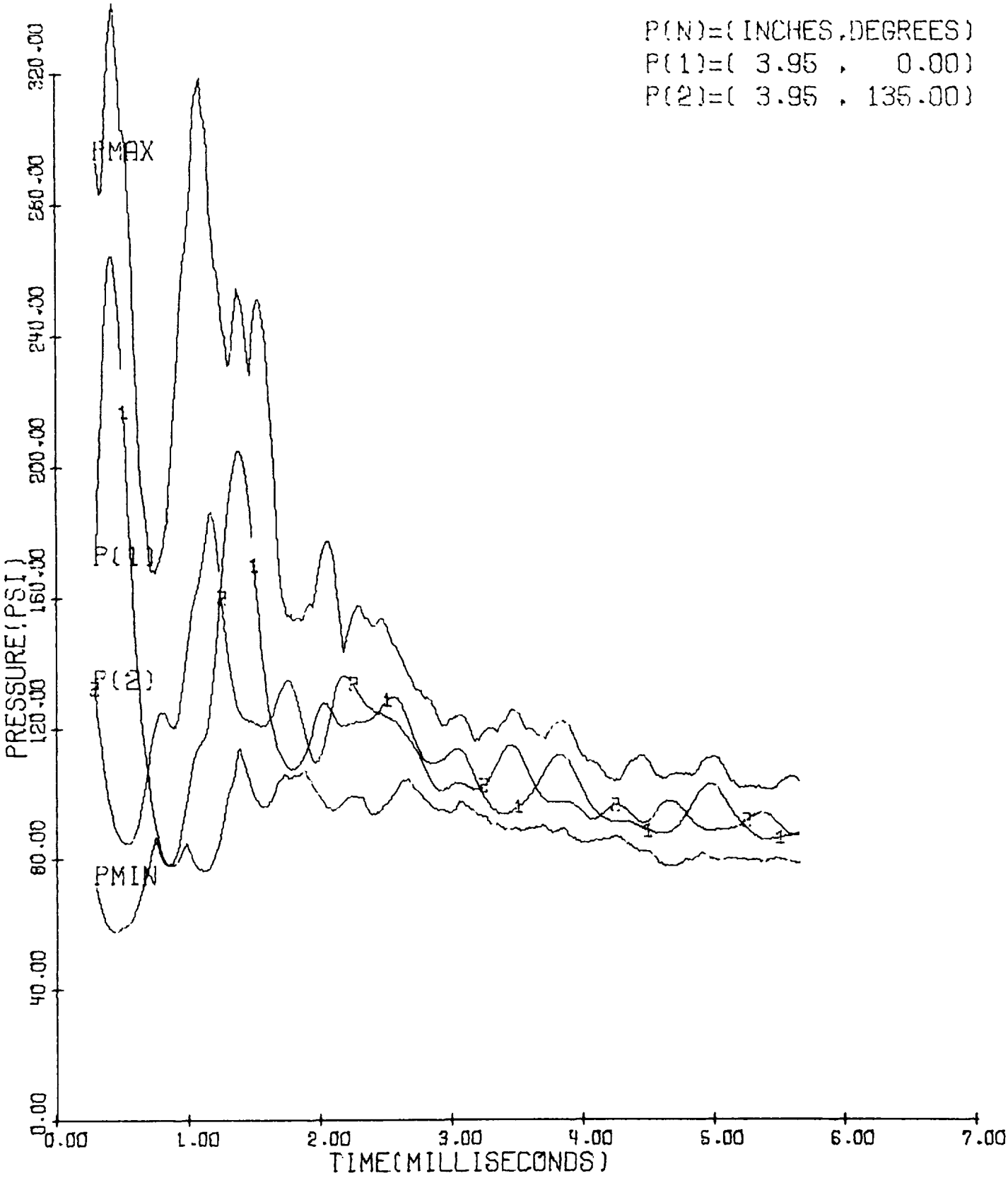

Figure 38

UNBAFFLED, $\dot{m}=0.35$, $A_t/A_c=0.5025$, $\lambda=1.2$

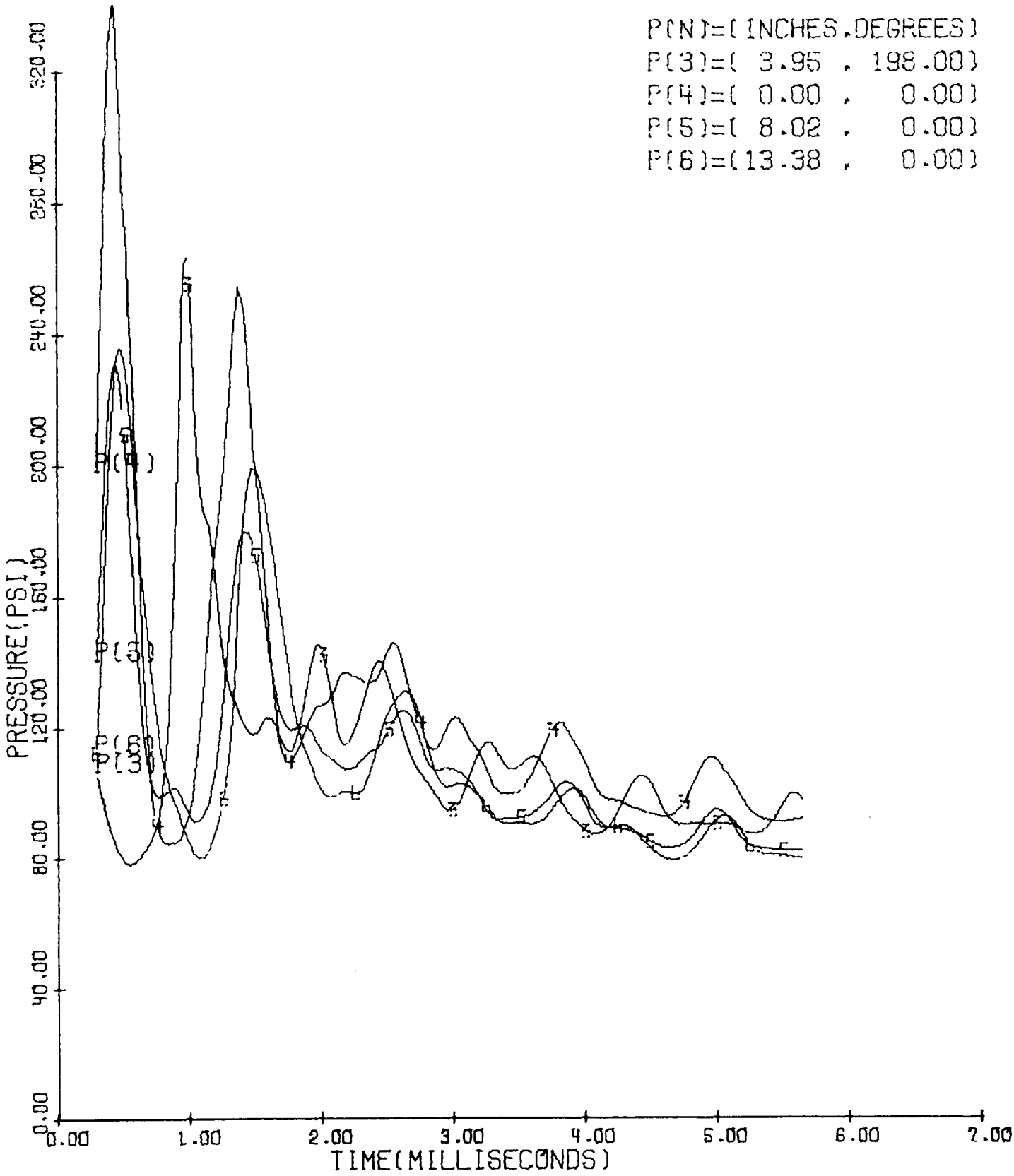

Figure 39

BAFFLED, ℓ=5.375",$\dot{m}$=0.35, A_t/A_c=0.5025, λ=0.5

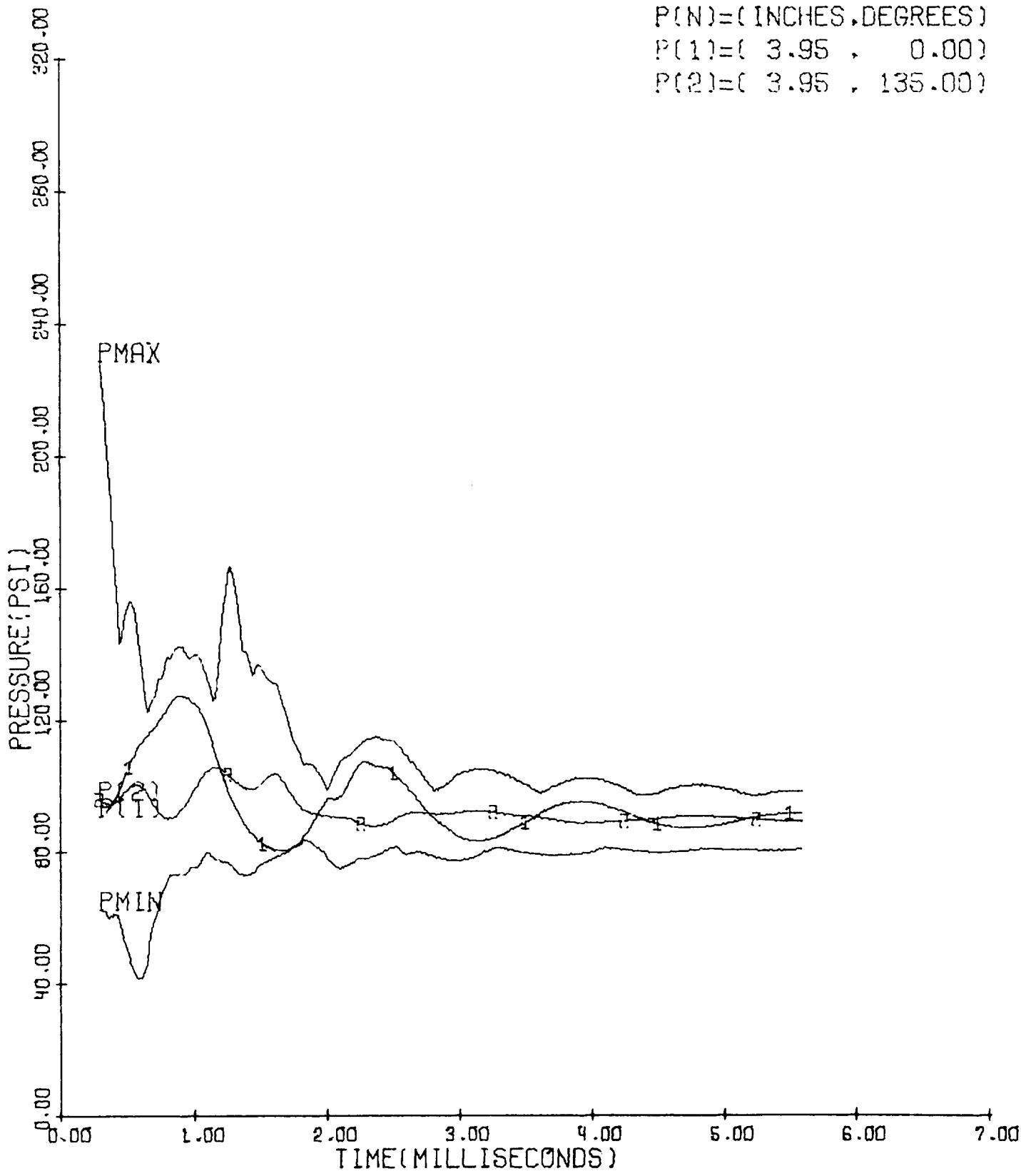

Figure 40

BAFFLED, ℓ=5.375", $\dot{m}$=0.35, A_t/A_c=0.5025, λ=0.5

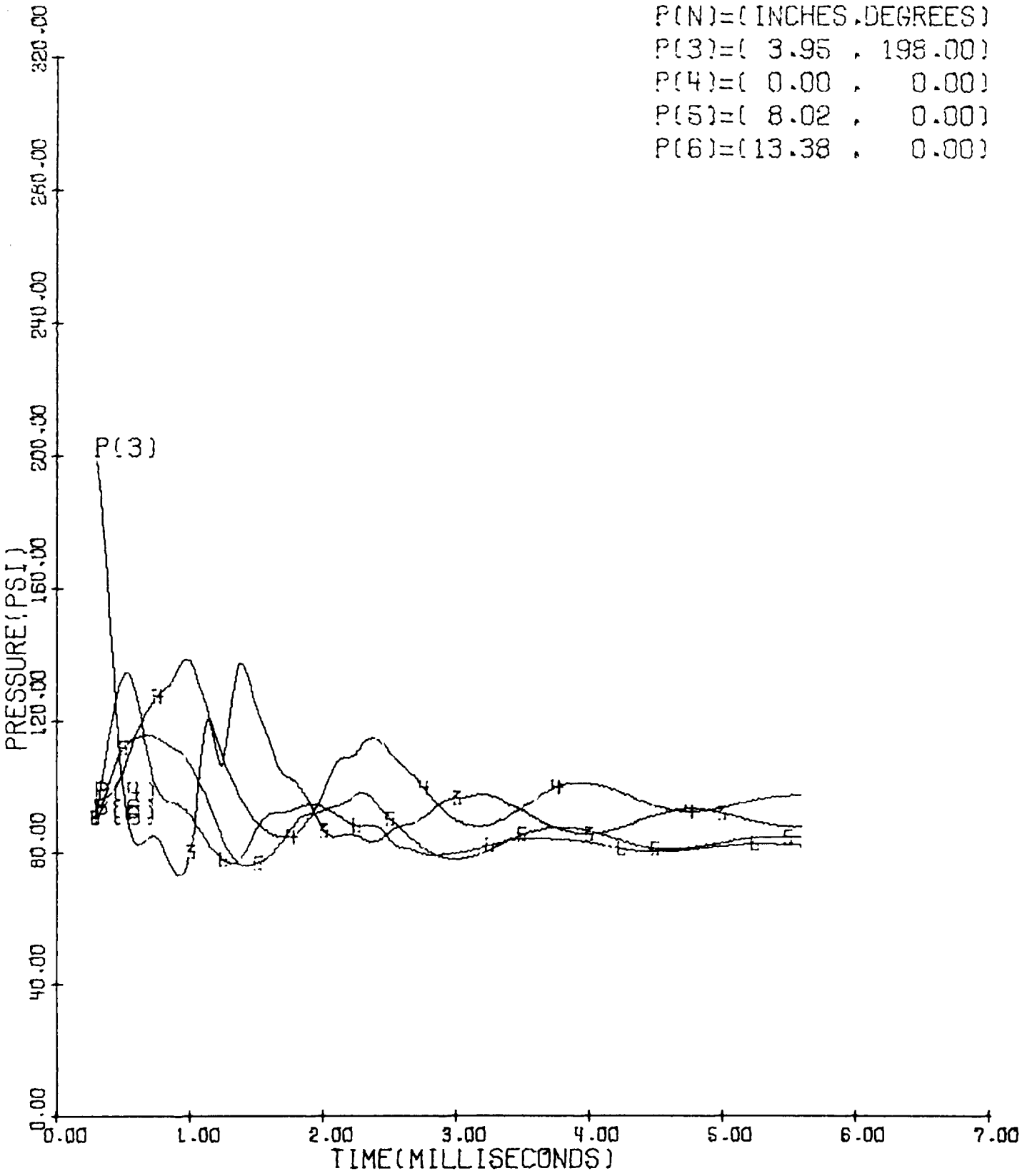

Figure 41

BAFFLED, ℓ=4.375",$\dot{m}$=0.35, A_t/A_c=0.5025, λ=0.5

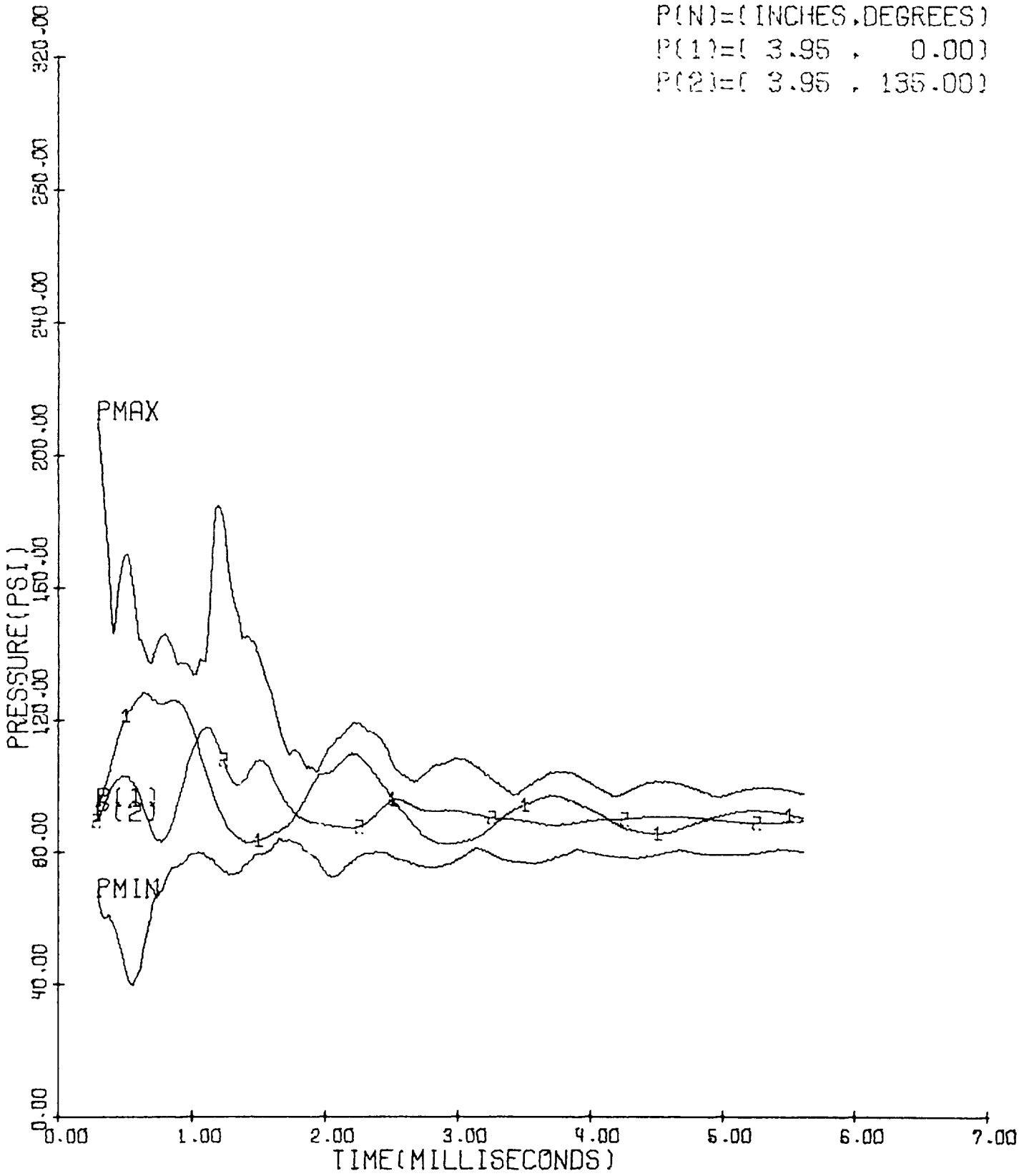

Figure 42

BAFFLED, ℓ=4.375",$\dot{m}$=0.35, A_t/A_c=o.5025, λ=0.5

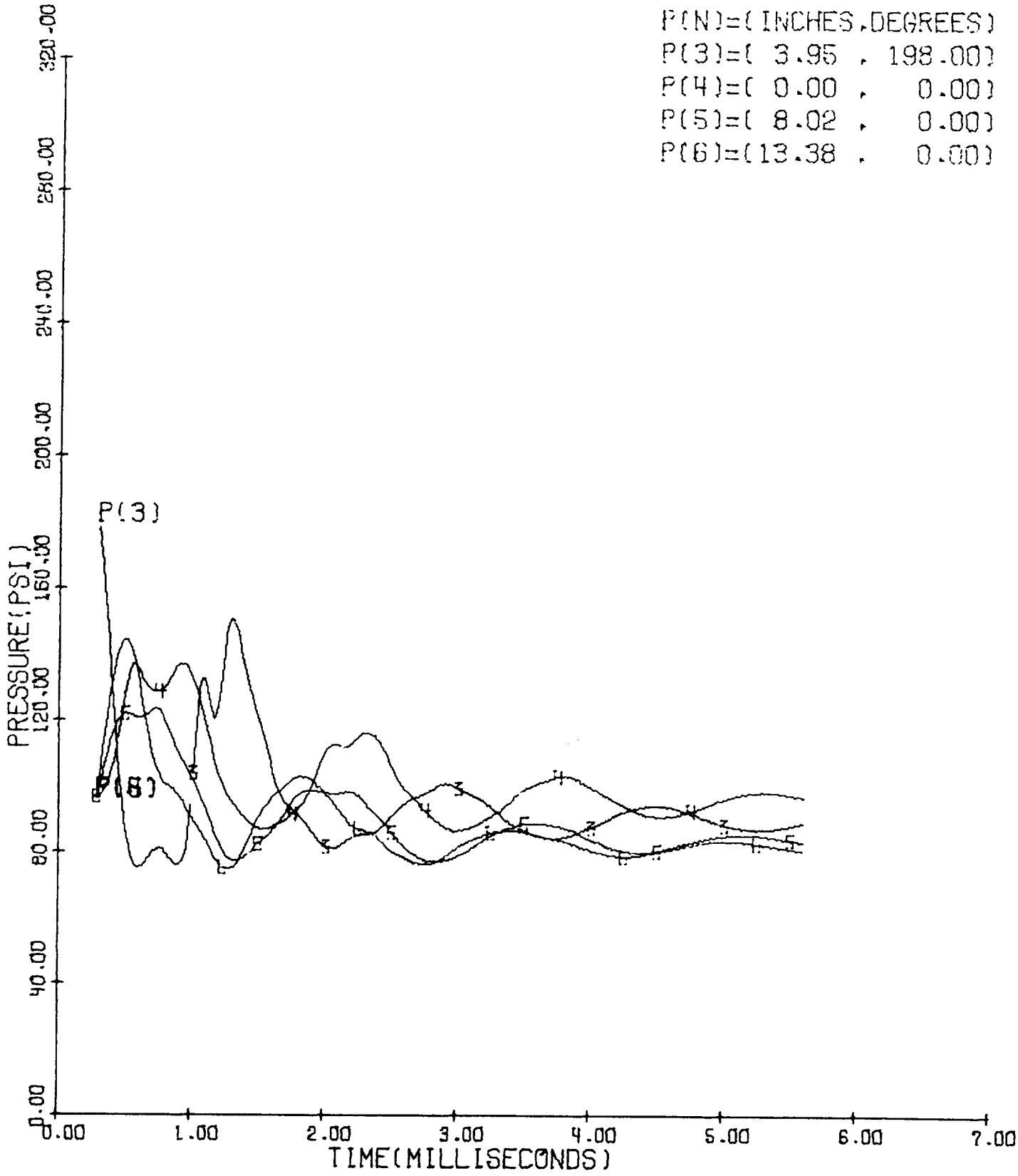

Figure 43

BAFFLED, ℓ=2.875",$\dot{m}$=0.35, A_t/A_c=0.5025, λ=0.5

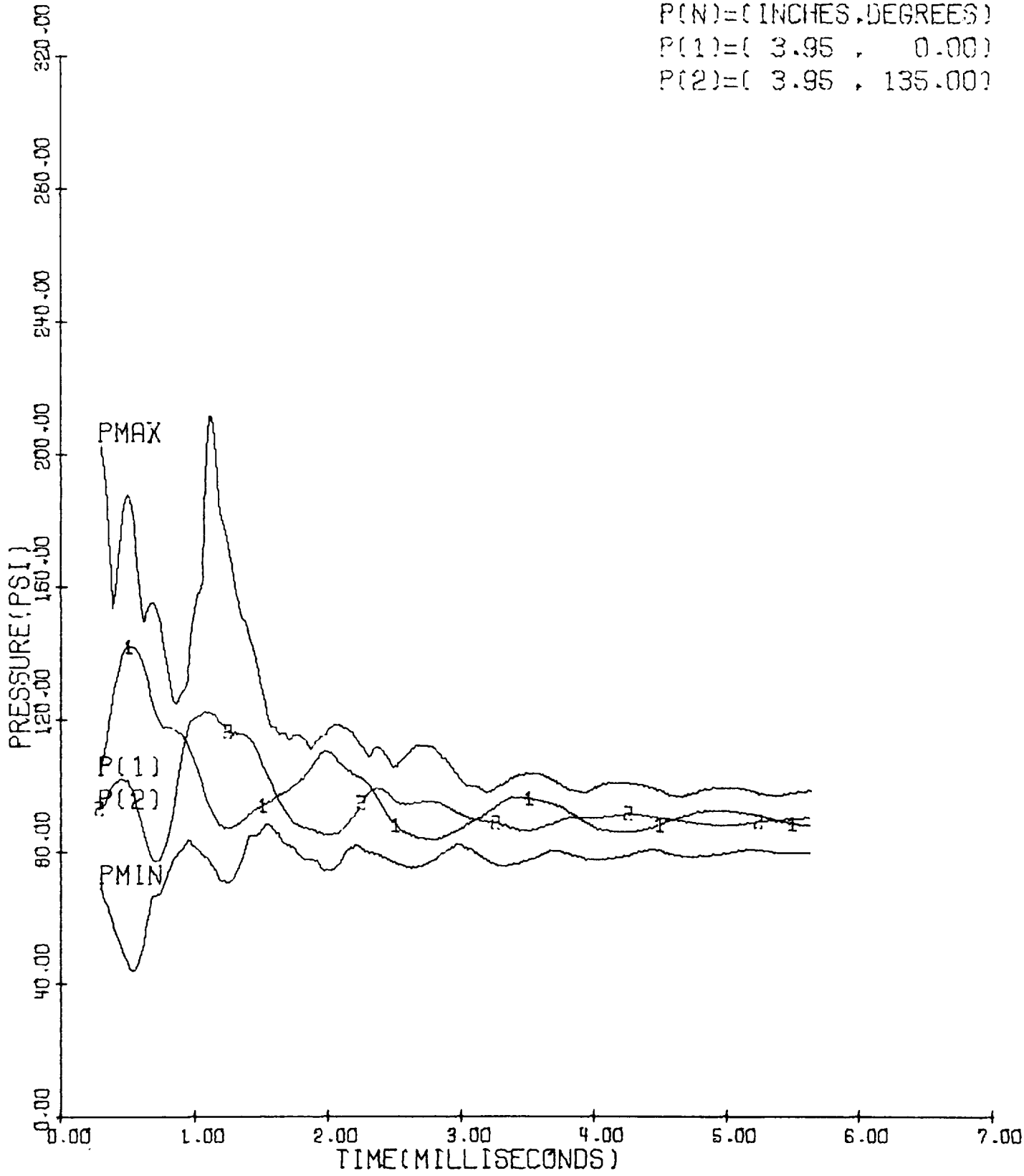

Figure 44

BAFFLED, ℓ=2.875",$\dot{m}$=0.35, A_t/A_c=0.5025, λ=0.5

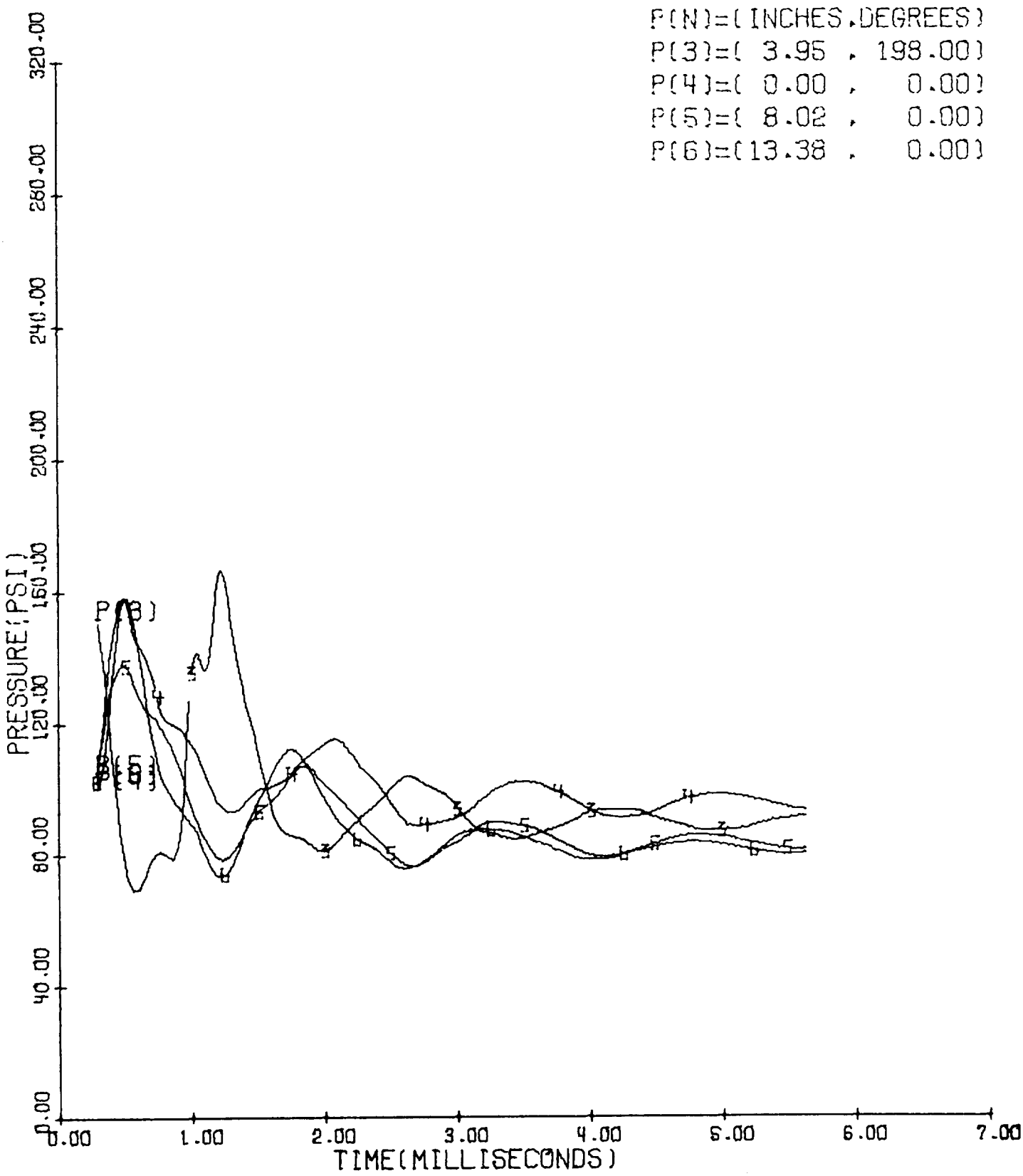

Figure 45

UNBAFFLED, $\dot{m}=0.35$, $A_t/A_c=0.5025$, $\lambda=0.1$

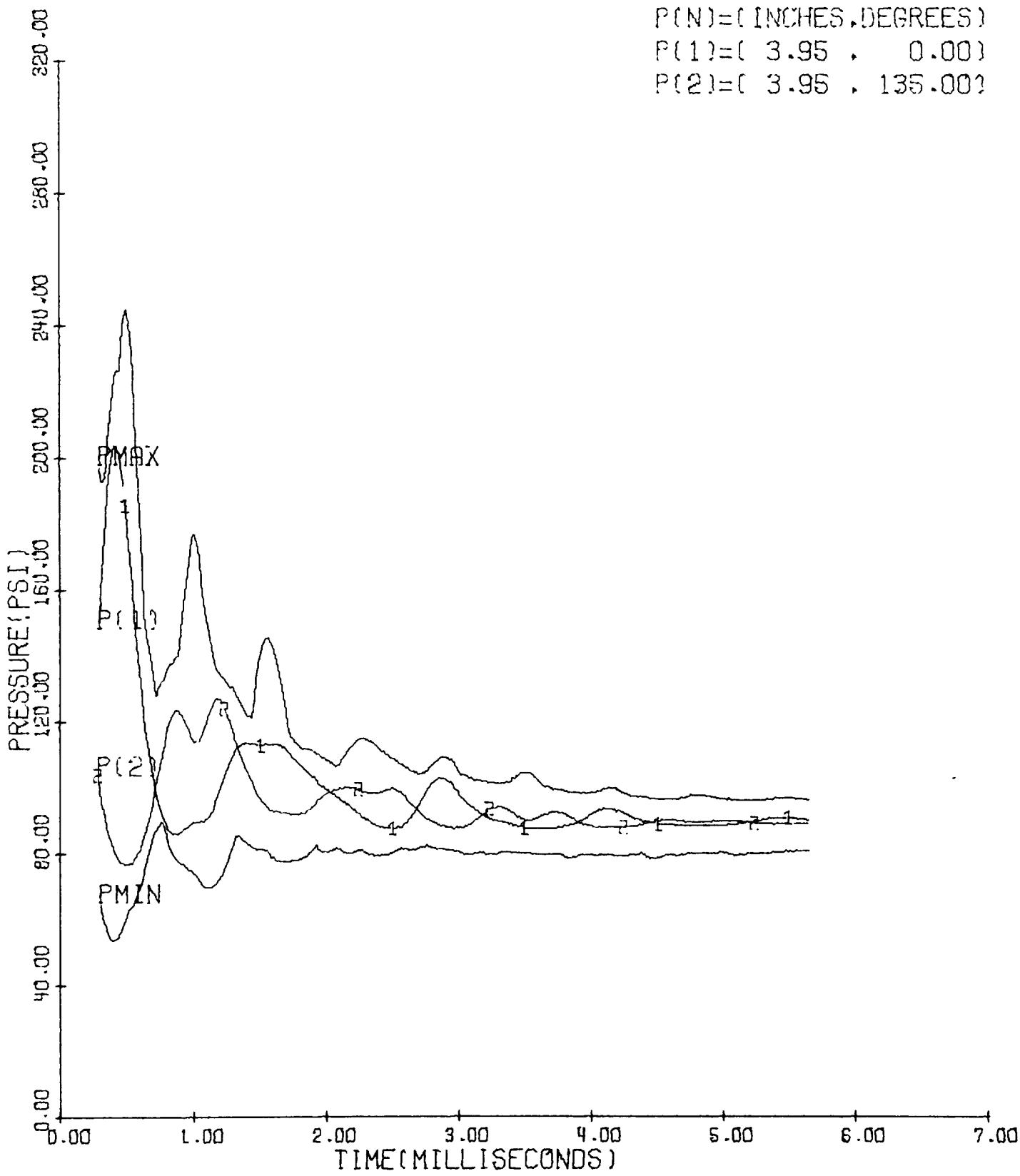

Figure 46

UNBAFFLED, $\dot{m}=0.35$, $A_t/A_c=0.5025$, $\lambda=0.1$

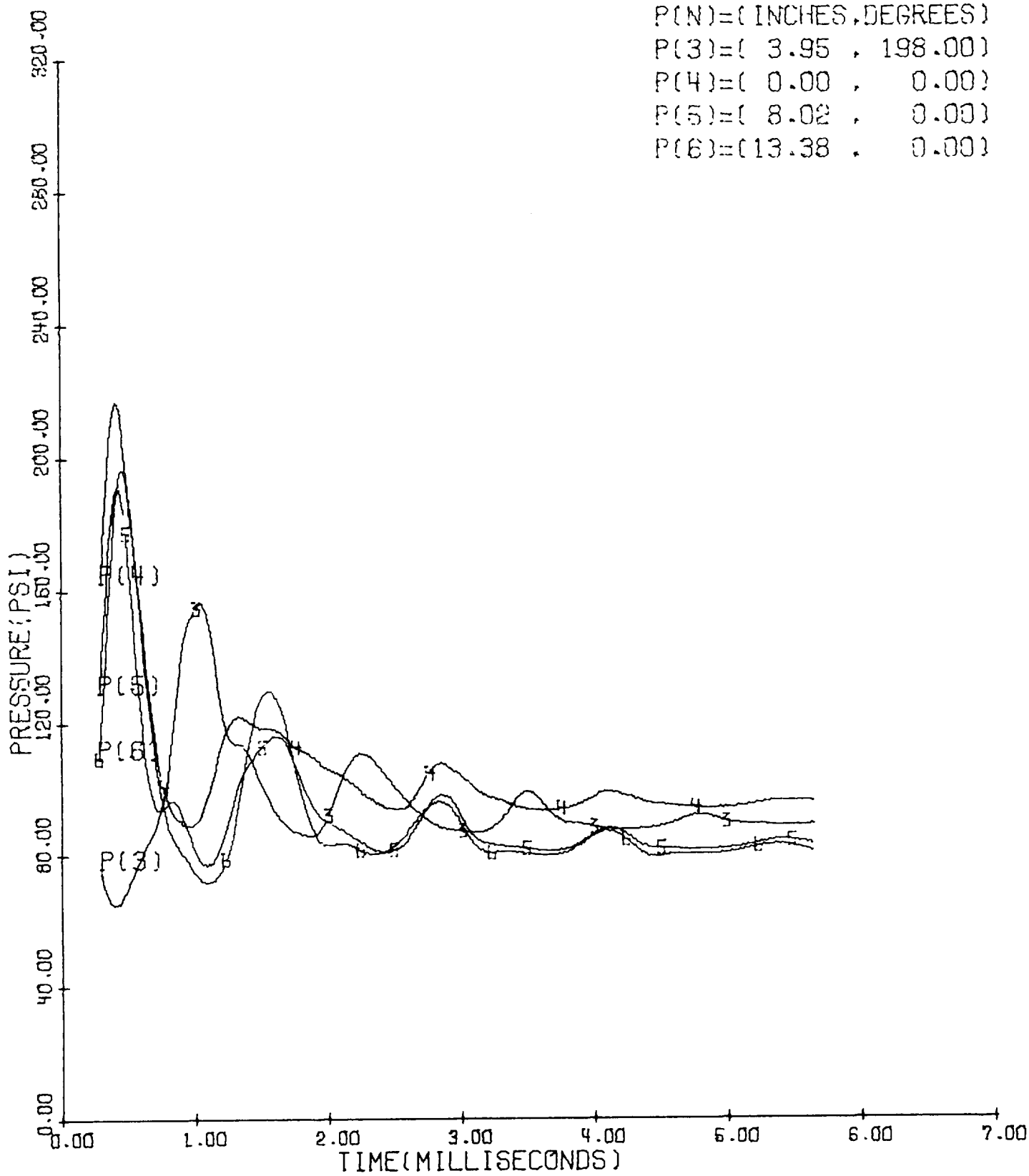

Figure 47

UNBAFFLED, $\dot{m}=0.28$, $A_t/A_c=0.5025$, $\lambda=0.5$

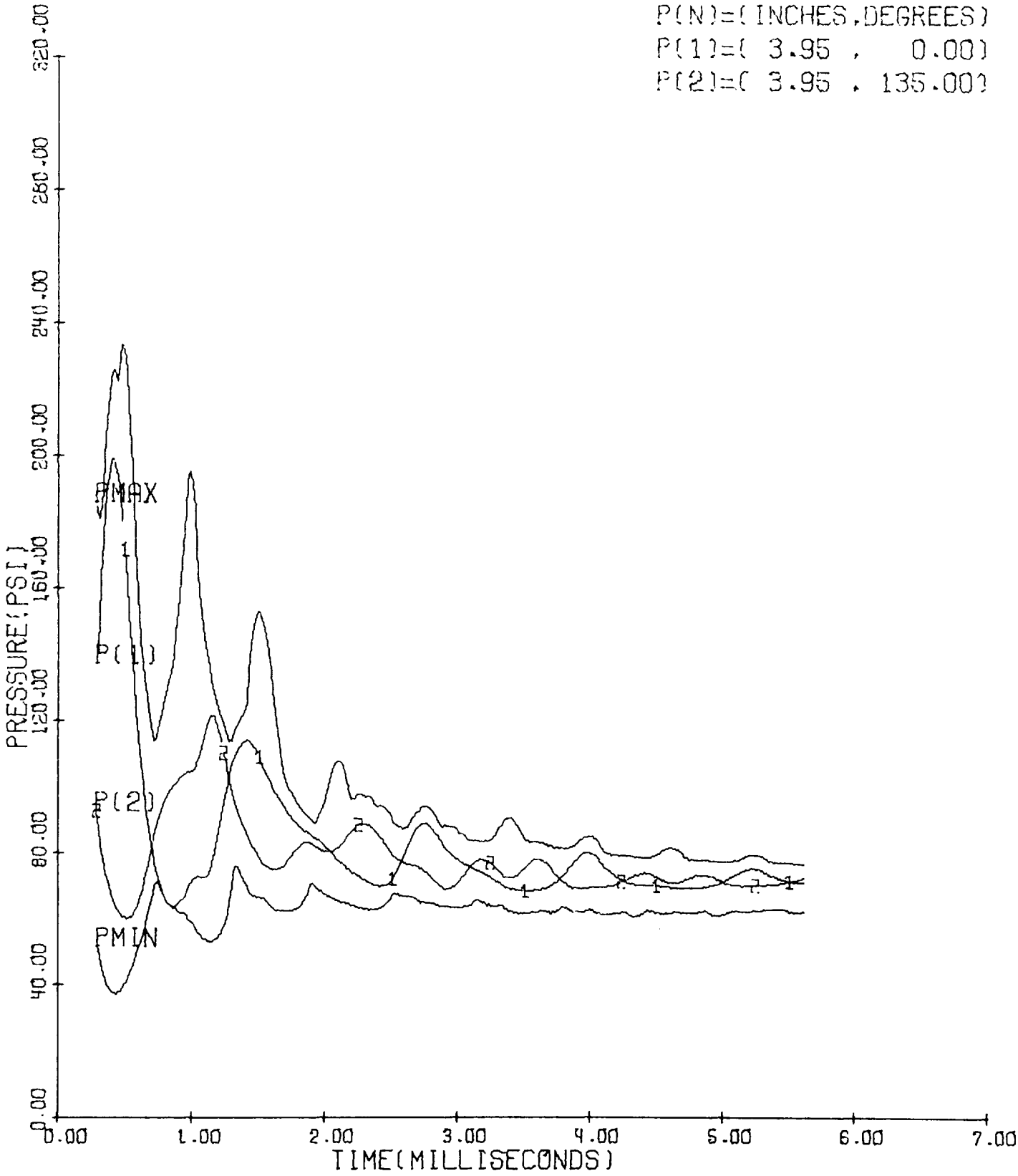

Figure 48

UNBAFFLED, $\dot{m}=0.28$, $A_t/A_c=0.5025$, $\lambda=0.5$

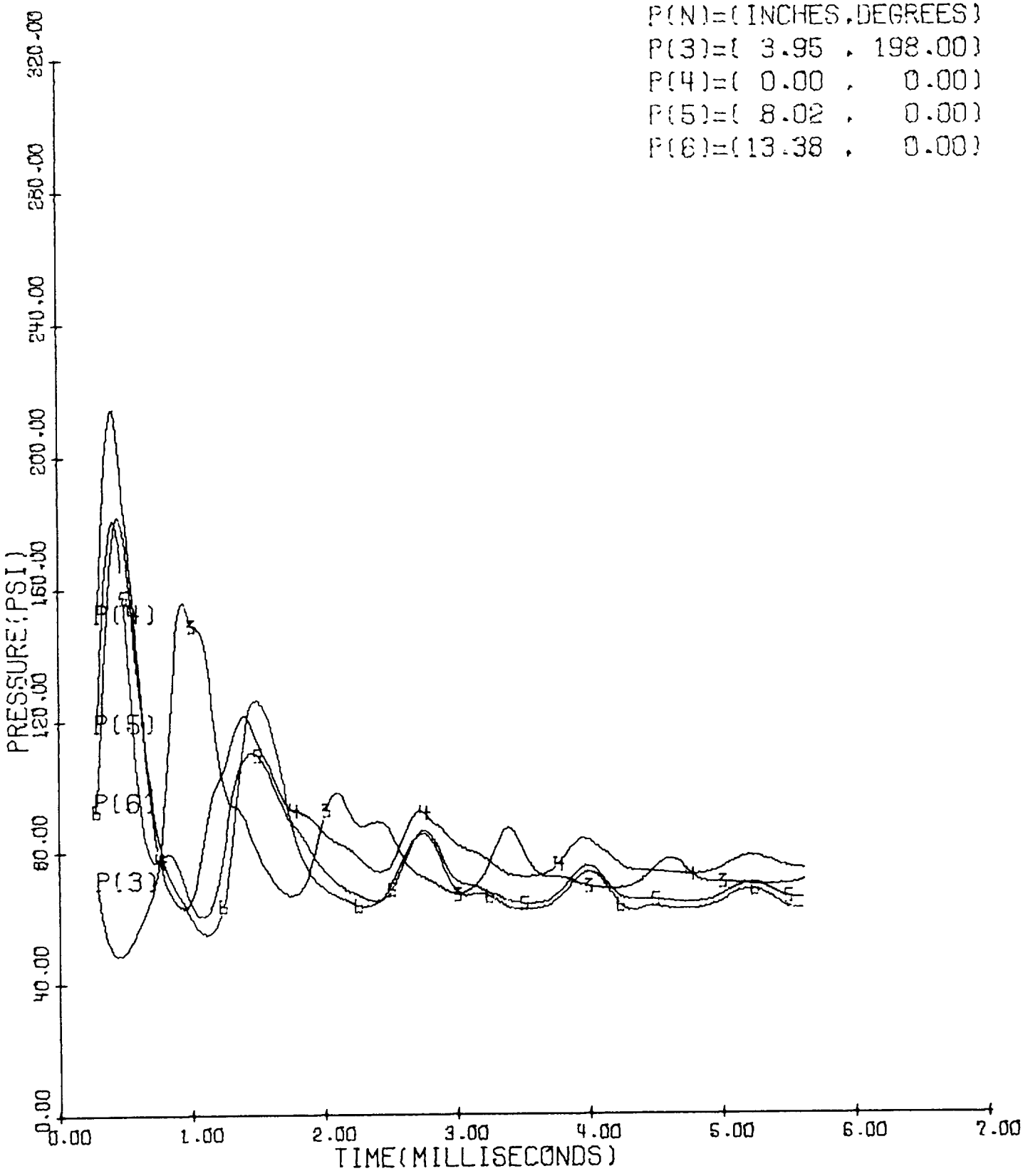

Figure 49

UNBAFFLED, $\dot{m}=0.28$, $A_t/A_c=0.3750$, $\lambda=0.5$

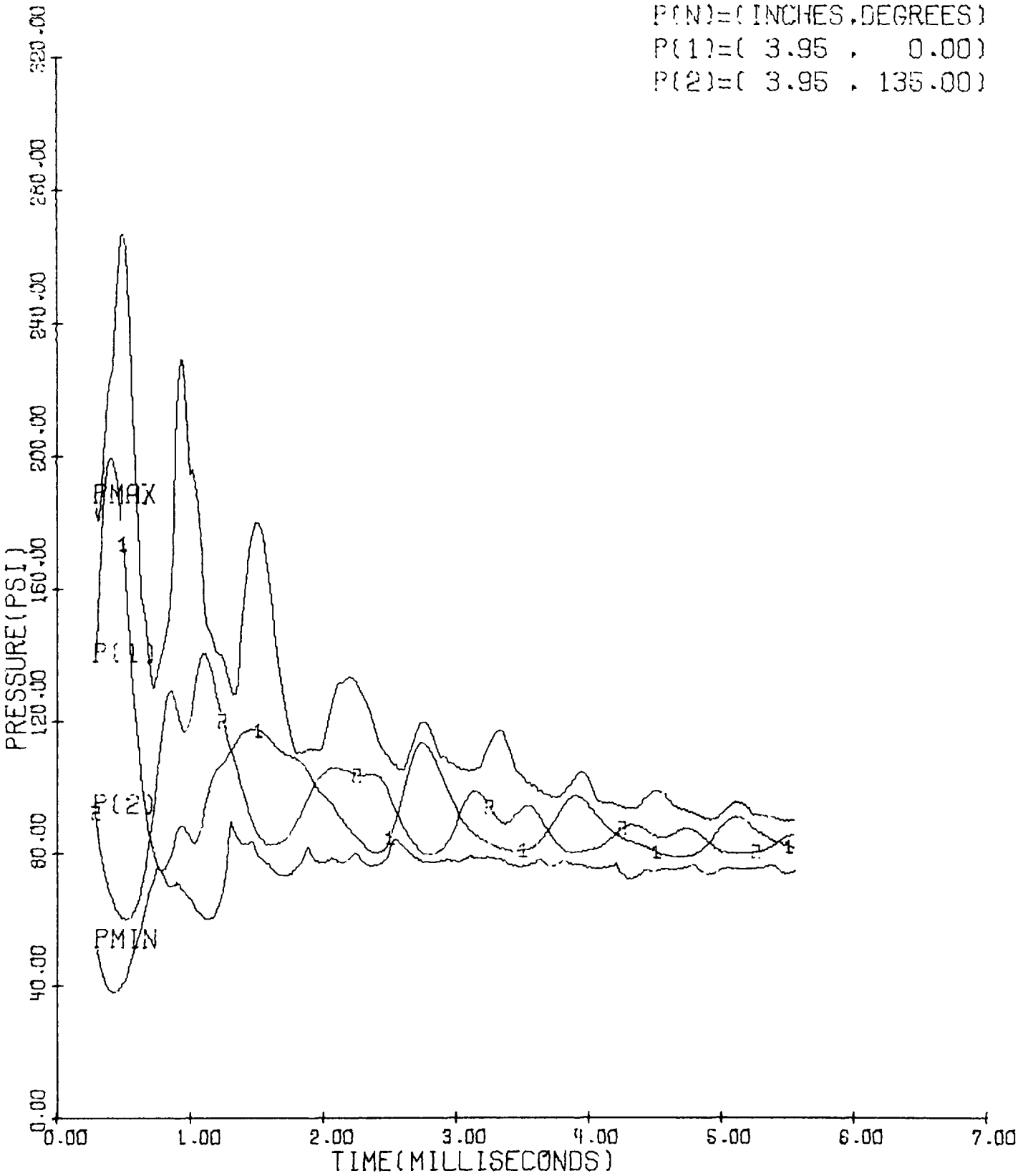

Figure 50

UNBAFFLED, $\dot{m}$=0.28, A_t/A_c=0.3750, λ=0.5

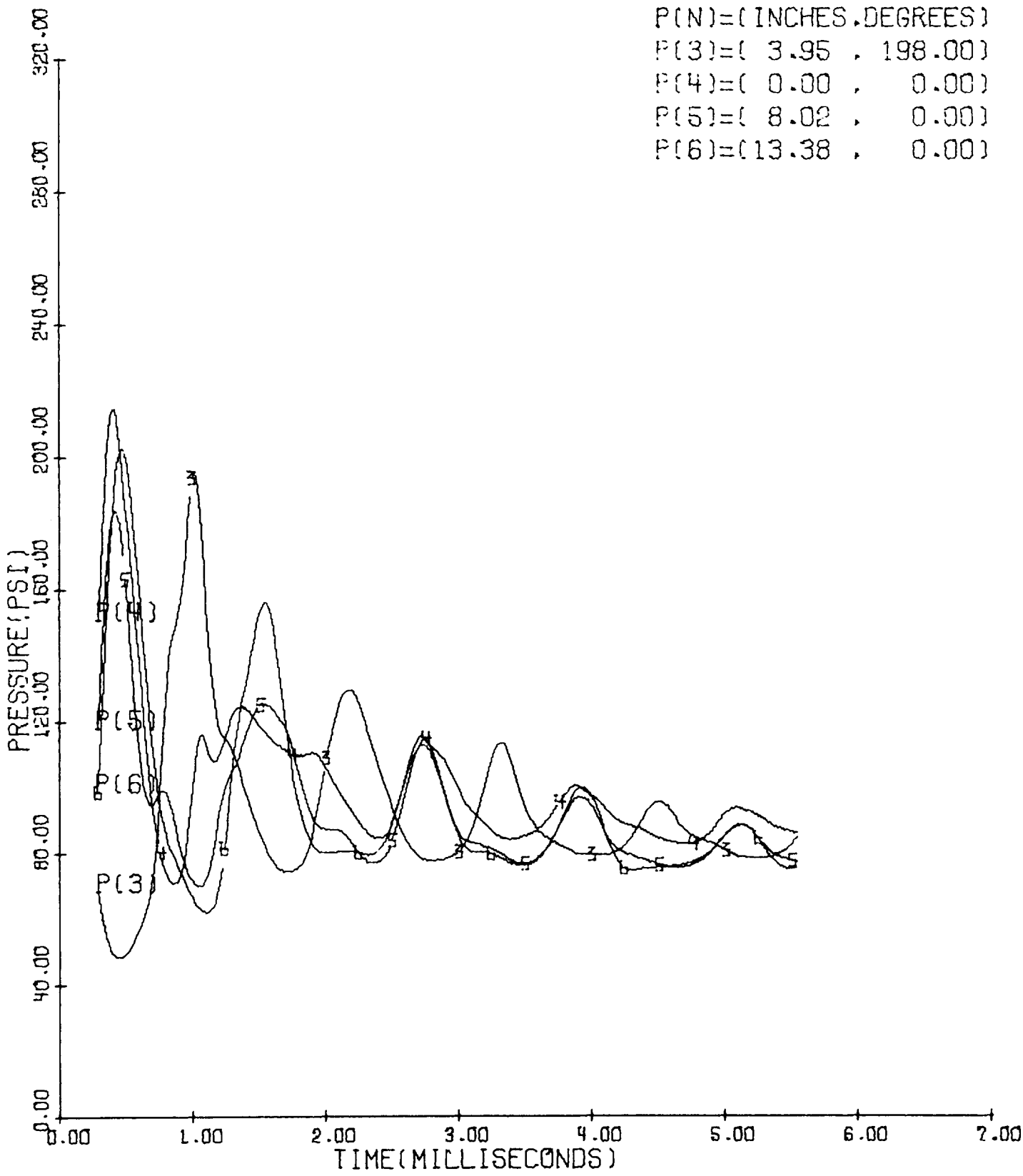

Figure 51

UNBAFFLED, $\dot{m}$=0.28, A_t/A_c=0.6250, λ=0.5

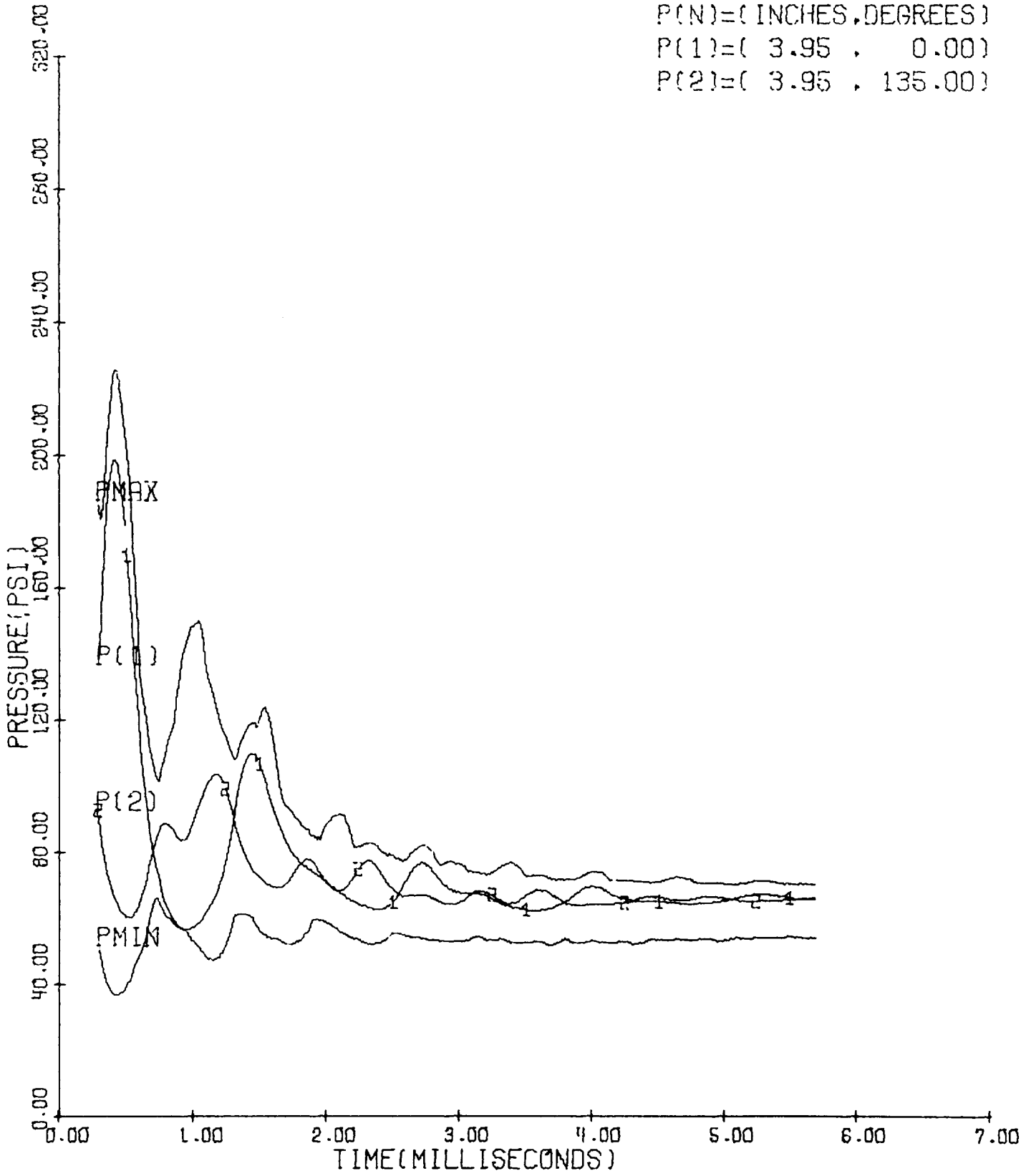

Figure 52

UNBAFFLED, $\dot{m}$=0.28, A_t/A_c=0.6250, λ=0.5

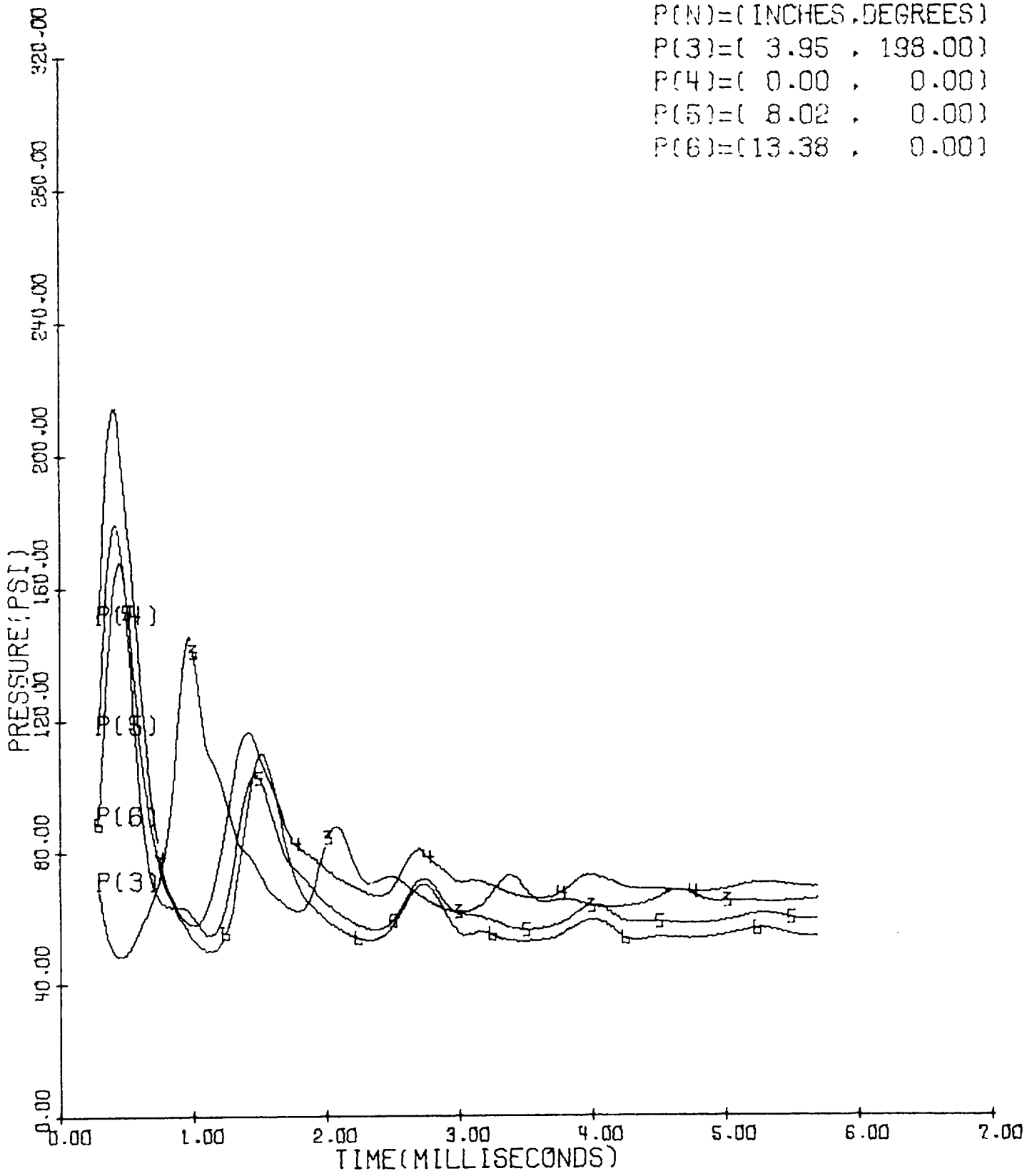

Figure 53

UNBAFFLED, $\dot{m}=0.28$, $A_t/A_c=0.5025$, $\lambda=1.2$

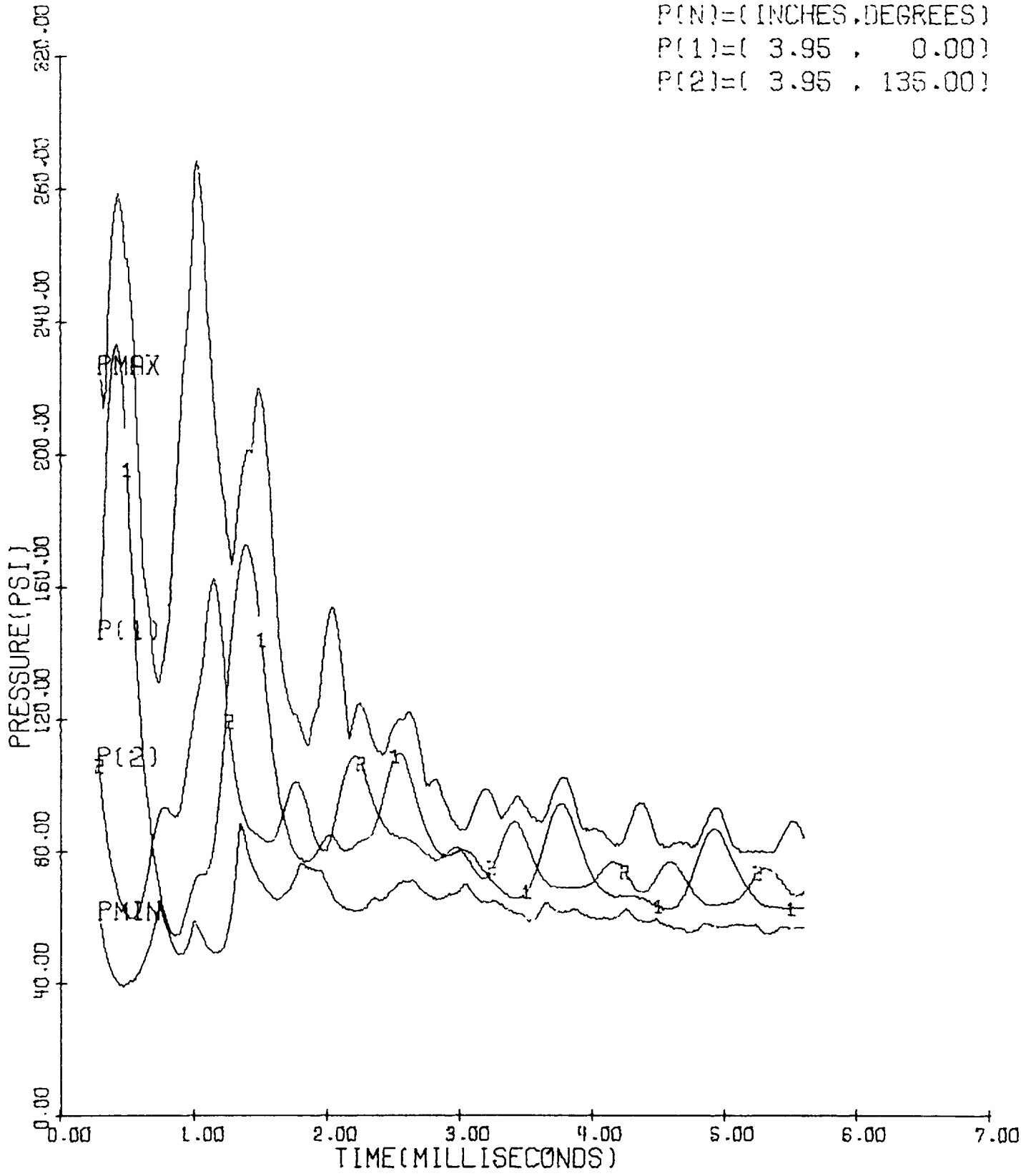

Figure 54

UNBAFFLED, $\dot{m}=0.28$, $A_t/A_c=0.5025$, $\lambda=1.2$

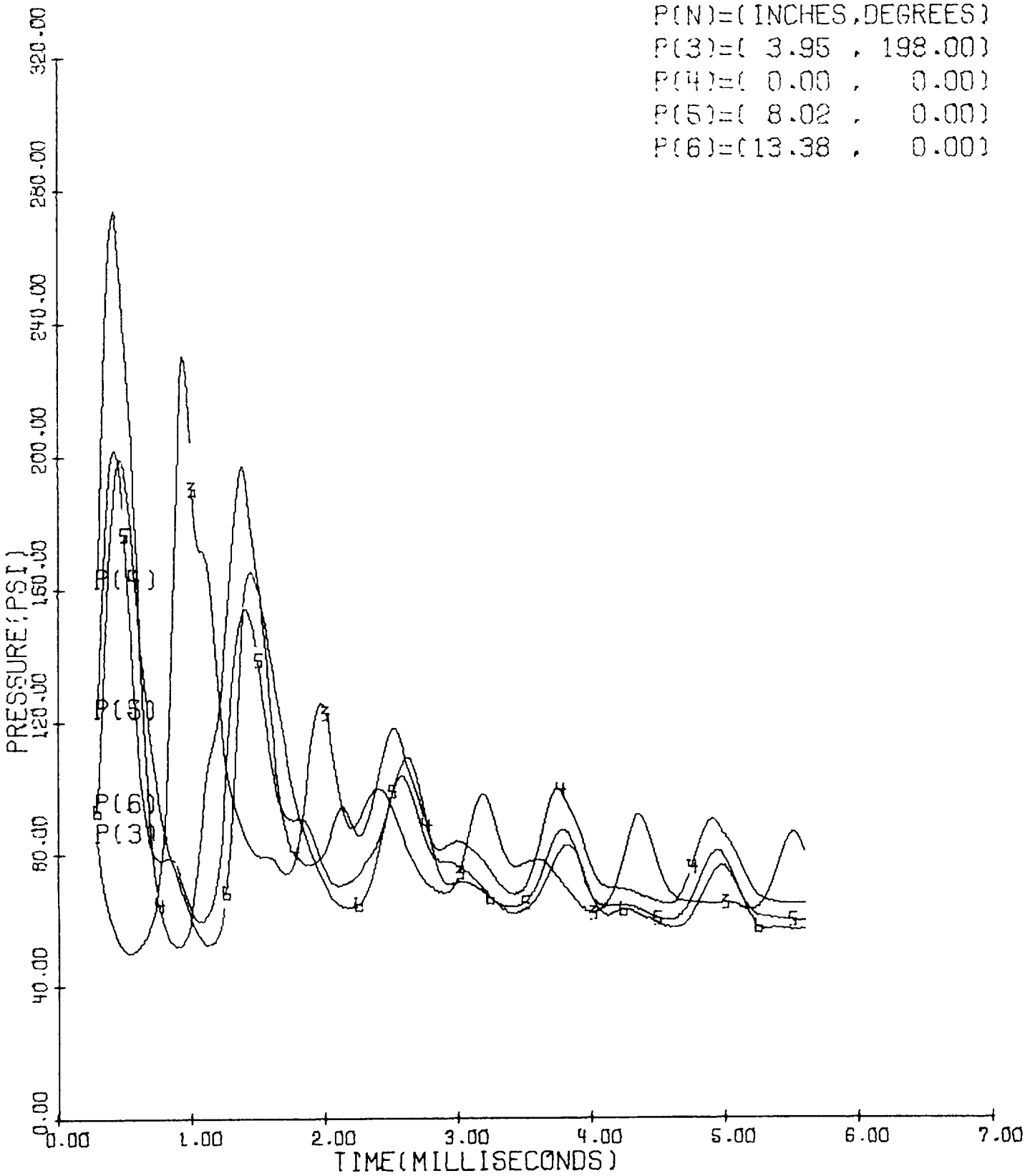

Figure 55

UNBAFFLED, $\dot{m}=0.28$, $A_t/A_c=0.5025$, $\lambda=0.1$

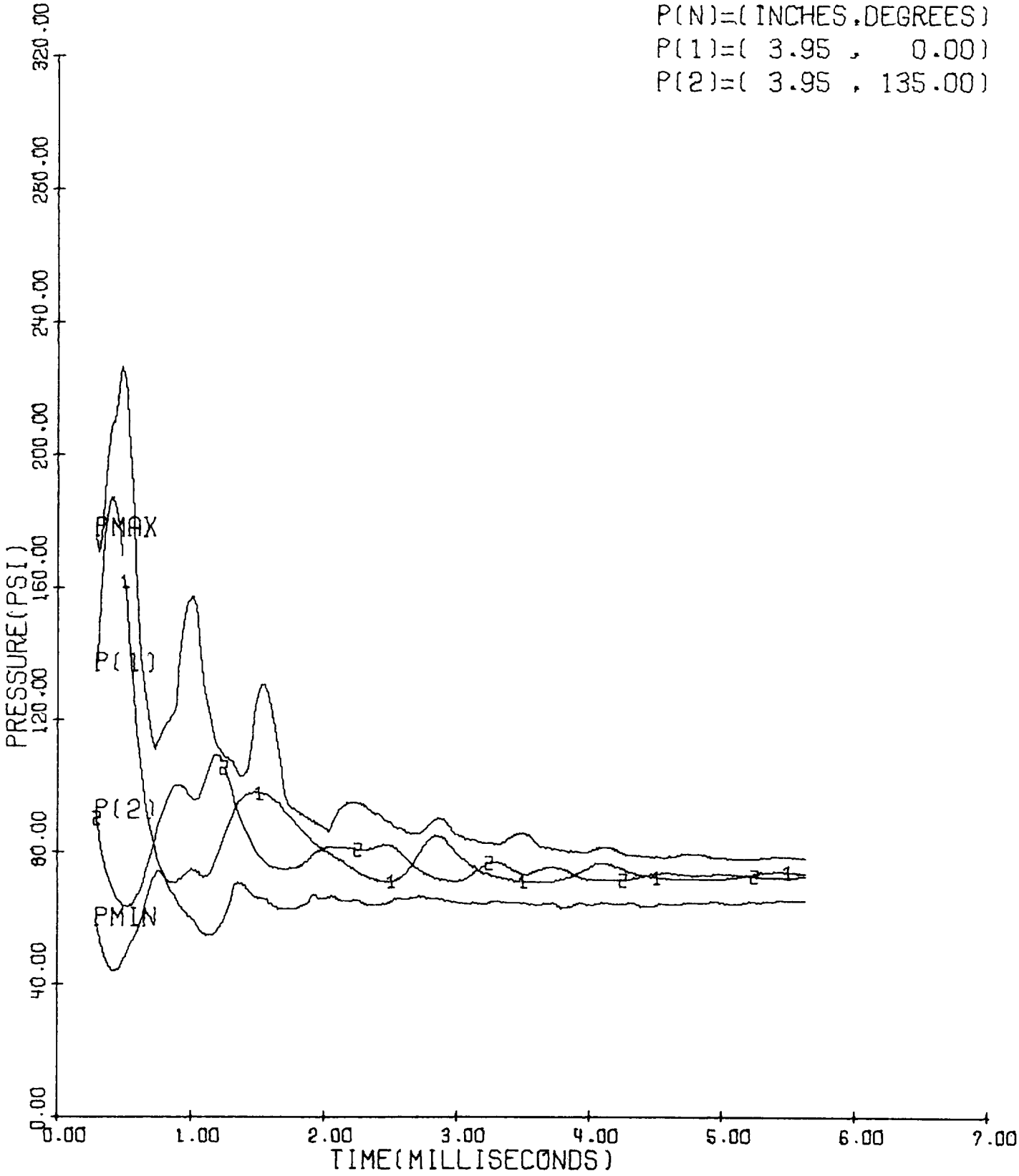

Figure 56

UNBAFFLED, $\dot{m}=0.28$, $A_t/A_c=0.5025$, $\lambda=0.1$

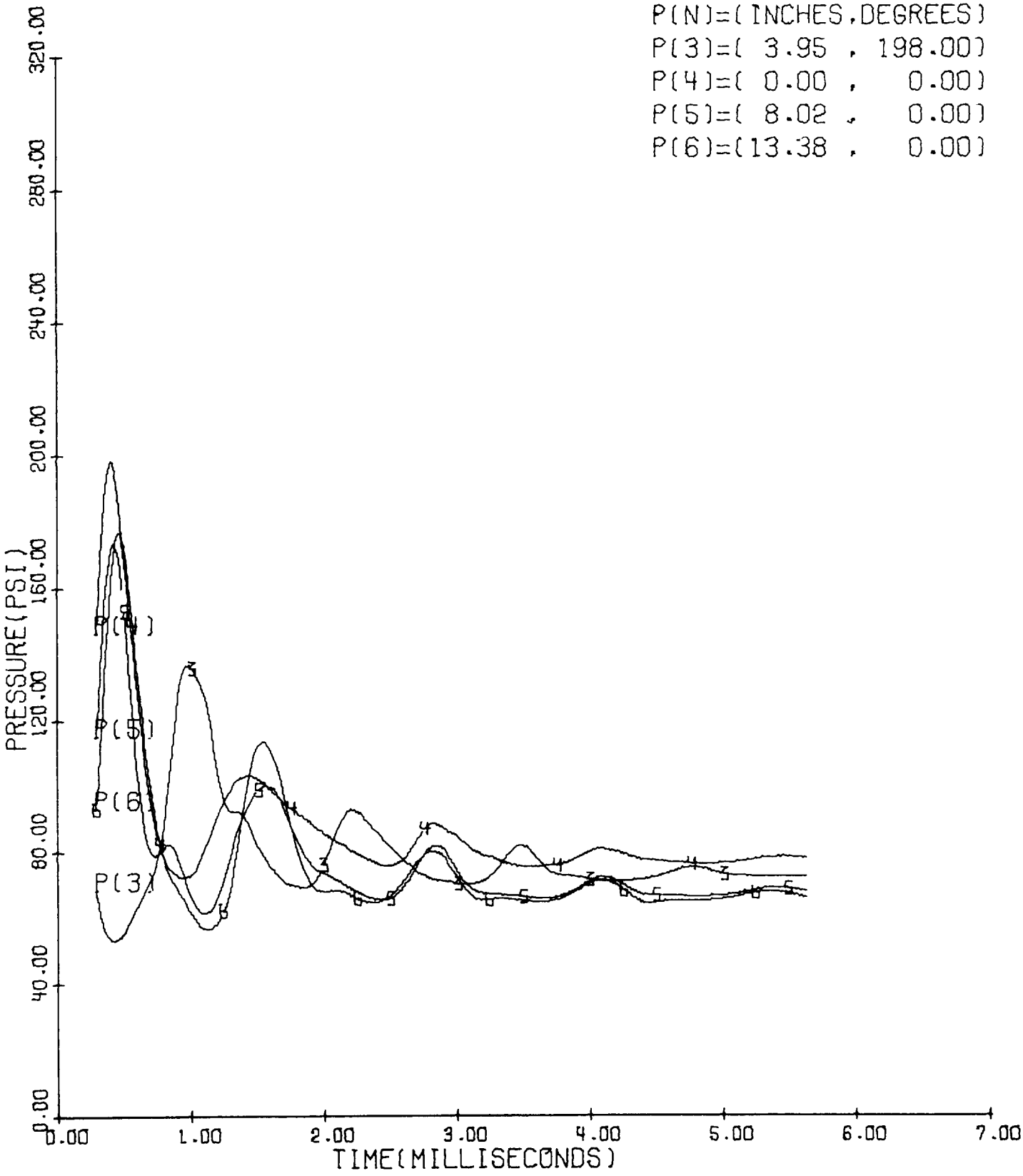

Figure 57

BAFFLED, ℓ=5.375",$\dot{m}$=0.28, A_t/A_c=0.5025, λ=0.5

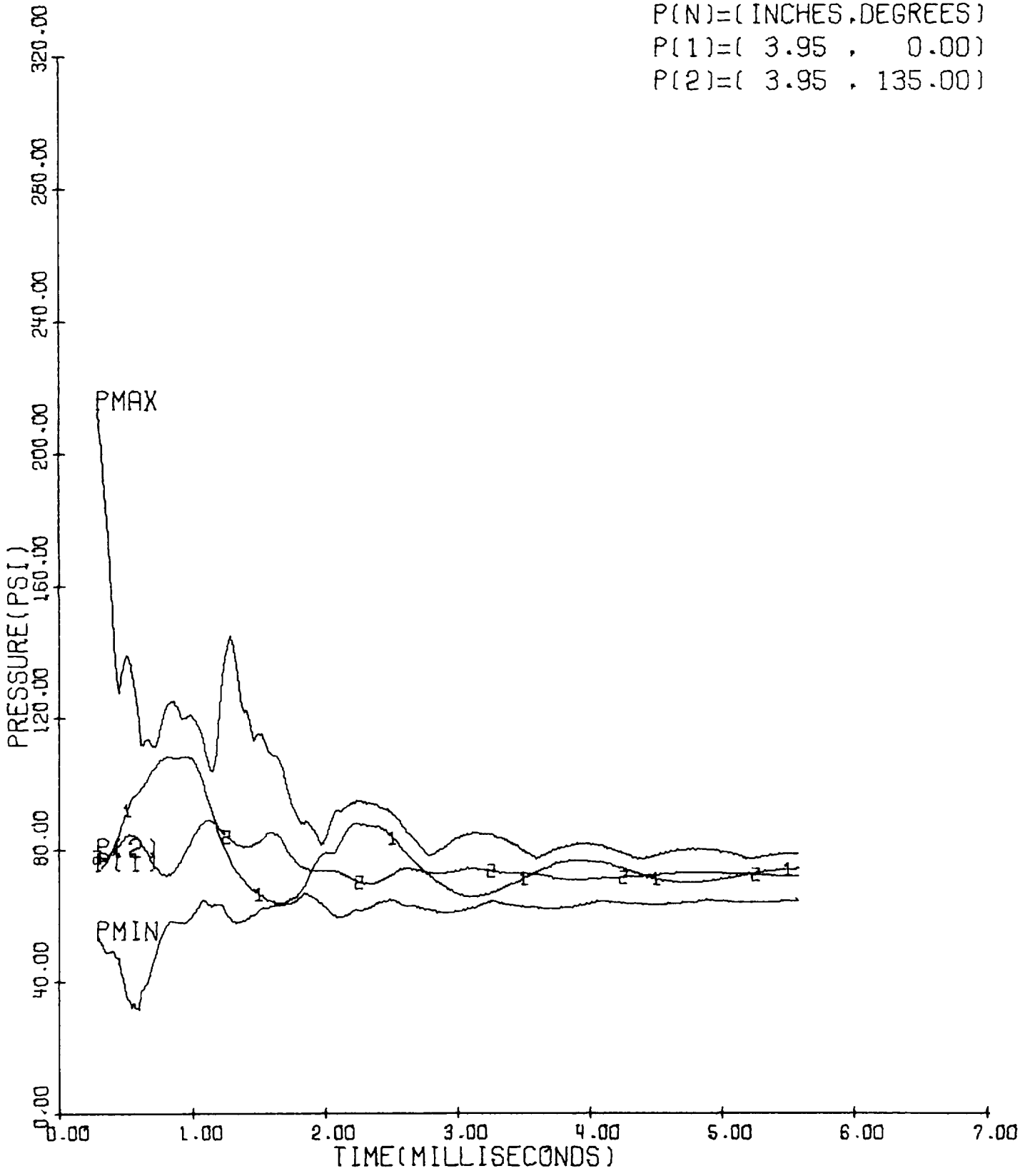

Figure 58

BAFFLED, ℓ=5.375",$\dot{m}$=0.28, A_t/A_c=0.5025, λ=0.5

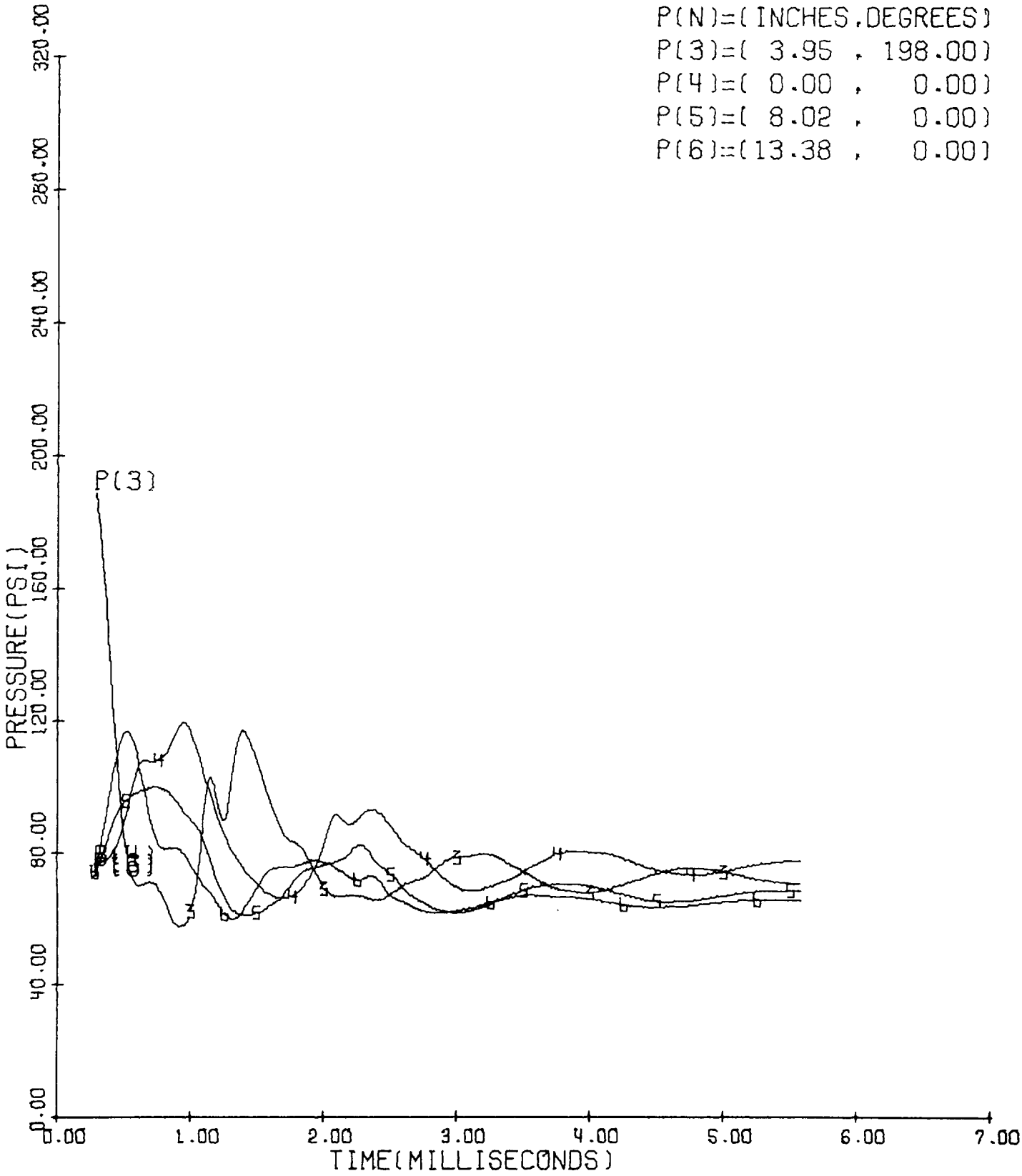

Figure 59

BAFFLED, ℓ=4.375",$\dot{m}$=0.28, A_t/A_c=0.5025, λ=0.5

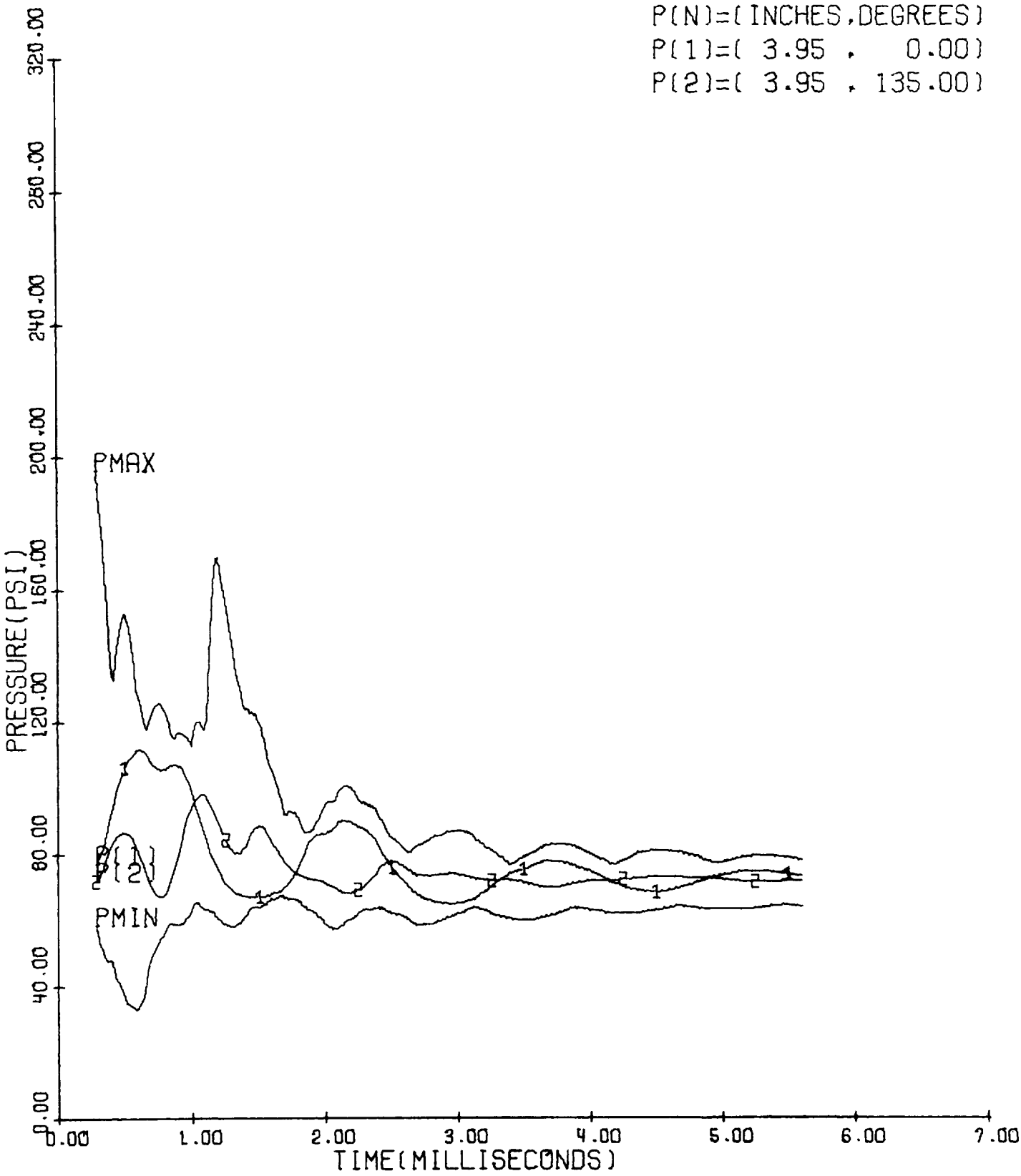

Figure 60

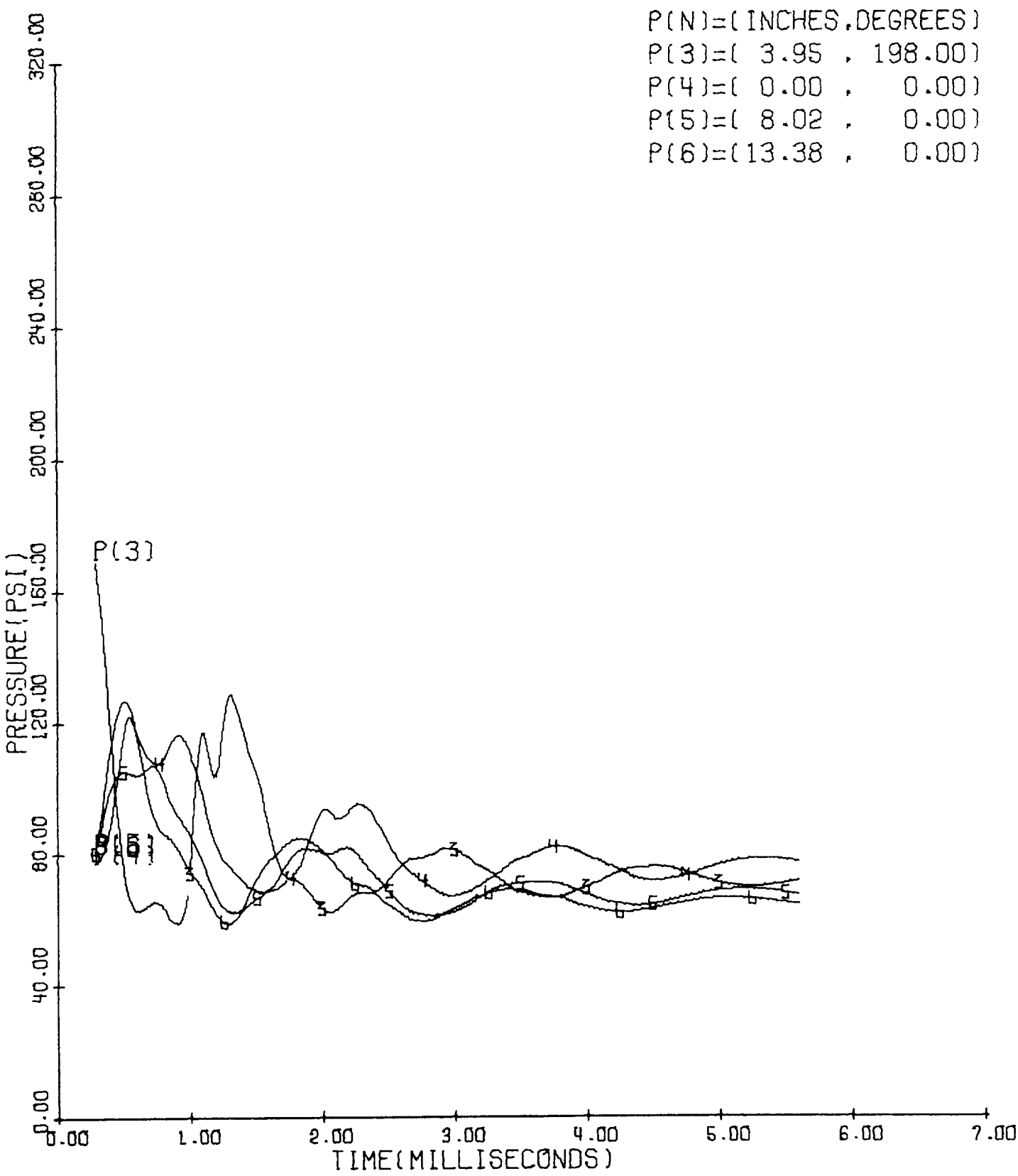
BAFFLED, ℓ=4.375",ṁ=0.28, A_t/A_c=0.5025, λ=0.5
P(N)=(INCHES,DEGREES)
P(3)=(3.95 , 198.00)
P(4)=(0.00 , 0.00)
P(5)=(8.02 , 0.00)
P(6)=(13.38 , 0.00)
P(3)
PRESSURE(PSI)
0.00
40.00
80.00
120.00
160.00
200.00
240.00
280.00
320.00
0.00
1.00
2.00
3.00
4.00
5.00
6.00
7.00
TIME(MILLISECONDS)

Figure 61

BAFFLED, ℓ=2.875",m=0.28, A_t/A_c=0.5025, λ=0.5

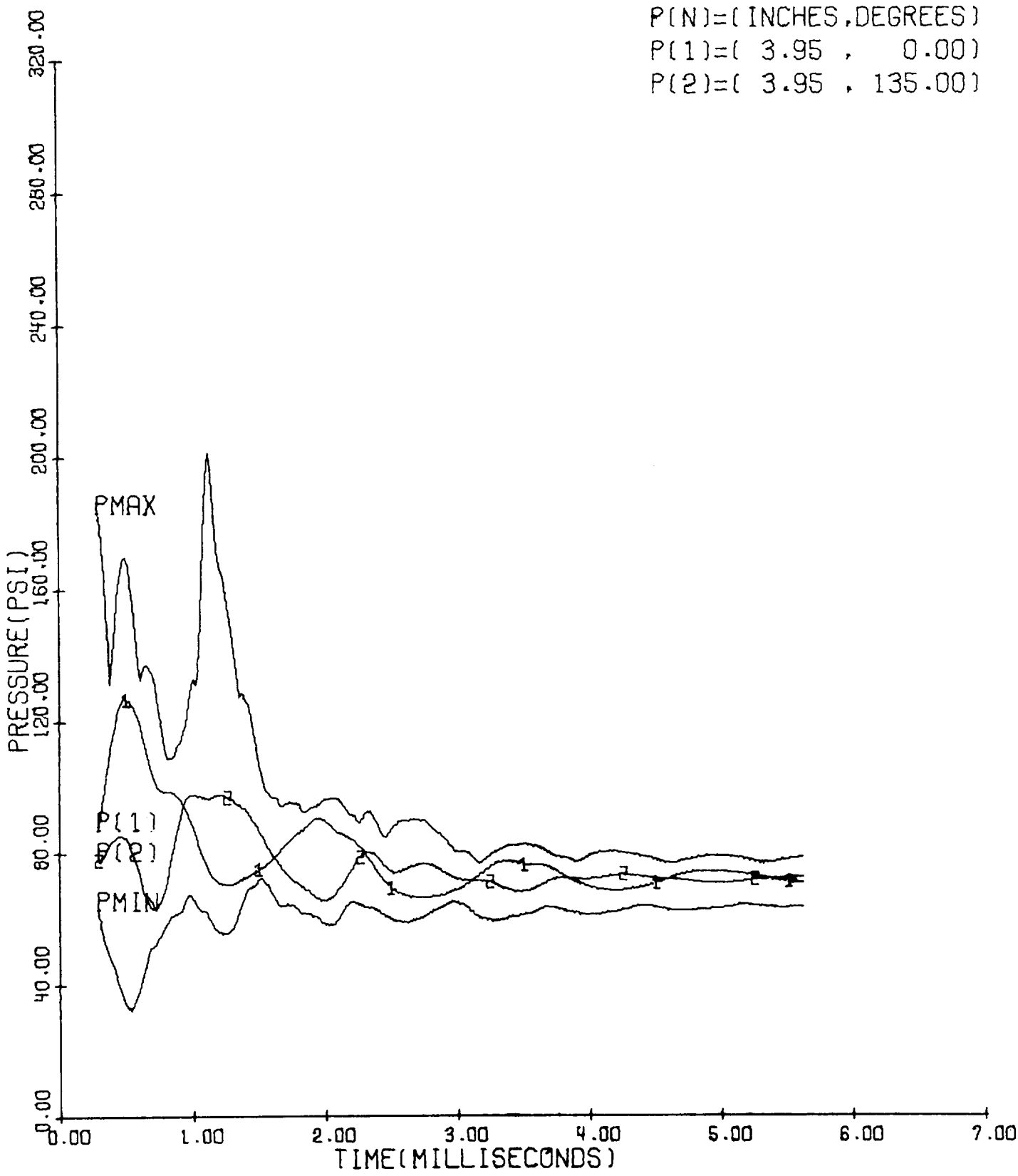

Figure 62

BAFFLED, ℓ=2.875",$\dot{m}$=0.28, A_t/A_c=0.5025, λ=0.5

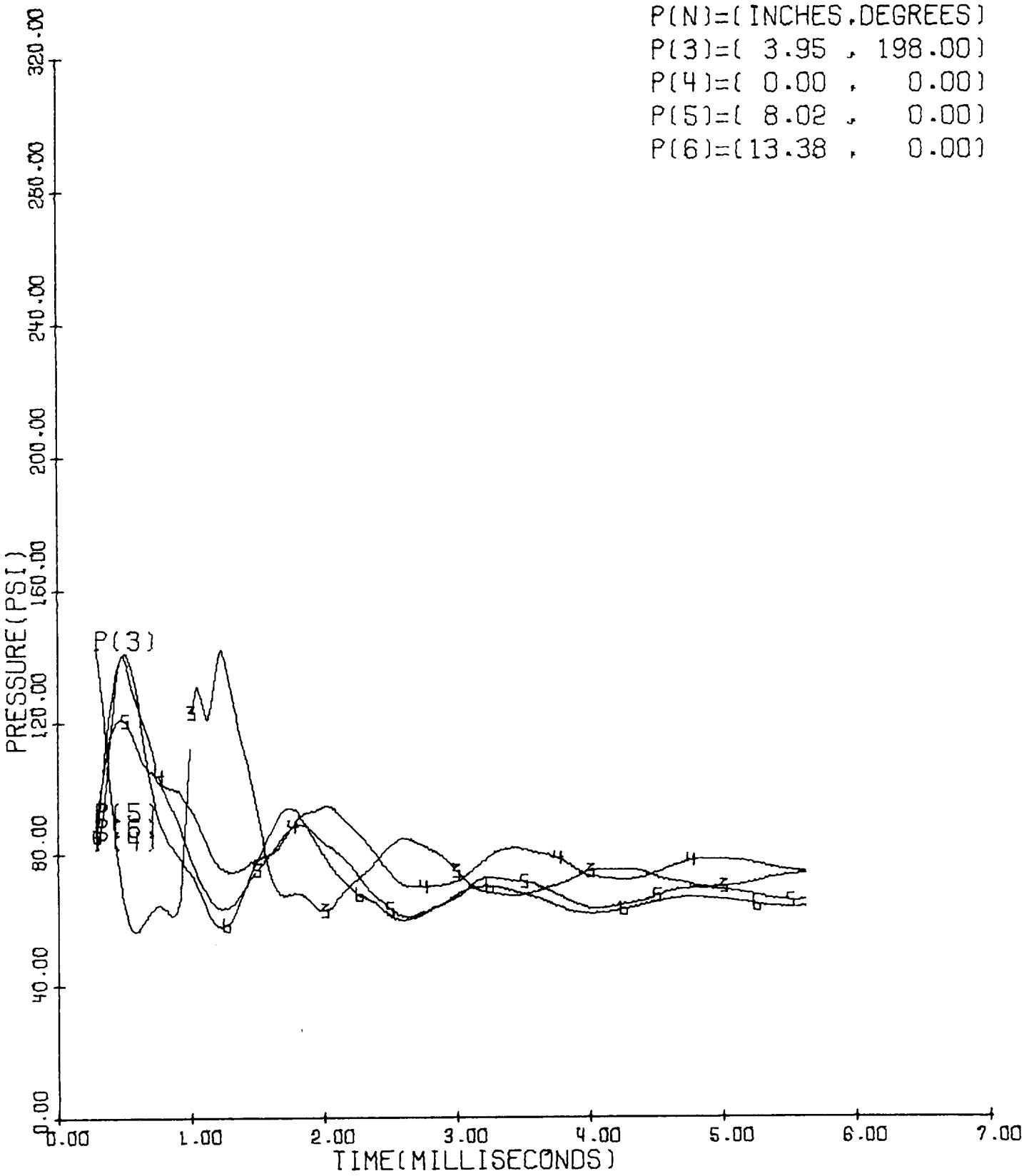

Figure 63

UNBAFFLED, $\dot{m}=0.42$, $A_t/A_c=0.5025$, $\lambda=0.5$

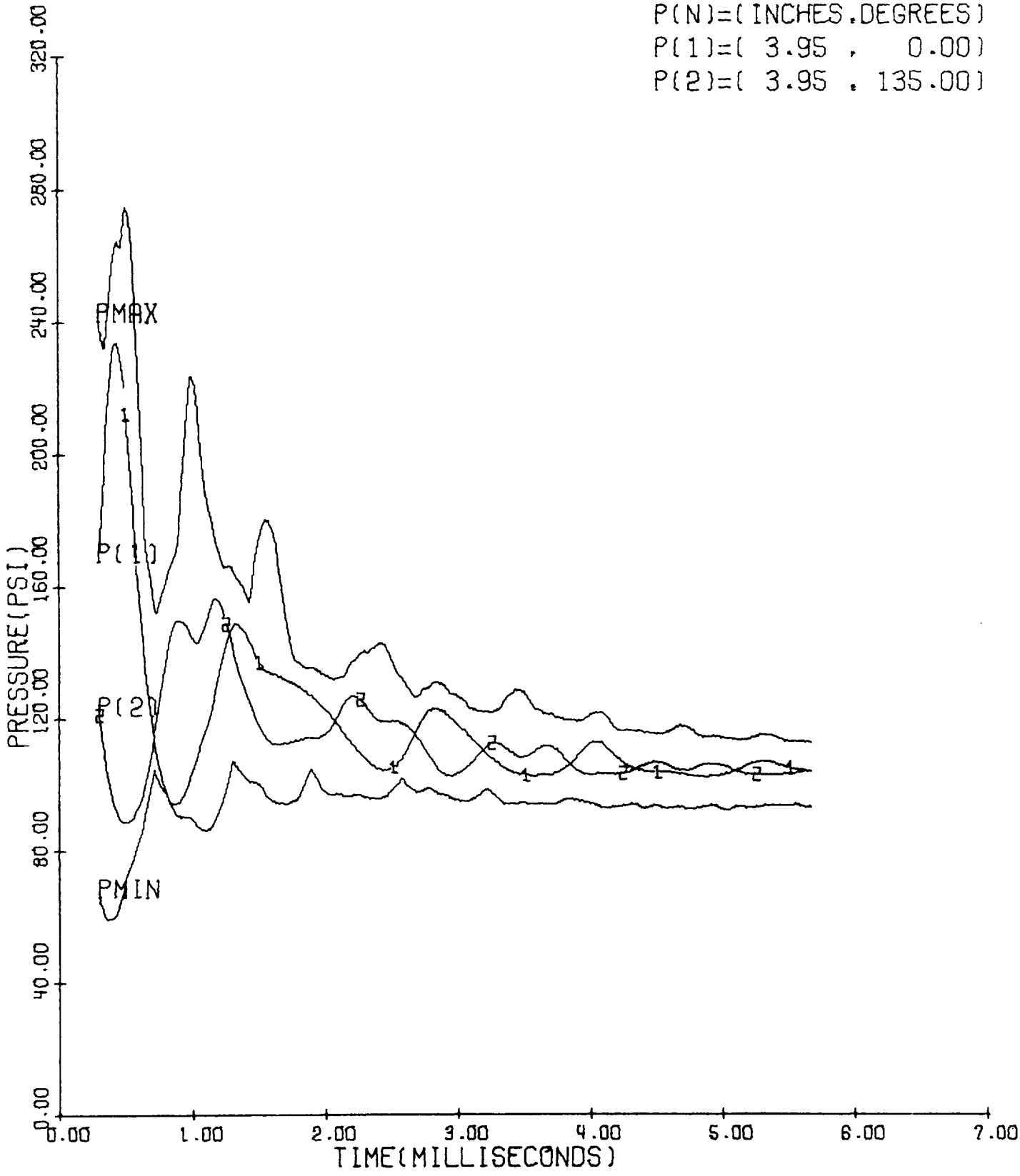

Figure 64

UNBAFFLED, $\dot{m}=0.42$, $A_t/A_c=0.5025$, $\lambda=0.5$

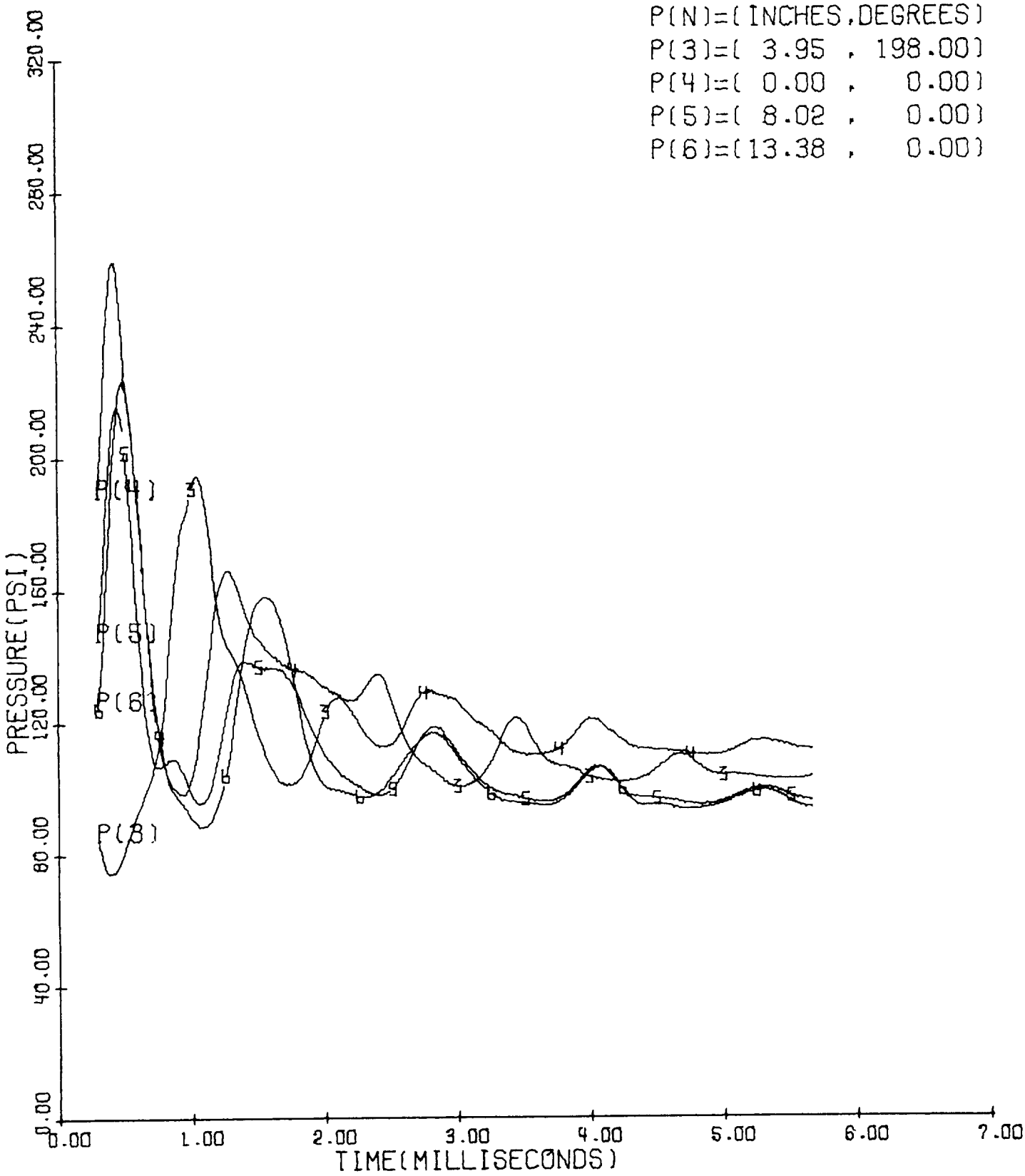

Figure 65

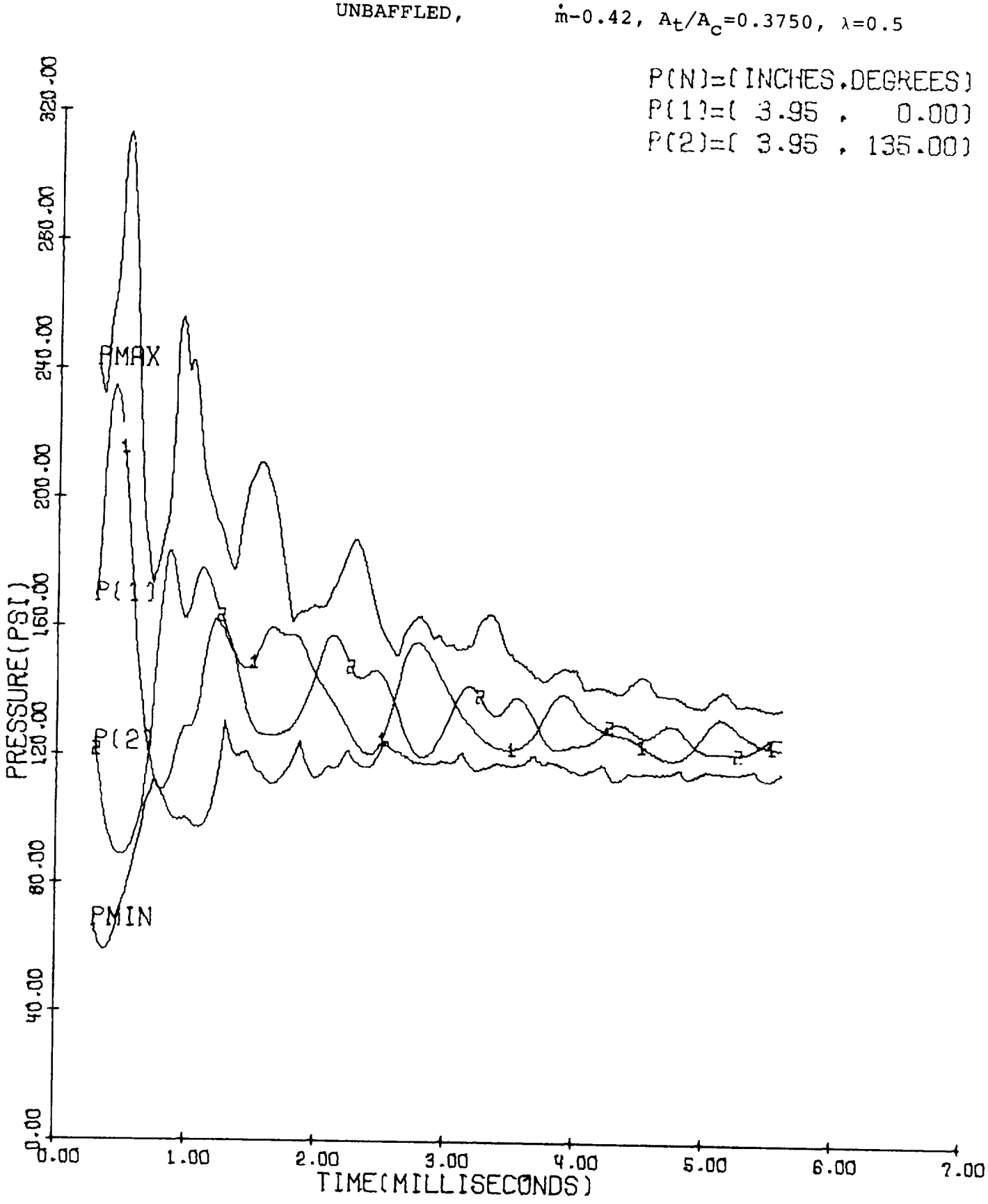
UNBAFFLED, ṁ-0.42, A_t/A_c=0.3750, λ=0.5
P(N)=(INCHES,DEGREES)
P(1)=(3.95 , 0.00)
P(2)=(3.95 , 135.00)
PMAX
P(1)
P(2)
PMIN
PRESSURE(PSI)
320.00
280.00
240.00
200.00
160.00
120.00
80.00
40.00
0.00
0.00
1.00
2.00
3.00
4.00
5.00
6.00
7.00
TIME(MILLISECONDS)

Figure 66

UNBAFFLED, $\dot{m}=0.42$, $A_t/A_c=0.3750$, $\lambda=0.5$

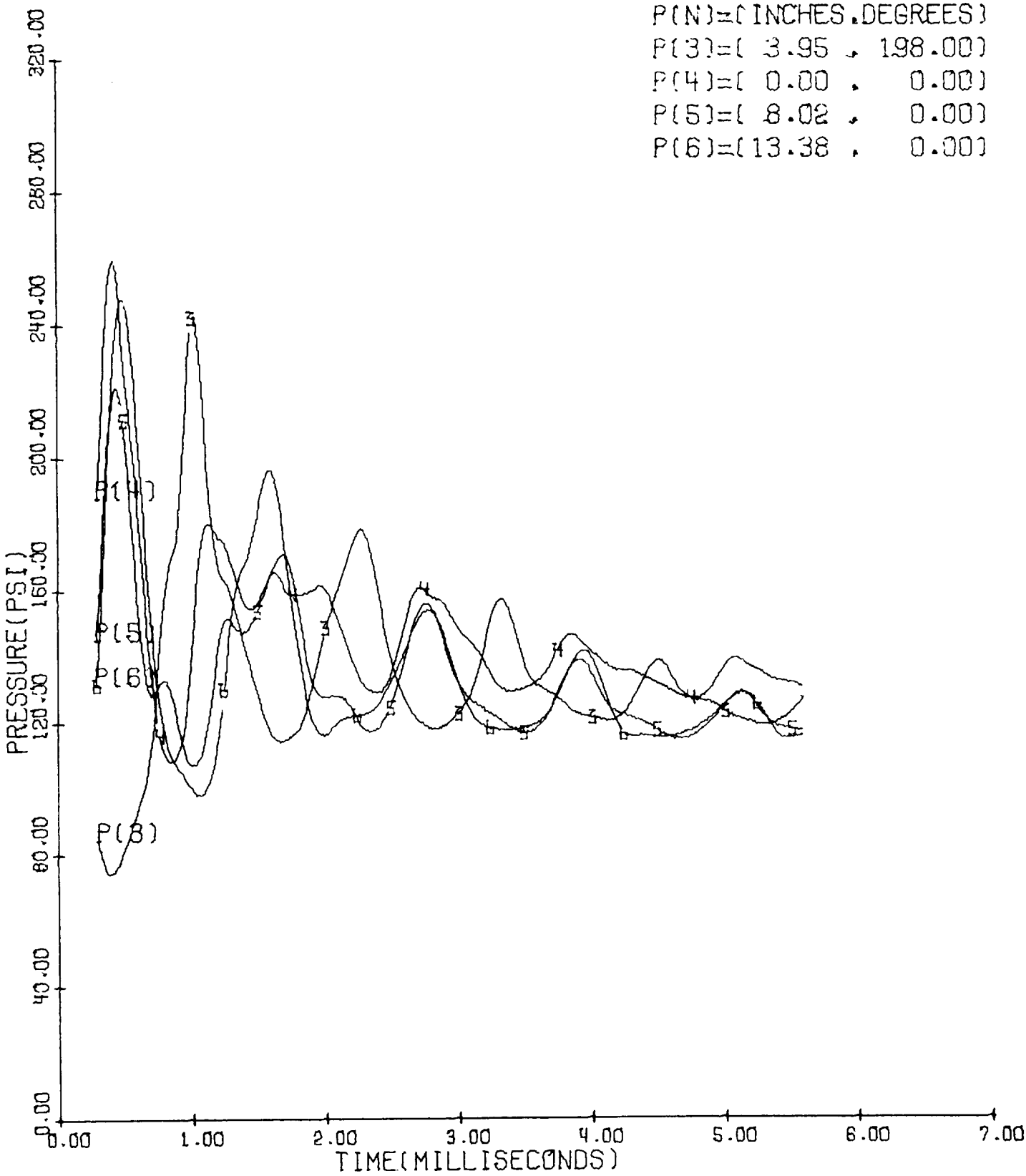

Figure 67

UNBAFFLED, $\dot{m}$=0.42, A_t/A_c=0.6250, λ=0.5

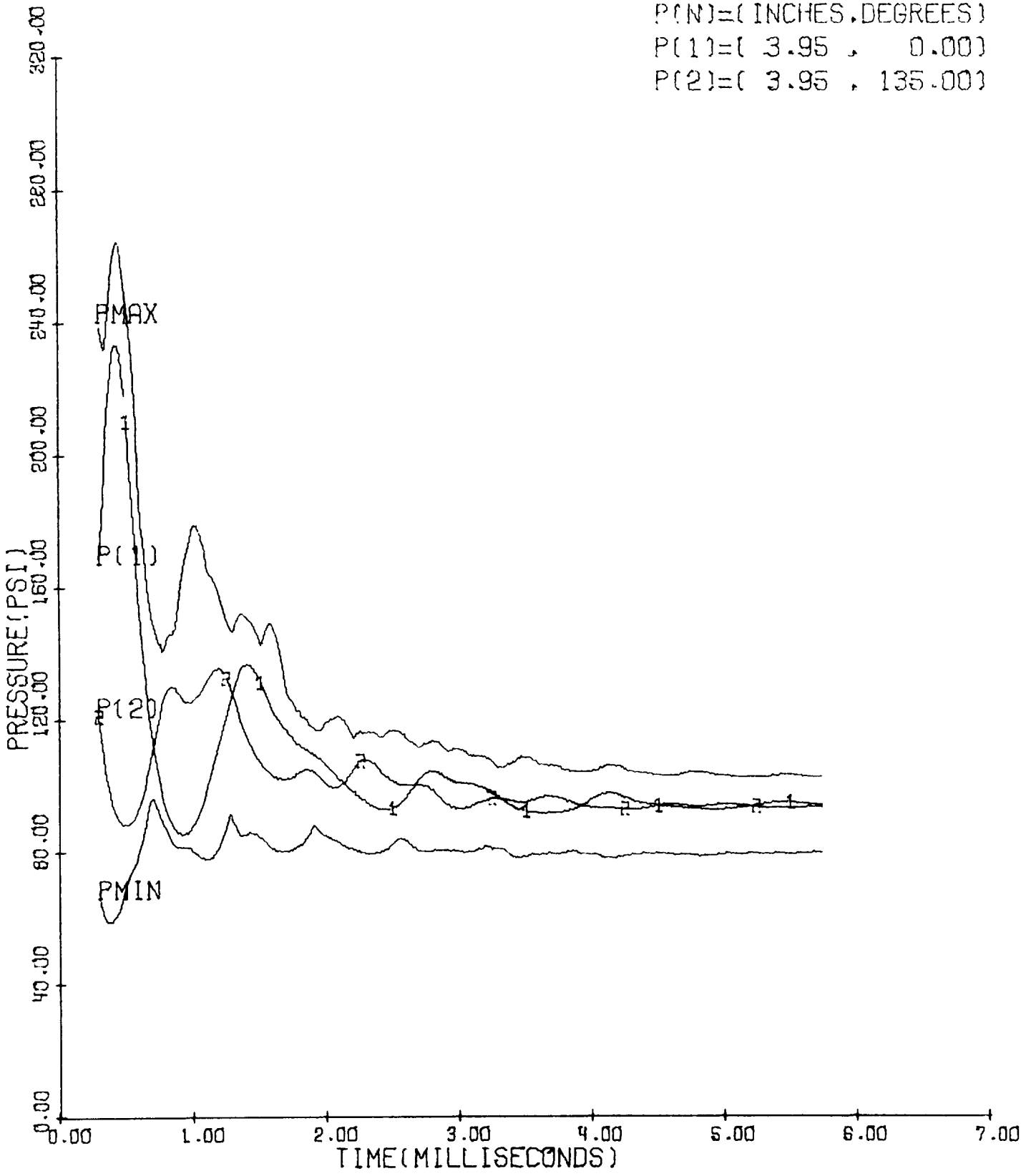

Figure 68

UNBAFFLED, $\dot{m}=0.42$, $A_t/A_c=0.6250$, $\lambda=0.5$

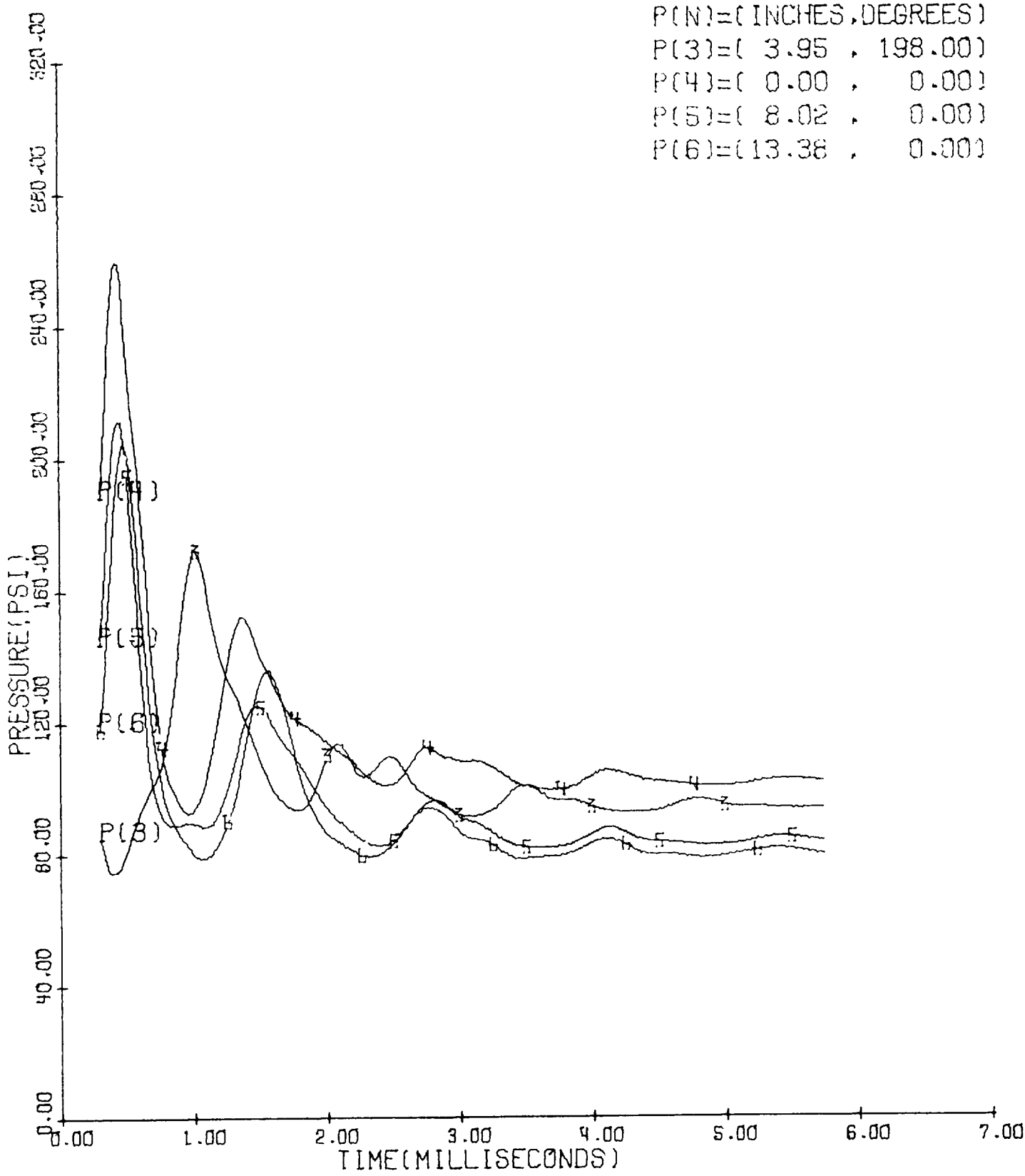

Figure 69

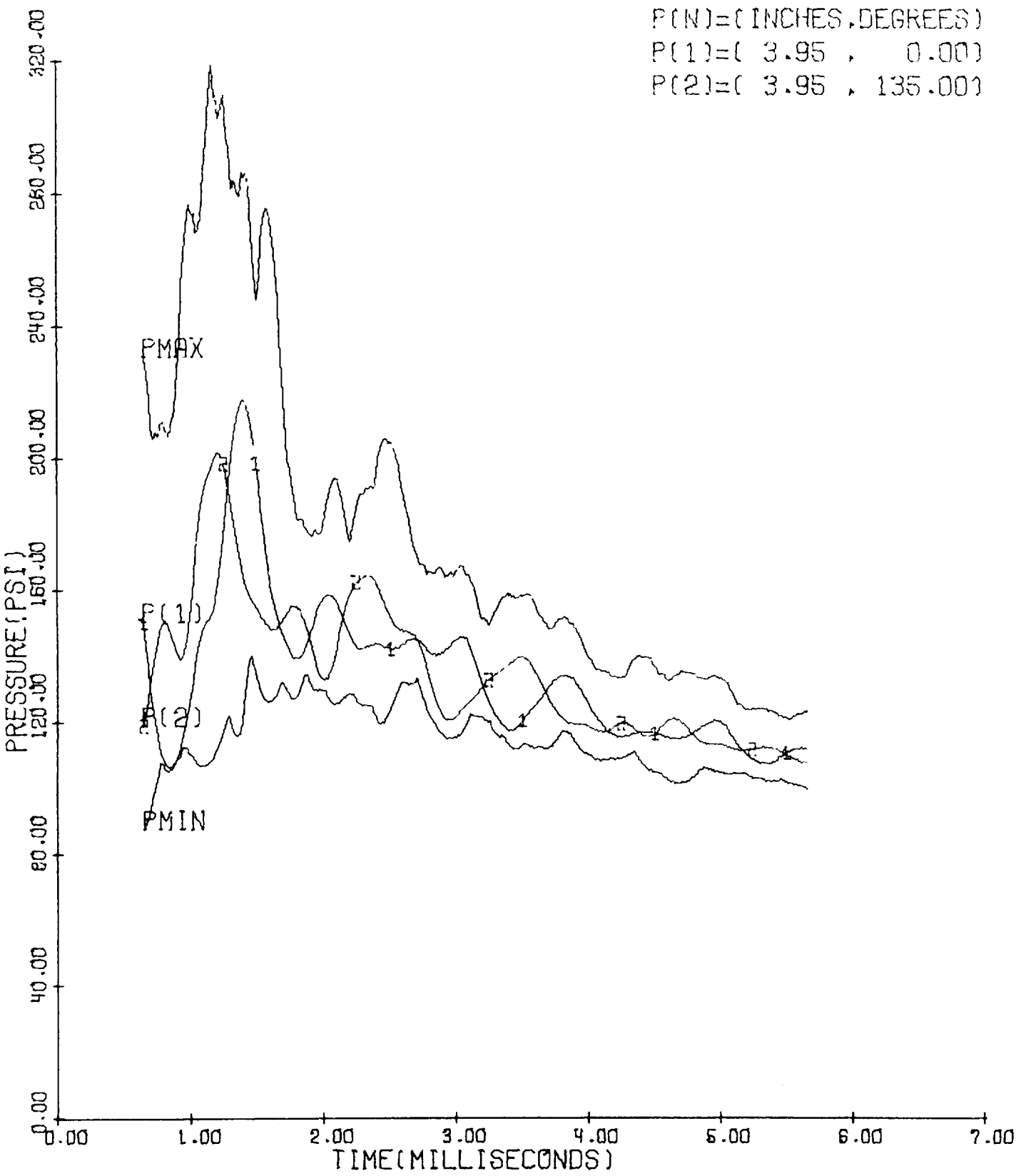
UNBAFFLED, $\dot{m}$=0.42, A_t/A_c=0.5025, λ=1.2
P(N)=(INCHES,DEGREES)
P(1)=(3.95 , 0.00)
P(2)=(3.95 , 135.00)
PMAX
P(1)
P(2)
PMIN
PRESSURE(PSI)
0.00
40.00
80.00
120.00
160.00
200.00
240.00
280.00
320.00
0.00
1.00
2.00
3.00
4.00
5.00
6.00
7.00
TIME(MILLISECONDS)

Figure 70

UNBAFFLED, $\dot{m}=0.42$, $A_t/A_c=0.5025$, $\lambda=1.2$

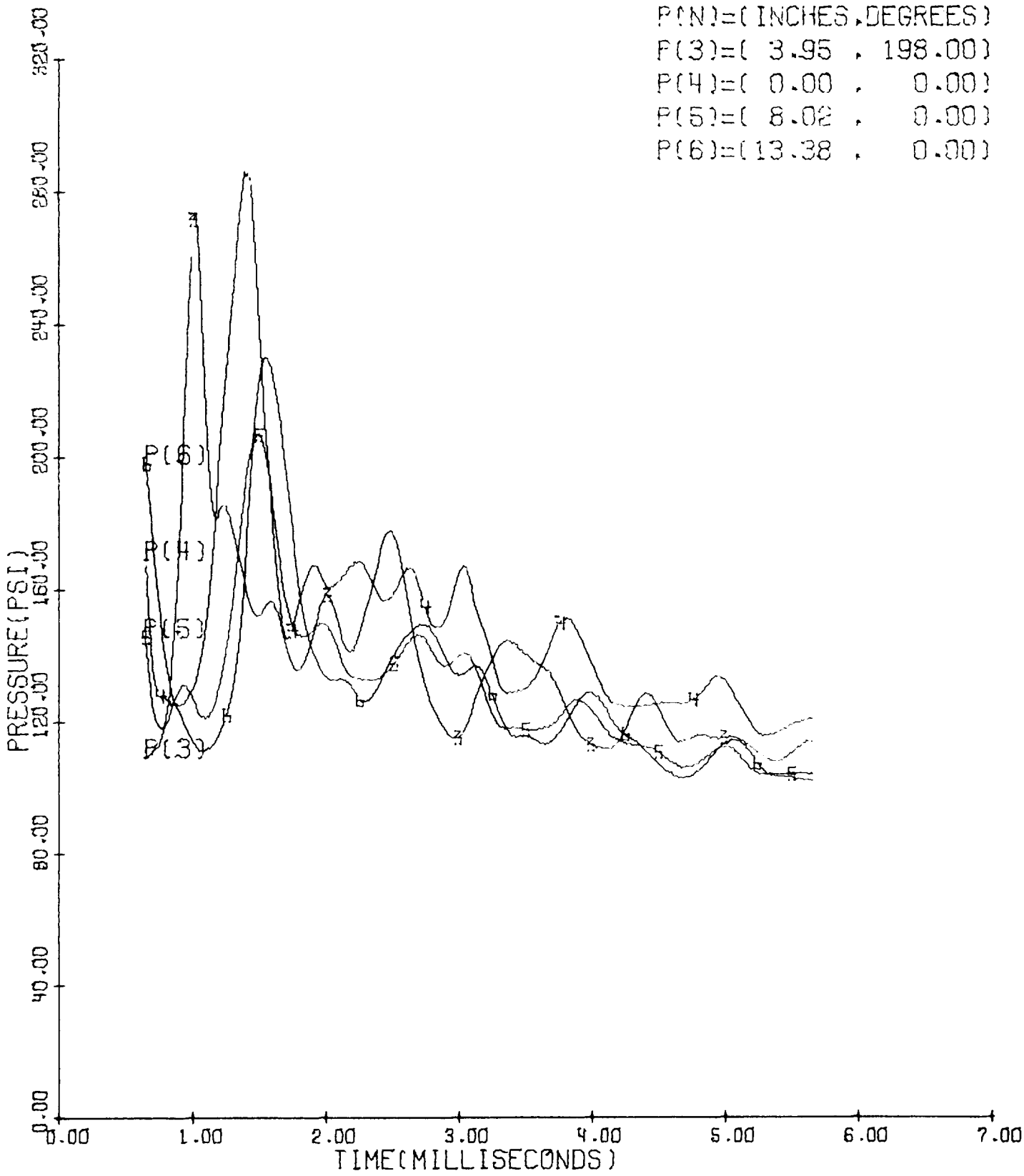

Figure 71

UNBAFFLED, $\dot{m}$=0.42, A_t/A_c=0.5025, λ=0.1

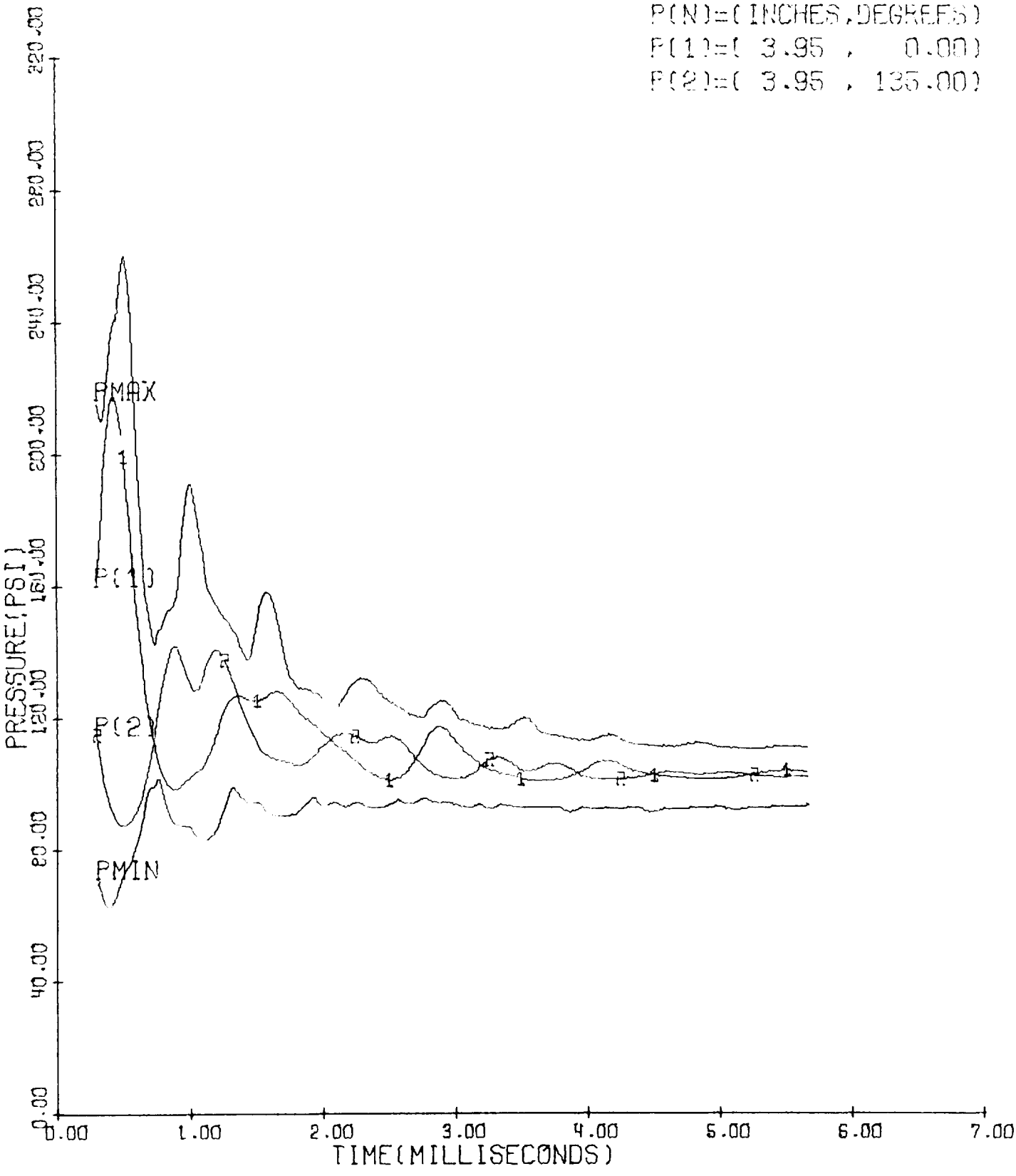

Figure 72

UNBAFFLED, $\dot{m}=0.42$, $A_t/A_c=0.5025$, $\lambda=0.1$

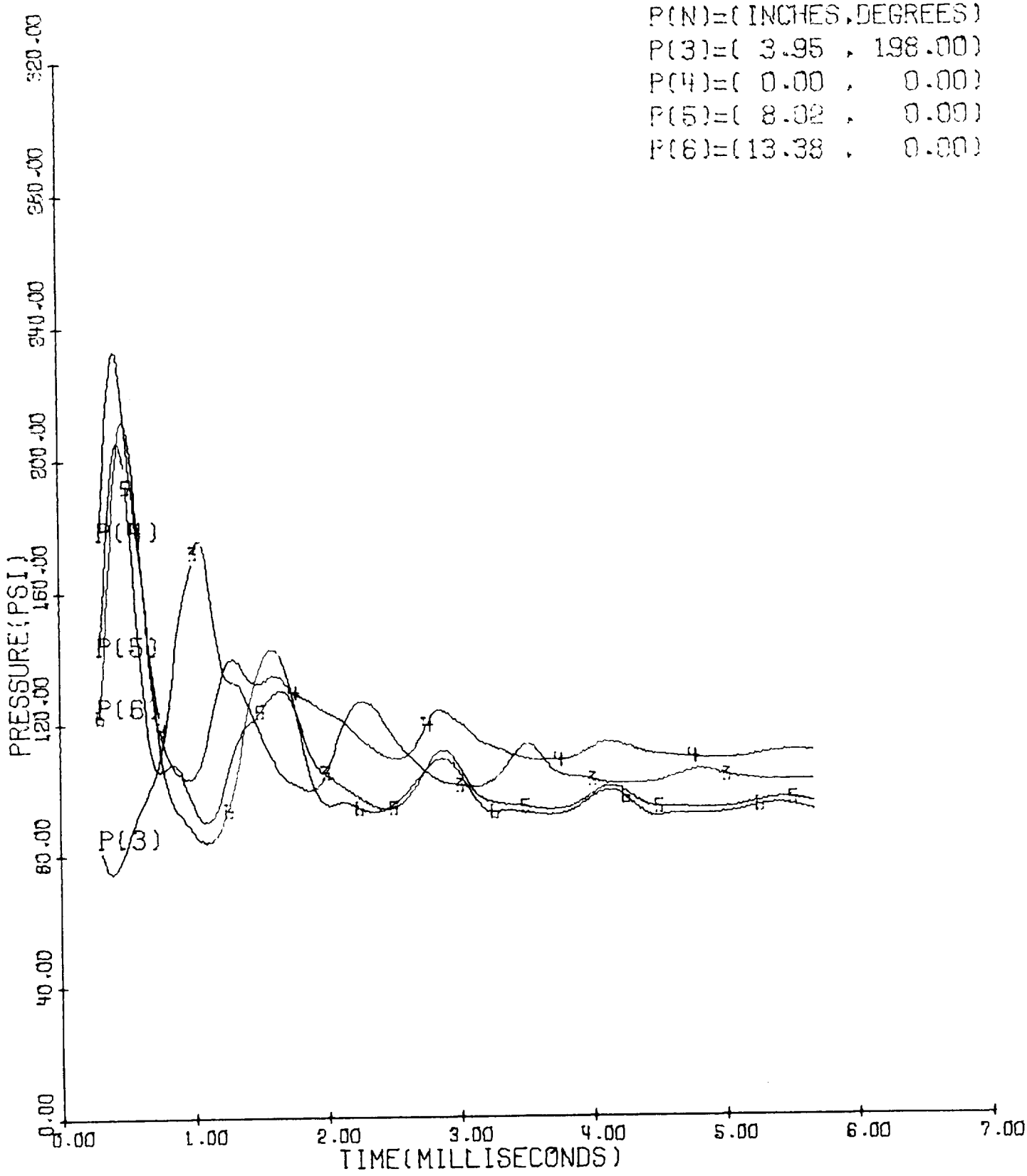

Figure 73

BAFFLED, ℓ=5.375",$\dot{m}$=0.42, A_t/A_c=0.5025, λ=0.5

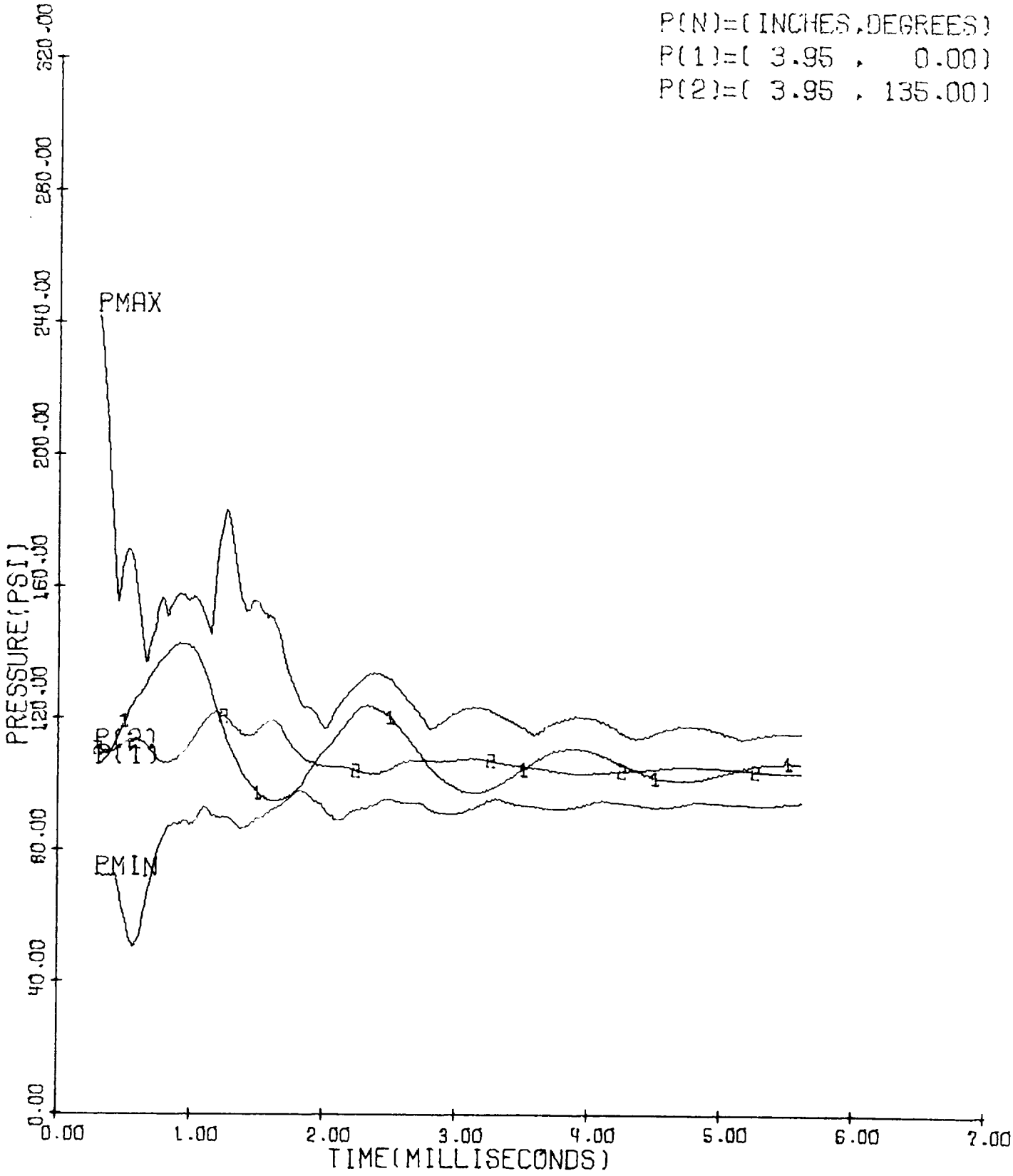

Figure 74

BAFFLED, ℓ=5.375",$\dot{m}$=0.42, A_t/A_c=0.5025, λ=0.5

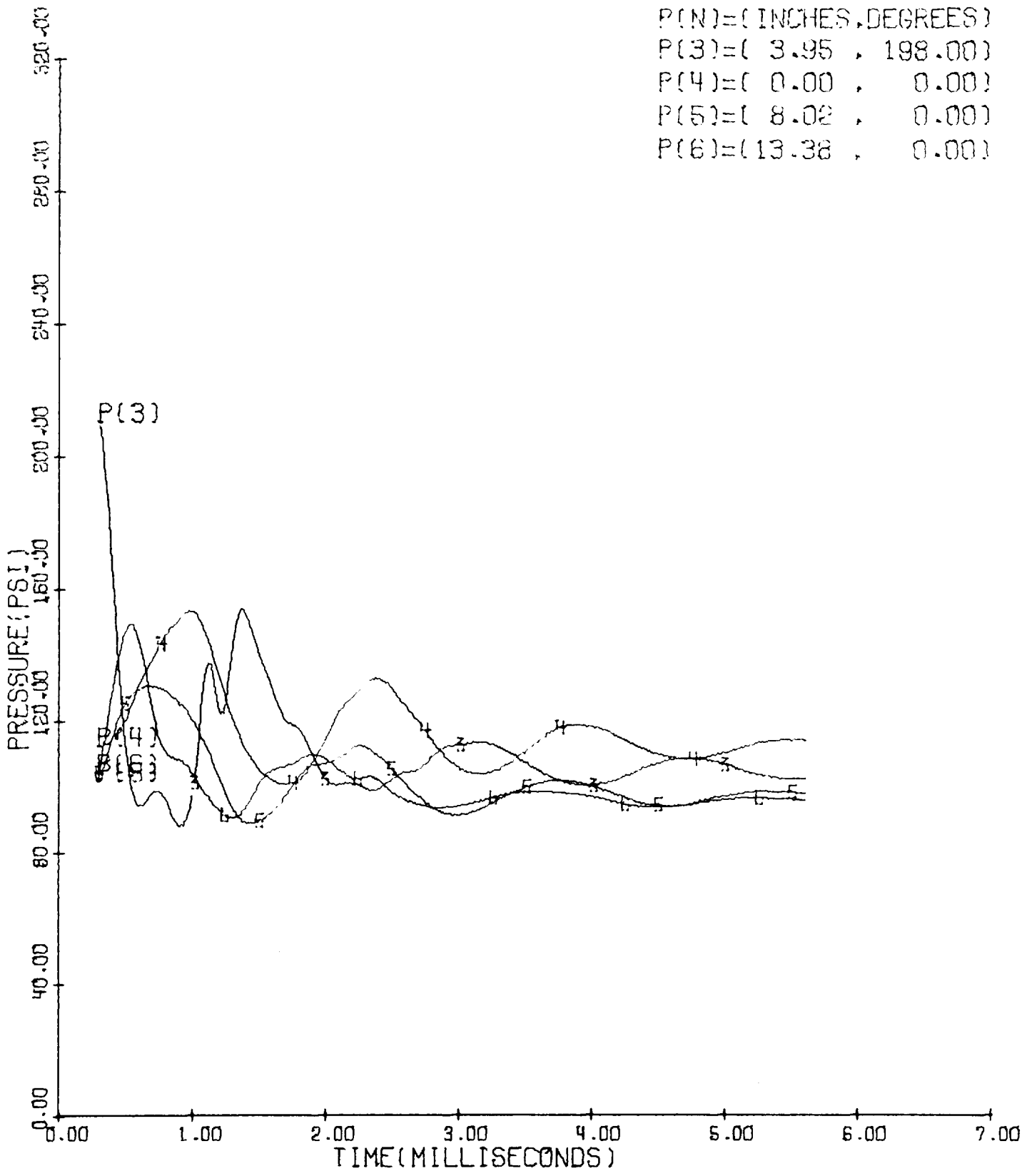

Figure 75

BAFFLED, ℓ=4.375",$\dot{m}$=0.42, A_t/A_c=0.5025, λ=0.5

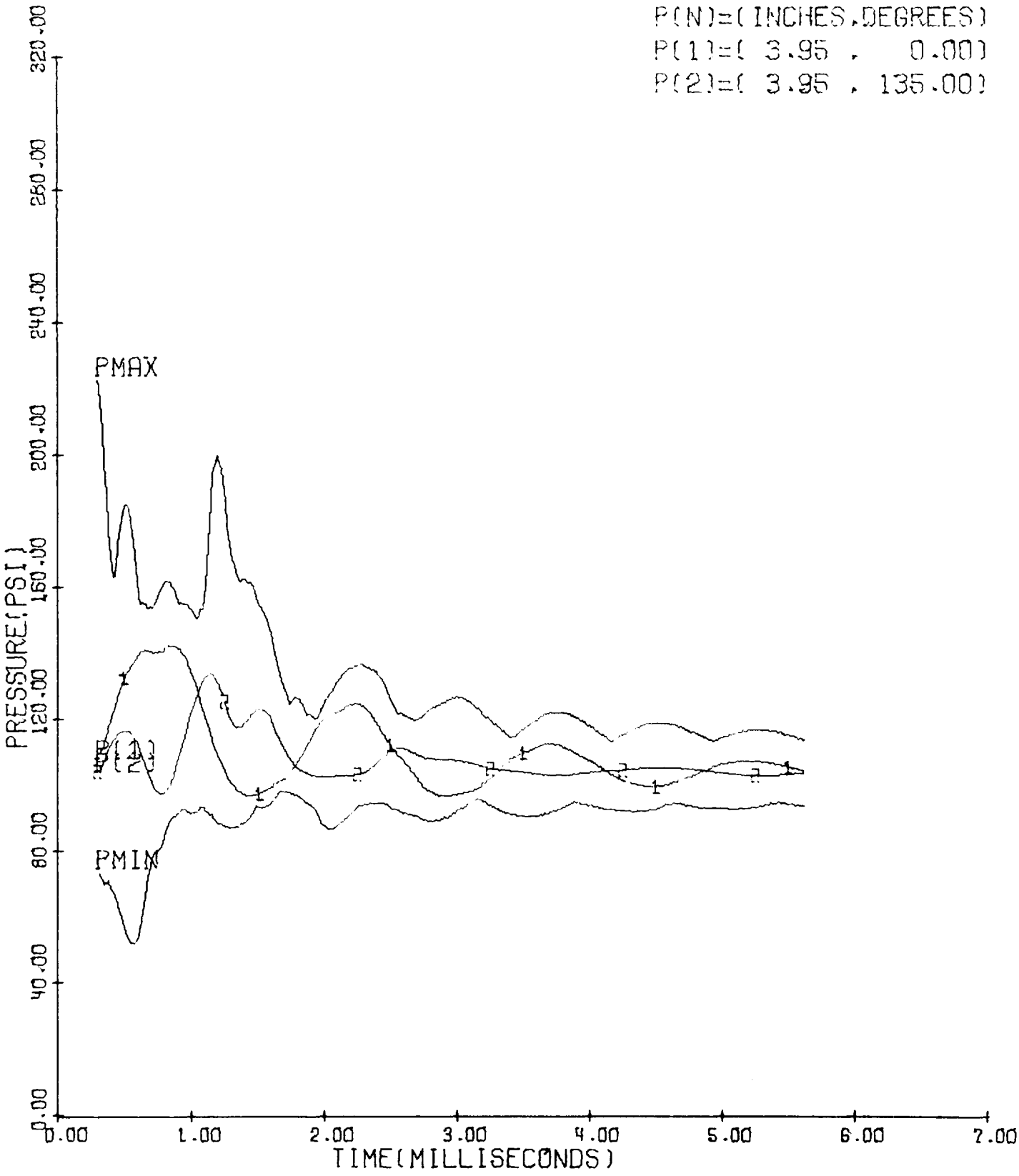

Figure 76

BAFFLED, ℓ=4.375", $\dot{m}$=0.42, A_t/A_c=0.5025, λ=0.5

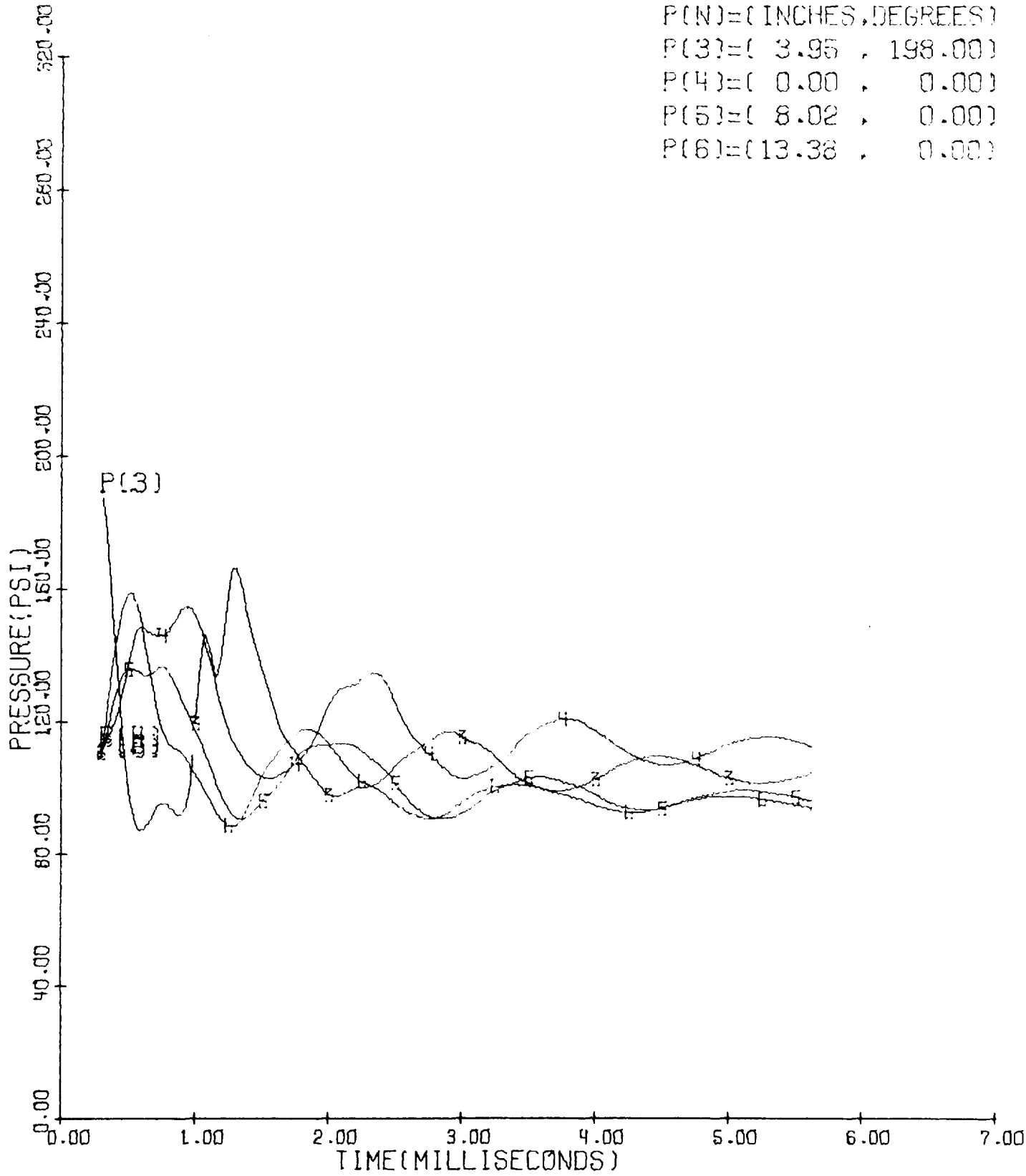

Figure 77

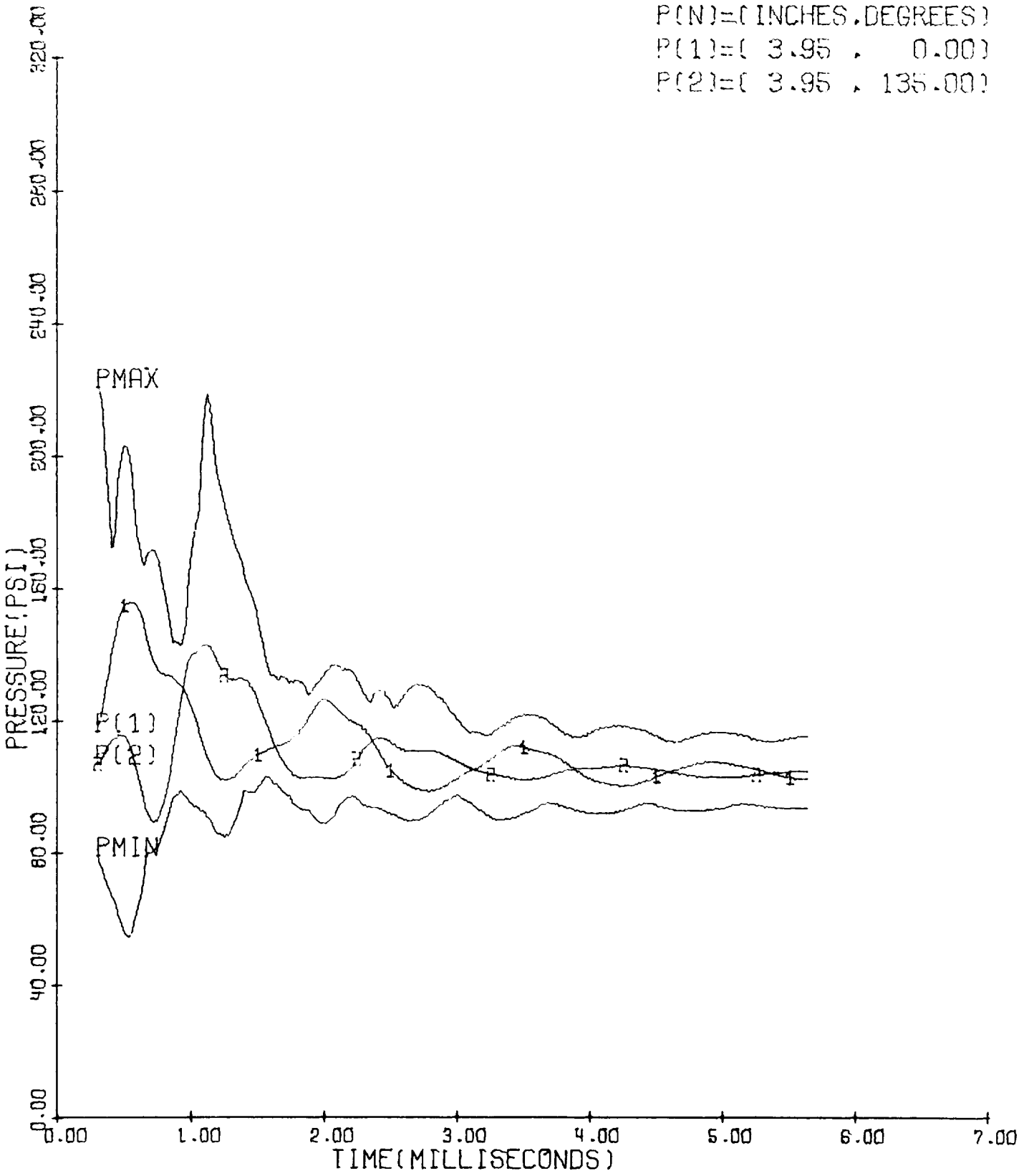
BAFFLED, ℓ=2.875",ṁ=0.42, A_t/A_c=0.5025, λ=0.5
P(N)=(INCHES,DEGREES)
P(1)=(3.95 , 0.00)
P(2)=(3.95 , 135.00)
PMAX
P(1)
P(2)
PMIN
PRESSURE(PSI)
TIME(MILLISECONDS)
0.00
40.00
80.00
120.00
160.00
200.00
240.00
280.00
320.00
1.00
2.00
3.00
4.00
5.00
6.00
7.00

Figure 78

BAFFLED, ℓ=2.875", $\dot{m}$=0.42, A_t/A_c=0.5025, λ=0.5

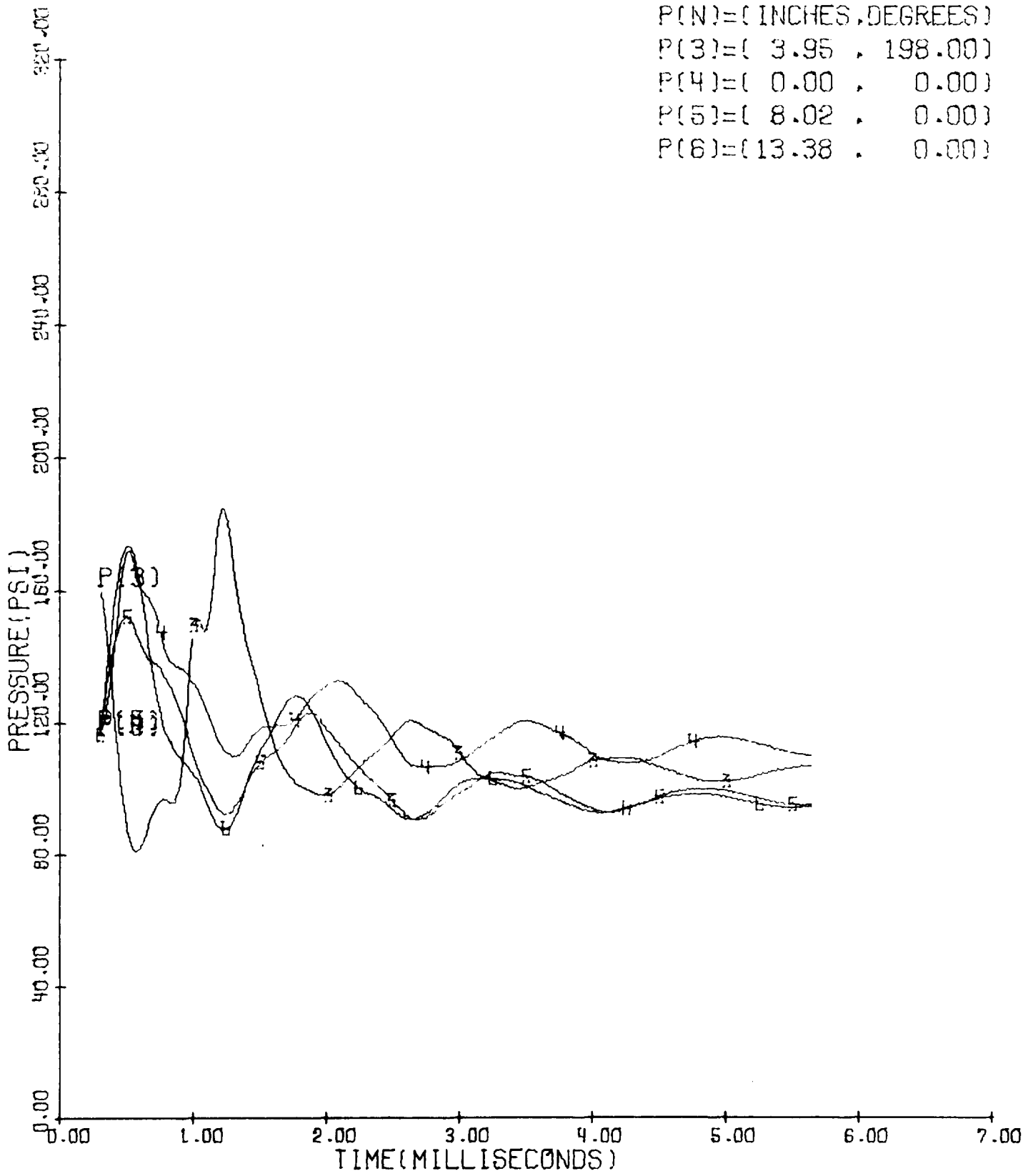

Figure 79

APPENDIX

In addition to the gas and droplet equations, which couple to each other through nonlinear inhomogeneous terms, it is required to describe the spray characteristics through a droplet distribution function

$$f(r_\ell, z, \theta, u_\ell, v_\ell, t)dr_\ell dz d\theta du_\ell dv_\ell dt$$

which describes the number of drops with radius lying between r_ℓ and $r_\ell+dr_\ell$, located in the region of space bounded between z and z+dz, θ and $\theta+d\theta$, having the velocity components in the axial direction and tangential direction lying between u_ℓ and $u_\ell+du_\ell$ and v_ℓ and $v_\ell+dv_\ell$ in the time interval dt. The differential equation describing the evolution of f is given in terms of a hyper-control volume in this six-dimensional space similar to the differential conservation law of the gas dynamic field, i.e.

$$\frac{\partial f}{\partial t} + \frac{\partial}{\partial r_\ell}(Lf) + \frac{\partial}{\partial z}(u_\ell f) + \frac{\partial}{\partial \theta}(v_\ell f) + \frac{\partial}{\partial u_\ell}(F_{u_\ell} f) + \frac{\partial}{\partial v_\ell}(F_{v_\ell} f) = 0 \qquad (A.1)$$

Here we have neglected the source and sink terms due to droplet breakup and coalescence. Hence, we imply that our model is described by a dilute spray. The term $L=dr_\ell/dt$ is the rate of change of droplet radius due to evaporation or droplet heating. The force terms $F_{u_\ell}=du_\ell/dt$, $F_{v_\ell}=dv_\ell/dt$ are per unit mass and are due to aerodynamic forces while $u_\ell=dz/dt$, $v_\ell=d\theta/dt$ are the rate of

change of droplet position which we have denoted previously as the local droplet velocity components. For steady-state spray combustion $\partial f/\partial t=0$ can be used to simplify (A.1). In addition, if the reasonable behavior of f, i.e. $|f(u_\ell,v_\ell)|\to 0$ as $|u_\ell|\to\infty$ and $|v_\ell|\to\infty$ is used when (A.1) is integrated over velocity space, the use of the divergence theorem leads to the vanishing of the last two terms of (A.1). Then if one defines the average quantities

$$\bar{L} = \int Lf du_\ell dv_\ell / \int f du_\ell dv_\ell$$

$$\bar{u}_\ell = \int u_\ell f du_\ell dv_\ell / \int f du_\ell dv_\ell$$

$$\bar{v}_\ell = \int v_\ell f du_\ell dv_\ell / \int f du_\ell dv_\ell$$

and the number density n of droplets per unit volume per unit radius (per unit time if there is time dependence in f)

$$n = \int_{-\infty}^{\infty} f du_\ell dv_\ell$$

Equation (A.1) becomes

$$\frac{\partial n}{\partial t} + \frac{\partial}{\partial r_\ell}(n\bar{L}) + \frac{\partial}{\partial z}(n\bar{u}_\ell) + \frac{\partial}{\partial \theta}(n\bar{v}_\ell)=0 \qquad \text{(A.2)}$$

If the combustion model is truly time dependent and two-dimensional then (A.2) cannot be simplified any further and one seeks a solution $n=n(r,z,\theta,t)$ which satisifes (A.2) subject to the mean

quantities $\bar{L}=\bar{L}(r_\ell,z,\theta,t)$, $\bar{u}_\ell=\bar{u}_\ell(r_\ell,z,\theta,t)$ and $\bar{v}_\ell=\bar{v}_\ell(r_\ell,z,\theta,t)$. The dependence of $\bar{u}_\ell$ and $\bar{v}_\ell$ on r_ℓ implies that the velocity distribution of the particles will depend on size. This will be true if different drag laws are used for different drop sizes and if a single drag law depends on drop size groups when the forces on the droplets are computed.

To help solve (A.2), one may consider a single droplet size which is a mean value for the spray. Then (A.2) is solved for this single drop along with the conservation laws applied to this single drop group. This equation is still complicated because it is to be solved in four-dimensional space. Rather than carry this project out, even using finite difference methods, we choose a more restricted dependence on the distribution function f.

Our model assumes that f is independent of time, i.e. f is prescribed to be

$$f=n(r,z,\theta_i)\delta(u-u_\ell)\delta(v-v_\ell) \qquad (A.3)$$

with

$$n=\delta(\theta-\theta_i)\delta(r-r_\ell)N(z) \quad 0\leq z\leq L$$

where L is the combustor length and θ_i is defined below. Here δ is the one-dimensional Dirac delta function which satisfies

$$\delta(x-x_o) = 1 \text{ if } x=x_o$$

$$= 0 \text{ otherwise}$$

and

$$\int \delta(x-x_o)dx = 1$$

If $x=x_o$ is in the range of integration.

The above definition for f insures that the spray properties are dependent on a single discrete value of drop radius and velocity; f is defined at discrete theta points. Here $\theta_i=\theta_o+i\Delta\theta$, $i=1,2,\ldots,J$; $J=2\Pi/N_\theta$ and N_θ is the number of intervals in the tangential direction.

We use

$$N(z) = N \text{ if } 0.1r_\ell^o \leq r_\ell(z) \leq r_\ell^o$$

$$= 0 \text{ otherwise} \qquad (A.4)$$

With this choice of distribution function, (A.3) and (A.4) satisfies (A.2). The constant N, which has the units drops per unit volume, is so chosen that the flow through the combustion chamber, when no disturbances are present, results in a prescribed pressure level at the injector, z=0. Then to compute the inhomogeneous term in the continuity equation, $\dot{m}$, and in the energy equation, $\dot{E}$, for the gas dynamic equations we use

$$\dot{m} = N\dot{m}_\ell$$

$$\dot{E} = N\dot{E}_\ell \qquad (A.5)$$

where $\dot{m}_\ell$ and $\dot{E}_\ell$ are the mass and energy release rates per drop.

DISTRIBUTION LIST

CONTRACT NAS 7 752

COPIES	RECIPIENT	DESIGNEE
	NASA HEADQUARTERS WASHINGTON, D.C. 20546	
1	CONTRACTING OFFICER	%X"
1	PATENT OFFICE	%X"
	NASA LEWIS RESEARCH CENTER 21000 BROOKPARK RD. CLEVELAND, OHIO 44135	
1	OFFICE OF TECHNICAL INFORMATION	%X"
1	DR. R. J. PRIEM	%X"
	NASA MANNED SPACECRAFT CENTER HOUSTON, TEXAS 77001	
1	OFFICE OF TECHNICAL INFORMATION	%X"
	NASA MARSHALL SPACE FLIGHT CENTER HUNTSVILLE, ALABAMA 35812	
1	TECHNICAL LIBRARY	%X"
1	DALE BURROWS, S+E, ATTN-PJ BLDG 4666	%X"
	NASA PASADENA OFFICE 4800 OAK GROVE DRIVE PASADENA, CALIFORNIA 91103	
1	PATENTS AND CONTRACTS MANAGEMENT	%X"
	JET PROPULSION LABORATORY 4800 OAK GROVE DR. PASADENA, CALIF. 91103	
2	JACK H. RUPE	%X"
3	CHIEF, LIQUID PROPULSION TECHNOLOGY RPL OFFICE OF ADVANCED RESEARCH AND TECHNOLOGY NASA HEADQUARTERS WASHINGTON, D.C., 20546	%X"
1	DIRECTOR, TECHNOLOGY UTILIZATION DIVISION OFFICE OF TECHNOLOGY UTILIZATION NASA HEADQUARTERS WASHINGTON, D.C., 20546	%X"

COPIES	RECIPIENT	DESIGNEE
25	NASA SCIENTIFIC AND TECHNICAL INFORMATION FACILITY P.O.BOX 33 COLLEGE PARK, MARYLAND 20740	%X"
1	DIRECTOR, LAUNCH VEHICLES AND PROPULSION, SV OFFICE OF SPACE SCIENCE AND APPLICATIONS NASA HEADQUARTERS WASHINGTON, D.C., 20546	%X"
1	DIRECTOR, ADVANCED MANNED MISSIONS, MT OFFICE OF MANNED SPACE FLIGHT NASA HEADQUARTERS WASHINGTON, D.C., 20546	%X"
1	MISSION ANALYSIS DIVISION NASA AMES RESEARCH CENTER MOFFETT FIELD, CALIFORNIA 24035	%X"

NASA FIELD CENTERS

1	AMES RESEARCH CENTER MOFFETT FIELD, CALIF. 94035	ALBERTA ALKSNE N-203-9
2	LEWIS RESEARCH CENTER 21000 BROOKPARK ROAD CLEVELAND, OHIO 44135	E. W. CONRAD ALLEN J. METZLER
1	GODDARD SPACE FLIGHT CENTER GREENBELT, MARYLAND 20771	MERLAND L. MOSESON CODE 620
2	JET PROPULSION LABORATORY CALIFORNIA INSTITUTE OF TECHNOLOGY 4800 OAK GROVE DRIVE PASADENA, CALIFORNIA 91103	HENRY BURLAGE, JR PROPULSION DIV. 38
2	LANGLEY RESEARCH CENTER LANGLEY STATION HAMPTON, VIRGINIA 23365	ED CORTWRIGHT DIRECTOR
2	LEWIS RESEARCH CENTER 21000 BROOKPARK ROAD CLEVELAND, OHIO 44135	DR. ABE SILVERSTEIN DIRECTOR

COPIES	RECIPIENT	DESIGNEE
2	MANNED SPACECRAFT CENTER HOUSTON, TEXAS 77001	J.G. THIBODAUX, JR. CHIEF, PROP. + POWER
2	JOHN F. KENNEDY SPACE CENTER, NASA COCOA BEACH, FLORIDA 32931	DR. KURT H. DEBUS

GOVERNMENT INSTALLATIONS

1	AERONAUTICAL SYSTEMS DIVISION AIR FORCE SYSTEMS COMMAND WRIGHT-PATTERSON AIR FORCE BASE DAYTON, OHIO 45433	D.L. SCHMIDT CODE ASRCNC-2
1	ARNOLD ENGINEERING DEVELOPMENT CENTER ARNOLD AIR FORCE STATION TULLAHOMA, TENNESSEE 37388	DR. H. K. DOETSCH
1	BUREAU OF NAVAL WEAPONS DEPARTMENT OF THE NAVY WASHINGTON, D.C., 20546	J. KAY RIMS-41
1	DEFENSE DOCUMENTATION CENTER HEADQUARTERS CAMERON STATION, BUILDING 5 5010 DUKE STREET ALEXANDRIA, VIRGINIA 22314 ATTN: TISIA	
1	PICATINNY ARSENAL DOVER, NEW JERSEY 07801	I. FORSTEN, CHIEF LIQUID PROPULSION LABORATORY,
2	AIR FORCE ROCKET PROPULSION LABORATORY RESEARCH AND TECHNOLOGY DIVISION AIR FORCE SYSTEMS COMMAND EDWARDS, CALIFORNIA 93523	RPRPD/MR. H. MAIN
1	U. S. ARMY MISSILE COMMAND REDSTONE ARSENAL ALABAMA 35809	MR. WALTER WHARTON
1	U. S. BUREAU OF MINES 4800 FORBES AVE. PITTSBURGH, PENN. 15213	MR. HENRY PERLEE

COPIES	RECIPIENT	DESIGNEE
1	U. S. NAVAL ORDNANCE TEST STATION CHINA LAKE CALIFORNIA 93557	D. COUCH
1	AIR FORCE OFFICE OF SCIENTIFIC RESEARCH 1400 WILSON BLVD. ARLINGTON, VIRGINIA 22209	B. T. WOLFSON

CPIA

1	CHEMICAL PROPULSION INFORMATION AGENCY APPLIED PHYSICS LABORATORY 8621 GEORGIA AVENUE SILVER SPRING, MARYLAND 20910	TOM REEDY

INDUSTRY CONTRACTORS

1	AEROJET-GENERAL CORPORATION P.O.BOX 296 AZUSA, CALIFORNIA 91703	W. L. ROGERS
1	SPACE DIVISION AEROJET-GENERAL CORPORATION 9200 EAST FLAIR DR. EL MONTE, CALIFORNIA 91734	S. MACHLAWSKI
1	AEROSPACE CORPORATION 2400 EAST EL SEGUNDO BOULEVARD P.O.BOX 95085 LOS ANGELES, CALIFORNIA 90045	O. W. DYKEMA
1	ATLANTIC RESEARCH CORPORATION EDSALL ROAD AND SHIRLEY HIGHWAY ALEXANDRIA, VIRGINIA 22314	LIBRARIAN
1	BELL AEROSYSTEMS COMPANY P.O.BOX 1 BUFFALO, NEW YORK 14240	W. M. SMITH
1	BOEING COMPANY P.O.BOX 3707 SEATTLE, WASHINGTON 98124	J. D. ALEXANDER

COPIES	RECIPIENT	DESIGNEE
1	WRIGHT AERONAUTICAL DIVISION CURTISS-WRIGHT CORPORATION WOOD-RIDGE, NEW JERSEY 07075	G. KELLEY
1	RESEARCH CENTER FAIRCHILD HILLER CORPORATION GERMANTOWN, MARYLAND	RALPH HALL
1	MISSILE AND SPACE SYSTEMS CENTER GENERAL ELECTRIC COMPANY VALLEY FORGE SPACE TECHNOLOGY CENTER P.O.BOX 8555 PHILADELPHIA, PA.	F. MEZGER F. E. SCHULTZ
1	GRUMMAN AIRCRAFT ENGINEERING CORP. BETHPAGE, LONG ISLAND NEW YORK 11714	JOSEPH GAVIN
1	HONEYWELL, INC. AEROSPACE DIV. 2600 RIDGWAY RD. MINNEAPOLIS, MINN.	MR. GORDON HARMS
1	HUGHES AIRCRAFT CO. AEROSPACE GROUP CENTINELA AND TEALE STREETS CULVER CITY, CALIF. 90230	E. H. MEIER V.P. AND DIV. MGR., RESEARCH + DEV. DIV.
1	ARTHUR D. LITTLE, INC. 20 ACORN PARK CAMBRIDGE, MASSACHUSETTS 02140	LIBRARY
1	LOCKHEED PROPULSION COMPANY P.O.BOX 111 REDLANDS, CALIFORNIA 92374.	H. L. THACKWELL
1	THE MARQUARDT CORPORATION 16555 SATICOY STREET VAN NUYS, CALIFORNIA 91409	HOWARD MC FARLAND
1	DENVER DIVISION MARTIN MARIETTA CORPORATION P.O.BOX 179 DENVER, COLORADO 80201	DR. MORGANTHALER A. J. KULLAS
1	ASTROPOWER LABORATORY MC DONNELL-DOUGLAS AIRCRAFT CO. 2121 PAULARINO NEWPORT BEACH, CALIF. 92663	DR. GEORGE MOC DIRECTOR, RESEARCH

COPIES	RECIPIENT	DESIGNEE
1	MISSILE AND SPACE SYSTEMS DIVISION MC DONNELL-DOUGLAS AIRCRAFT CO. 3000 OCEAN PARK BOULEVARD SANTA MONICA, CALIF. 90406	MR. R. W. HALLET CHIEF ENGINEER ADV. SPACE TECH.
1	SPACE + INFORMATION SYSTEMS DIVISION NORTH AMERICAN ROCKWELL 12214 LAKEWOOD BOULEVARD DOWNEY, CALIFORNIA 90241	LIBRARY
1	ROCKETDYNE C/0 LIBRARY 586-306 6633 CANOGA AVENUE CANOGA PARK, CALIF. 91304	DR. R. J. THOMPSON S. F. IACOBELLIS
1	NORTHROP SPACE LABORATORIES 3401 WEST BROADWAY HAWTHORNE, CALIFORNIA 90250	DR. WILLIAM HOWARD
1	STANFORD RESEARCH INSTITUTE 333 RAVENSWOOD AVENUE MENLO PARK, CALIFORNIA 94025	DR. GERALD MARKSMAN
1	TRW SYSTEMS GROUP TRW INCORPORATED ONE SPACE PARK REDONDO BEACH, CALIF. 90278	G. W. ELVERUM
1	REACTION MOTORS DIVISION THIOKOL CHEMICAL CORPORATION DENVILLE, NEW JERSEY 07832	DWIGHT S. SMITH
1	RESEARCH LABORATORIES 400 MAIN ST. EAST HARTFORD, CONN. 06108	ERLE MARTIN
1	UNITED TECHNOLOGY CENTER 587 METHILDA AVENUE P.O.BOX 358 SUNNYVALE, CALIFORNIA 94088	DR. DAVID ALTMAN
1	ROCKETDYNE A DIV. OF NORTH AMERICAN ROCKWELL 6633 CANOGA AVENUE CANOGA PARK, CALIFORNIA 91304	R. B. LAWHEAD

COPIES	RECIPIENT	DESIGNEE
1	PRATT ? WHITNEY AIRCRAFT FLORIDA RESEARCH ? DEVELOPMENT CTR. P.O.BOX 2691 WEST PALM BEACH, FLORIDA 33402	G. D. LEWIS
1	DEFENSE RESEARCH CORPORATION P.O.BOX 3587 SANTA BARBARA, CALIFORNIA 93105	. GRAY
1	AEROJET-GENERAL CORPORATION P.O.BOX 1947 SACRAMENTO, CALIFORNIA 95809	DAVID KORS
1	DYNAMIC SCIENCE 2400 MICHELSON DRIVE IRVINE, CALIF. 92664	THOMAS TYSOM
1	MATHEMATICAL APPLICATIONS GROUP, INC. 180 SO. BROADWAY WHITE PLAINS, NEW YORK 10605	DR. S. Z. BURNSTEIN
	UNIVERSITIES	
1	OHIO STATE UNIVERSITY DEPT. OF AERONAUTICAL ENG. COLUMBUS, OHIO 43210	R. EDSE
1	PENNSYLVANIA STATE UNIV. MECH. ENGINEERING DEPT. 207 MECHANICAL ENGINEERING BLVD. UNIVERSITY PARK, PA. 16802	G. M. FAETH
1	UNIVERSITY OF SOUTHERN CALIF. DEPT. OF MECH ENG UNIVERSITY PARK LOS ANGELES, CALIF. 90007	M. GERSTEIN
1	PRINCETON UNIVERSITY FORRESTAL CAMPUS GUGGENHEIM LABORATORIES PRINCETON, NEW JERSEY 08540	D. HARRJE I. GLASSMAN
1	UNIVERSITY OF WISCONSIN MECHANICAL ENG DEPT 1513 UNIVERSITY AVE. MADISON, WISCONSIN 53705	P. S. MYERS

COPIES	RECIPIENT	DESIGNEE
1	UNIVERSITY OF MICHIGAN AEROSPACE ENGINEERING ANN ARBOR, MICHIGAN 48104	J. A. NICHOLLS
1	UNIVERSITY OF CALIF. DEPT. OF CHEM. ENG. 6161 ETCHEVERRY HALL BERKELEY, CALIF. 94720	A. K. OPPENHIEM R. SAWYER
1	PURDUE UNIV SCHOOL OF MECH ENG LAFAYETTE, INDIANA 47907	J. R. OSBORN
1	SACRAMENTO STATE COLLEGE ENGINEERING DIVISION 60000 J. STREET SACRAMENTO, CALIFORNIA 95818	E. H. REARDON
1	ILLINOIS INSTITUTE OF TECH RM 200 M. H. 3300 S. FEDERAL STREET CHICAGO, ILLINOIS 60616	T. P. TORDA
1	POLYTECHNIC INSTITUTE OF BROOKLYN GRADUATE CENTER ROUTE 110 FARMINGDALE, NEW YORK	V. D. AGOSTA
1	GEORGIA INST OF TECH ATLANTA, GEORGIA 30332	B. T. ZINN
1	UNIVERSITY OF DENVER RESEARCH INSTITUTE DENVER, COLORADO	W. H. MCLAIN
1	NEW YORK UNIVERSITY DEPT. OF CHEM. ENG. UNIVERSITY HEIGHTS NEW YORK 53, NEW YORK	LEONARD DAUERMAN
1	THE JOHNS HOPKINS UNIVERSITY APPLIED PHYSICS LABORATORY 8621 GEORGIA AVE. SILVER SPRINGS, MARYLAND 20910	W. G. BERL

COPIES	RECIPIENT	DESIGNEE
	FOREIGN UNIVERSITIES	
1	THE UNIVERSITY OF SHEFFIELD DEPT. OF FUEL TECHNOLOGY ST. GEORGE'S SQUARE SHEFFIELD 1, YORKS ENGLAND	MR. J. SWITHENBANK
1	MOTORLAR ENSTITUSU PROFESSOR ZUBEYIR DEMIRGUE DIRECTOR OF ENGINE INSTITUTE ISTANBUL - GUMUSSUYU	
1	INSTITUTO NACIONAL DE TECNICA AEROESPACIAL CARLOS SANCHEZ-TARIFA SERRANO 43 MADRID, SPAIN	